10.13 Planetary Atmospheres

DC Catling, University of Washington, Seattle, WA, USA

10.13.1 Introduction and Scope

The enormous topic of planetary atmospheres ranges from the origin of atmospheres to the fluid dynamics of small weather systems, so here, I restrict the scope to broad essentials at a level suitable for a PhD research student. I assume knowledge of calculus, plus basic physics and chemistry, but little else. The audience could also include researchers in allied fields – for example, planetary geologists, geochemists, or astronomers. I focus on atmospheres in the solar system. Exoplanets represent

a new frontier that should reveal a larger diversity of atmospheres (Seager, 2010; Seager and Deming, 2010; Seager et al., 2010). But at the moment, only a little can be said about exoplanet atmospheres with any certainty. Currently, observational data from such atmospheres are arguably much sparser than data were for atmospheres in our solar system before the Space Age. Rather than speculate, I concentrate on key principles associated with the planetary atmospheres that we know best. In fact, these are what will be needed to interpret exoplanet atmospheres correctly (see Chapter 10.21).

Until the last 5 years or so, introductory syntheses about atmospheres were mostly confined to the Earth (e.g., Houghton, 2002; Wallace and Hobbs, 2006), with a few exceptions (Chamberlain and Hunten, 1987; Yung and DeMore, 1999), but now, the coverage of planetary atmospheres is more available. A primer by Ingersoll (2013) is a good read for all levels, while Taylor (2010) provides a useful introduction aimed at mid-level undergraduates. At the research level, general texts are Pierrehumbert (2010), Sanchez-Lavega (2010), and Catling and Kasting (in press). In a more specialized area, Yung and Demore (1999) provided a detailed monograph on photochemistry. Recent papers have also reviewed the probable atmospheric circulation regimes of exoplanets (Showman et al., 2010, 2013).

The structure of this review is as follows. In order to discuss atmospheres, I start with an overview of composition and basic physical properties, including the layers of atmospheres. Thus, **Section 10.13.2** describes structure and thermodynamics. Atmospheric composition determines physical properties, which in turn affects climate through the greenhouse effect. A planet's climate requires a grasp of the radiative transfer of energy, which is discussed in **Section 10.13.3**. A brief overview of the photochemistry of atmospheres is then given in **Section 10.13.4** to provide an appreciation of the globally averaged bulk composition and vertical distribution of constituents. However, atmospheric motions transport heat and constituents, including condensable species, and are indispensable for several aspects of climate and chemistry. Principles of atmospheric motion are described in **Section 10.13.5**. Together, these various topics – thermodynamics, radiation, chemistry, and dynamics – provide the essentials of planetary atmospheres. Finally, in **Section 10.13.6**, I very briefly note some key outstanding questions.

One topic is missing: atmospheric origin and evolution. This subject is of profound interest but involves considerable geochemistry and familiarity with all the topics of this review, so the reader is referred to Catling and Kasting (in press) that comprehensively reviews this area (see **Chapter 10.14**).

10.13.2   Composition and Vertical Structure

10.13.2.1   The Observed Compositional Diversity of Atmospheres

A physically meaningful classification of the composition of planetary atmospheres falls into two chemical categories: reducing and oxidizing. A redox (reduction–oxidation) state indicates the chemical character of atmospheres, for example, whether elements such as carbon are likely to be found in their reduced form (methane, CH_4) or oxidized variety (carbon dioxide, CO_2).

The solar system contains several examples of oxidizing and reducing atmospheres. Reducing atmospheres are those that are relatively rich in reducing gases, typically hydrogen-bearing gases, such as hydrogen itself (H_2), methane (CH_4), and possibly ammonia (NH_3). Examples include all the giant planets and Saturn's largest moon, Titan (**Table 1**). In principle, an atmosphere dominated by carbon monoxide (CO) would also be reducing (perhaps applicable to some hot giant exoplanet

atmospheres (Moses et al., 2011) or early Mars (Zahnle et al., 2008)), although we do not have an example in the modern solar system, and such an atmosphere would likely contain considerable H_2 as well. The atmosphere of the early Earth was also reducing, albeit weakly, before its oxygenation at 2.4 Ga (Ga=giga anna=billions of years ago) (Catling, 2014; Lyons et al., 2014). In contrast, oxidizing atmospheres are relatively poor in reducing hydrogen-bearing gases and include modern Earth and Mars (**Table 2**). Molecular O_2 has a volume abundance of 21 and 0.15% on Earth and Mars, respectively, which greatly exceeds the amount of hydrogen-bearing reducing gases of 1.8 ppmv (parts per million by volume) CH_4 on Earth (Hartmann et al., 2013) and 15 ± 5 ppmv H_2 on Mars (Krasnopolsky and Feldman, 2001). Venus is unusual. The upper atmosphere of Venus is oxidizing, with a tenuous ozone (O_3) layer at 90–105 km altitude on the nightside (Montmessin et al., 2011), while the atmosphere below ~20 km altitude is arguably weakly reducing because sulfur is converted into various reduced forms (Krasnopolsky and Pollack, 1994). Noting sulfur oxidation numbers in square brackets, these sulfur species include sulfur dioxide (SO_2) [+4], carbonyl sulfide (OCS)[−2], hydrogen sulfide (H_2S) [−2], and elemental sulfur allotropes of 1–8 atoms ($S-S_8$)[0]. The OCS is sourced from weathering of sulfides on the surface, or volcanic outgassing, or the reduction of sulfur by carbon monoxide (e.g., S_2+CO), which is present at ~20 ppmv below 20 km (Fegley, 2014). Unlike Earth and Mars, O_2 is absent in Venus' atmosphere with an upper limit of <0.3 ppmv.

Broadly speaking, planetary formation theories from a Sun-like nebula (reviewed by Chambers, 2014) favor more hydrogen-rich atmospheres far from a star and more oxidizing atmospheres nearby, but this can be confounded in an extrasolar system if a planet's orbital distance changes in planetary migration. Also, the very early rocky planets in our own solar system may have had hydrogen-rich atmospheres (Abe, 2011).

Redox also indicates the possible chemistry of aerosols, which are fine particles found in atmospheres. In general, oxidizing atmospheres with sulfurous gases tend to produce sulfate aerosols at altitude (McGouldrick et al., 2011), such as in the Earth's stratosphere (Crutzen, 1976; Robock, 2000), on Venus (Thompson et al., 2011), or on Mars when it was volcanically active (Settle, 1979; Smith et al., 2014; Tian et al., 2010). In contrast, reducing atmospheres generate hydrocarbon aerosols, including the giant planets (Irwin, 2009; Moses et al., 2004; West et al., 1991, 2004, 2009), Titan (Krasnopolsky, 2010; Lavvas et al., 2008a,b; Wilson and Atreya, 2004), and probably the early Earth (Pavlov et al., 2001; Wolf and Toon, 2010; Zerkle et al., 2012).

In addition to the atmospheres discussed in the preceding text, some smaller bodies possess very thin atmospheres. Exospheres exist directly above the surfaces of several moons, which are defined as atmospheric layers of such low density that they are virtually collisionless. We find the following thin atmospheres, where the surface pressure is given in bar (1 bar=10^5 Pa) in parentheses:

(i) N_2-rich atmospheres above surfaces covered in N_2 ice: Triton ($\sim(14-20)\times10^{-6}$), the largest moon of Neptune, and Pluto ($\sim15\times10^{-6}$)

Table 1 The composition of reducing atmospheres

Species	Jupiter	Saturn	Uranus	Neptune	Titan
H_2	$86.4 \pm 2.6\%$	$88 \pm 2\%$	$82.5 \pm 3.3\%$	$80 \pm 3.2\%$	0.099%
He	$13.6 \pm 0.3\%$	$12 \pm 2\%$	$15.2 \pm 3.3\%$	$19.0 \pm 3.2\%$	
CH_4[a]	$0.204 \pm 0.049\%$	$0.47 \pm 0.2\%$	$\sim 2.3\%$ (below CH_4 clouds)	$\sim 1-2\%$ (below CH_4 clouds)	5.65% (1.48% in stratosphere)
$^{13}CH_4$	$1.9 \pm 0.1 \times 10^{-5}$	$5.1 \pm 0.2 \times 10^{-5}$			0.062%
N_2	–	–	–	–	94.2%
NH_3[a]	$5.74 \pm 0.22 \times 10^{-4}$ (8.9–11.7 bar, below NH_3 clouds)	$\sim 1.1 \times 10^{-4}$ ($p > 1$ bar, below NH_3 clouds)	$< 1 \times 10^{-7}$	6×10^{-7} (at 6 bar)	
H_2O[a]	$4.23 \pm 1.38 \times 10^{-4}$ (at 17.6–20.9 bar)	2.3×10^{-7} (upper troposphere)	$6-14 \times 10^{-9}$ (at $p < 0.03$ mbar)	$1.7-4.1 \times 10^{-9}$ (at $p < 0.6$ mbar)	$< 10^{-8}$
H_2S[a]	$6.7 \pm 0.4 \times 10^{-5}$ (at $p > 16$ bar)	$< 0.4 \times 10^{-6}$	$< 8 \times 10^{-7}$	$< 3 \times 10^{-6}$	–
Ne	1.99×10^{-5}				$< 2 \times 10^{-5}$ ^{20}Ne
Ar	$1.57 \pm 0.35 \times 10^{-5}$				3.4×10^{-5} ^{40}Ar 2.1×10^{-7} ^{36}Ar
C_2H_6	$5.8 \pm 1.5 \times 10^{-6}$ (stratosphere)	$7.0 \pm 1.5 \times 10^{-6}$ (stratosphere)	1.5×10^{-5} (at 0.5–1 mbar)	1.5×10^{-6} (stratosphere)	$\leq 1 \times 10^{-5}$
PH_3	$1.04 \pm 0.1 \times 10^{-6}$	$5.9 \pm 0.2 \times 10^{-6}$ ($p > 0.5$ bar)	$< 8.3 \times 10^{-7}$		-
C_2H_2	$\sim 4 \times 10^{-8}$ (at 5 mbar)	$3.0 \pm 0.2 \times 10^{-7}$ (at 1 mbar)	$\sim 1.0 \times 10^{-8}$ (stratosphere)	$6.0^{+14.0}_{-4.0} \times 10^{-9}$ (stratosphere)	$\leq 2 \times 10^{-6}$
C_2H_2	3.5×10^{-10} (at $p < 10$ mbar)	3.4×10^{-10} (at $p < 10$ mbar)	$4.0 \pm 0.5 \times 10^{-11}$ (at 0.1 mbar)	6×10^{-8} (at $p < 5$ mbar)	10^{-8} (above stratospheric condensation)
CO	$1.6 \pm 0.3 \times 10^{-9}$ (at 5–8 bar)	$< 10^{-7}$ (stratosphere)	$< 4 \times 10^{-8}$ (stratosphere)	$6.5 \pm 3.5 \times 10^{-6}$ (stratosphere)	4.7×10^{-5}
D/H	$2.3-2.6 \times 10^{-5}$	$1.7^{+0.75}_{-0.45} \times 10^{-5}$			$1.35 \pm 0.3 \times 10^{-4}$ in H_2 $1.32^{+0.15}_{-0.11} \times 10^{-4}$ in CH_4
$^{13}C/^{12}C$	0.0108 ± 0.0005	0.011			0.01099 ± 0.00017 in CH_4

[a]Condensable species, so levels are indicated.

Gases are given as volume mixing ratios. CH_4 is condensable on Titan, Uranus, and Neptune. H_2O and NH_3 are condensable on the giant planets, while H_2S reacts with NH_3 to form ammonium hydrosulfide (NH_4SH) clouds.

Source: Lodders K (2010) Atmospheric chemistry of the gas giant planets. *Geochemical News* 142: 1–11; Atreya SK, Mahaffy PR, Niemann HB, Wong MH, and Owen TC (2003) Composition and origin of the atmosphere of Jupiter – An update, and implications for the extrasolar giant planets. *Planetary and Space Science* 51: 105–112; Irwin P (2009) *Giant Planets of Our Solar System: Atmospheres, Composition, and Structure*, 2nd edn. Chichester, UK: Springer; Niemann HB, Atreya SK, Demick JE, Gautier D, Haberman JA, Harpold DN, Kasprzak WT, Lunine JI, et al. (2010) Composition of Titan's lower atmosphere and simple surface volatiles as measured by the Cassini–Huygens probe gas chromatograph mass spectrometer experiment. *Journal of Geophysical Research* 115.

(ii) O_2-rich exospheres above moons covered in water ice: Jupiter's moons, Europa ($\sim 10^{12}-10^{13}$ O_2), (Smyth and Marconi, 2006), Ganymede ($\sim 10^{-12}$ O_2) (Hall et al., 1998), and Callisto ($\sim 10^{-12}$ O_2 possibly + CO_2) (Carlson, 1999; Kliore et al., 2002; Liang et al., 2005), and Saturn's moons, Rhea ($\sim 10^{-12}$ O_2 and CO_2) (Teolis et al., 2010) and Dione ($\sim 10^{-12}$ O_2) (Tokar et al., 2012)

(iii) Volcanogenic atmospheres: SO_2 on Io ($\sim 10^{-7}-10^{-9}$), a moon of Jupiter, and a water vapor–CO_2 exosphere on Enceladus, a moon of Saturn

The tenuous N_2-rich atmospheres (with minor CH_4) on Triton and Pluto arise from vapor equilibrium with N_2 (and CH_4) ice at prevailing surface temperatures. The O_2-rich exospheres on the moons of Jupiter and Saturn come from the breakdown of water ice on the surfaces of these moons by radiolysis and sputtering (Johnson et al., 2009). Radiolysis is the chemical alteration of ices by charged particles, and sputtering is when charged particles collide and eject atoms or molecules. The faster escape of the hydrogen compared with that of the oxygen leaves oxygen lingering behind in an exosphere. The charged particles

come from magnetospheres, which are envelopes of ions around planets controlled by the planetary magnetic fields.

Volcanic small bodies have a different class of atmosphere. The very thin SO_2 atmosphere on Io, a rocky body, is sourced from high-temperature volcanism at a rate of 10^5 kg s^{-1} SO_2 (Lellouch et al., 2003). The SO_2 freezes to form frost away from the hot vents (Schmitt et al., 1994). Elemental sulfur is also volcanically outgassed, with $SO_2/S_2 \sim 3-12$ in the plume of the volcano Pele (Spencer et al., 2000). In contrast to Io, Enceladus is covered in water ice and affected by cryovolcanism, that is, a form of volcanism where ice turns to vapor or gets ejected as a result subsurface heating, unlike volcanism that involves molten rock. Plumes at the south pole of Enceladus release icy particles at a rate of 200 ± 30 kg s^{-1} (Hansen et al., 2011) from parallel lineaments called 'tiger stripes' (~ 500 m deep, ~ 130 km long, 2 km wide) (Porco et al., 2006), causing a very asymmetrical exosphere (Tenishev et al., 2010).

The very thin atmospheres described in the preceding text are mentioned for completeness. Henceforth, I restrict most of the discussion to thicker atmospheres, the thinnest being that of Mars.

Table 2   The composition and properties of oxidizing atmospheres (noting that the lower atmosphere of Venus could be considered somewhat reducing)

Parameter	Venus	Earth	Mars
Mean surface pressure (bar)	95.6	1.0	0.006
Mean surface temperature (K)	735	288	218
Mass relative to the Earth (5.97×10^{24} kg)	0.815	1.0	$0.107 \approx 1/9$
Mean radius relative to the Earth (6371 km)	0.950	1.0	$0.532 \approx 1/2$
Key gases in atmosphere (by volume)	CO_2 96.5%	N_2[a] 78.084%	CO_2 96.0 ± 0.7%
	N_2 3.5%	O_2[a] 20.946%	N_2 1.89 ± 0.01%
	SO_2[c]	H_2O 0.1 ppm – 4%	Ar 1.93 ± 0.01%
	• 150 ± 30 ppm	(varies)	O_2 0.145 ± 0.09%
	(22–42 km)	Ar 9340 ppm	CO 0.06%
	• 25 ± 150 ppm	CO_2[a,b]	H_2O ~0.03%
	(12–22 km)	• ~280 ppm	(varies)
	^{40}Ar 70 ± 25 ppm	(pre-industrial)	He 10 ppm
	$^{36+38}$Ar 75 ± 35 ppm	• 396.5 ppm	H_2 15 ± 5 ppm
	H_2O[e] 30 ± 15 ppm (5–45 km)	(year 2013)	Ne 2.5 ppm
	CO[c]	Ne 18.18 ppm	Kr 0.3 ppm
	• 45 ± 10 ppm	^{4}He 5.24 ppm	O_3 0–80 ppb
	(cloud top)	CH_4[a] 1.7 ppm	H_2O_2 0–40 ppb
	• 17 ± 1 ppm (12 km)	Kr 1.14 ppm	SO_2[d] <0.3 ppb
	He 12 (+24/−8) ppm	H_2[a] 0.55 ppm	
	Ne 7 ± 3 ppm	N_2O[a] ~320 ppb	
	H_2[c] 2.5 ± 1 ppm	CO[a] 125 ppb	
	(50–60 km)		
	HCl 0.4 ppm		
	(70 km)		
	^{84}Kr 50 ± 25 ppb		

[a]Biologically cycled and influenced.
[b]Currently increasing about 2 ppm per year because of anthropogenic emissions.
[c]Altitude-dependent.
[d]Indicates lack of volcanic outgassing.
Source: Lodders K and Fegley B (1998) *The Planetary Scientist's Companion*. New York: Oxford University Press; Pollack JB (1991) Kuiper prize lecture: Present and past climates of the terrestrial planets. *Icarus* 91: 173–198; Krasnopolsky VA and Lefevre F (2013) Chemistry of the atmospheres of Mars, Venus, and Titan. In: Mackwell SJ, Simon-Miller AA, Harder JW, and Bullock MA (eds.) *Comparative Climatology of Terrestrial Planets*, pp. 231–275. Tucson, AZ: University of Arizona Press; Mahaffy PR, Webster CR, Atreya SK, et al. (2013) Abundance and isotopic composition of gases in the martian atmosphere from the Curiosity Rover. *Science* 341: 263–266.

10.13.2.2   Nomenclature for the Vertical Structure of Atmospheres

Along with composition, a basic description of any atmospheres involves atmospheric structure. The term conventionally refers to the vertical temperature profile, which provides information about how chemical and physical processes change with altitude. The average thermal profile is also the basis for naming atmospheric layers using a system developed for Earth in the early 1900s (Lindemann and Dobson, 1923; Martyn and Pulley, 1936); thus, the nomenclature works with only some degree of success for other bodies. New atmospheric layers begin where there is a temperature inflection (Figure 1). On Earth, the five layers are the following: (i) the troposphere (tropos – Greek for the 'turning' of convection), where temperature declines from the surface to the tropopause (pause – Greek for 'stop'), which lies at an average pressure of 0.16 bar (Sausen and Santer, 2003). The tropopause altitude is 0.2 bar (11 km) in the US Standard Atmosphere but varies in detail with latitude from 0.1 to 0.3 bar (tropics to pole) (Hoinka, 1998). (ii) The stratosphere (stratus– Greek for 'layered'), where temperature increases from the tropopause to the stratopause at ~50 km altitude where the air pressure is ~100 Pa (1 mbar). (iii) The mesosphere from the stratopause to the mesopause, at ~85 km altitude, where the air pressure is about 1–0.1 Pa (0.01–0.001 mbar).

(iv) The thermosphere from the mesopause to the thermopause (or exobase) at that varies over altitudes of ~250–500 km as solar ultraviolet (UV) flux changes over cycles ranging from daily to the 11-year solar cycle. (v) The exosphere, which blends into interplanetary space.

Convection dominates lower troposphere. Solar radiation heats the surface of rocky planets or is absorbed in the deeper portions of troposphere on giant planets. Consequently, warm buoyant air rises to altitudes of lower pressure where it expands and cools. Cool air parcels sink and warm. The net effect of such convection is a decline of temperature with altitude. On Earth, the rate that temperature decreases, the lapse rate, averages ~6 K km^{-1} globally. In the upper troposphere where the air is thinner, radiation transfers energy instead of convection above a radiative–convective boundary. Higher still, emission of thermal infrared (IR) radiation from the air to space becomes so efficient that a temperature minimum or tropopause is achieved. The tropopause occurs near an average pressure of roughly 0.1 bar on Earth, Titan, and the giant planets. The similarity is because of a common scaling of broadband IR opacity and pressure. In upper troposphere, the IR opacity is pressure-dependent in the same way – varying approximately with the square of the pressure – while all these atmospheres are roughly similar in their strong opaqueness to IR at deeper pressures, such as 1 bar,
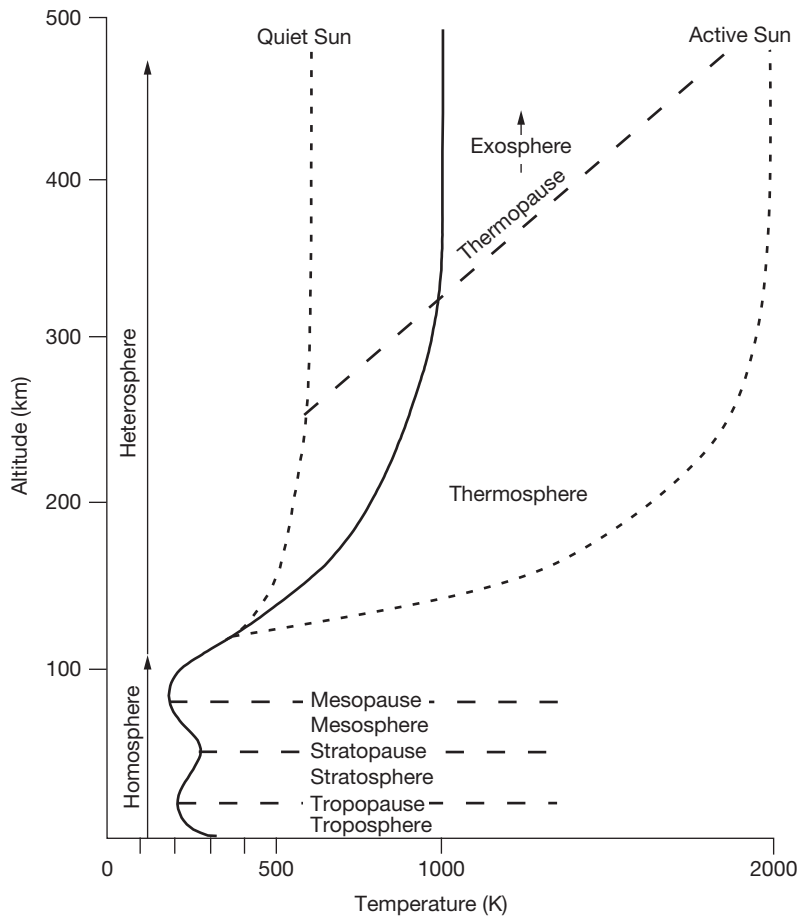
Figure 1   The terminology for vertical layers of the Earth's atmosphere, shown schematically. (Drawn by the author.)

despite the big differences in atmospheric composition and gravity (Robinson and Catling, 2014) (see **Section 10.13.3.4**).

In stratospheres, the absorption of shortwave solar radiation causes a temperature inversion, defined as a temperature increase with altitude. On Earth, the ozone absorbs UV radiation, whereas on the giant planets and Titan, aerosol particles and methane absorb at wavelengths in the UV, visible, and near-IR. Mars and Venus, which have predominantly CO_2 atmospheres, do not have strong shortwave absorbers above their troposphere, so in the global average, they lack stratospheric inversions and tropopause minima (see **Section 10.13.3.4**).

Above the Earth's stratosphere, CO_2 emission to space causes the mesosphere to have the lowest atmospheric temperatures. A cold mesopause forms the lower boundary of the thermosphere where temperature increases with altitude. Mesopauses occur around ∼1–0.1 Pa in planetary atmospheres in the solar system. They are cold because the air is so thin in upper mesospheres that energy-exchanging collisions between molecules become less frequent than photon emission at a level of radiative relaxation (Curtis and Goody, 1956; López-Puertas and Taylor, 2001). Consequently, excited molecules lose energy by radiation rather than by collisions.

In thermospheres, absorption of extreme ultraviolet radiation (EUV) (with wavelength shorter than ∼120 nm) causes temperature to increase. Molecules are broken apart by EUV and photochemical reactions, and EUV and x-rays ionize both molecules and atoms. In the tenuous gas, infrequent collisions between electrons and ions create an ionosphere, a shell of electrons and ions that extends on Earth from the mesosphere into the exosphere. The Earth's hot thermosphere (∼1000 K at 250 km altitude) reflects the slow rate of removing heat. Atoms and atomic ions do not have vibrational or rotational transitions and so are poor radiators, unlike molecules. Instead, heat is transferred inefficiently by conduction downward to the cold mesopause where radiative cooling is effective. Unlike the Earth, the upper thermospheres on Mars and Venus are relatively cold at ∼270 K for Mars and ∼250 K for Venus, because their ∼96% CO_2 causes efficient radiative cooling to space (Section 10.13.4.5). Finally, exospheres lie above thermospheres and are where atmospheres become collisionless.

Chemically, we can divide atmospheres into two big layers: a homosphere where bulk gases are well mixed up to a homopause and a heterosphere above the homopause where molecular diffusion becomes more important than turbulent mixing. The homopause occurs where the diffusion separation time and turbulent mixing time of gases are equal. This tends to occur within a few orders of magnitude of 0.01 Pa (or 0.1 μbar). On Earth, the homopause is at ∼100 km height. Above, at 250–1000 km altitude, diffusive separation causes atomic oxygen (O) to become the dominant species, while higher up, helium dominates, and then, hydrogen above 2500 km height.

Species escape from the base of exospheres (the exobase) if their upward velocity exceeds the escape velocity v_{esc}, which is given by a balance between gravitational energy and kinetic energy (KE):

$$\frac{1}{2}mv_{esc}^2 = \frac{GMm}{r} \Rightarrow v_{esc} = \sqrt{\frac{2GM}{r}} \Rightarrow \underbrace{v_{esc} \propto \sqrt{\frac{a^3}{a}} \propto a}_{\text{if same density body of radius } a} \quad [1]$$

Here, r is the radial distance, G is the universal gravitational constant $(6.672 \times 10^{-11} \, \text{N m}^2 \, \text{kg}^{-2})$, M is the mass of the planet, a is the planet's radius, and m is the molecular mass. Today, hydrogen escapes efficiently from Earth at a small rate $\sim 3 \, \text{kg s}^{-1}$. Hydrogen atoms at the exobase in the tail of the Maxwell–Boltzmann velocity distribution have enough thermal velocity to evaporate and escape even though the root-mean-square speed (given by $1/2mv^2 = (3/2)kT$, where $k = 1.381 \times 10^{-23} \, \text{J K}^{-1}$ is Boltzmann's constant and T is exobase temperature) is less than the Earth's escape velocity. Alternatively, the hydrogen is lost when chemical or charged particle reactions impart speed to hydrogen atoms. The rate-limiting step is not a loss from the exobase itself but diffusion from the homopause to the exobase. Consequently, hydrogen is said to be lost at an upper limit by diffusion-limited escape (Hunten, 1973; Walker, 1977). Diffusion-limited escape of hydrogen is an excellent theory given that data suggest that it happens on Venus, Earth, Mars, and Titan.

For completeness, there are three ways that gases escape from planets: (i) thermal escape, with end-member approximations of thermal evaporation (as mentioned in the preceding text) called Jean's escape at one end and pressure-driven hydrodynamic escape at the other (e.g., Catling and Zahnle, 2009; Johnson et al., 2013; Walker, 1982), (ii) nonthermal escape where an atom or molecule is boosted to escape velocity because of a chemical reaction or ionic interaction, and (iii) impact erosion where atmospheric gases are expelled as a result of the large body impacts. Helium escapes from the Earth today through nonthermal escape. However, bodies can lose their atmospheres in bulk. Theory demonstrates that the two mechanisms that most efficiently strip away substantial atmospheres are hydrodynamic escape driven by stellar irradiation (Lammer et al., 2008; Sekiya et al., 1980, 1981; Watson et al., 1981; Zahnle and Kasting, 1986; Zahnle et al., 1990) and impact erosion (Griffith and Zahnle, 1995; Melosh and Vickery, 1989; Walker, 1986; Zahnle et al., 1992). Currently, in the solar system, only Pluto's atmosphere is believed to be undergoing hydrodynamic escape (Trafton et al., 1997). The reader is referred to Catling and Kasting (in press) and Lammer (2013) for more discussion of escape processes.

10.13.2.3   The Equation of State, Atmospheric Composition, and the Hydrostatic Equation

The most basic physics of atmospheres involves connecting the distributions of pressure, temperature, and density with (i) an equation of state and (ii) a hydrostatic equation.

Except for deep within giant-planet atmospheres, the ideal gas law works well as for (i)

$$p = nkT = (n\overline{m})\left(\frac{k}{\overline{m}}\right)T \Rightarrow p = \rho\overline{R}T \quad [2]$$
$$\underbrace{\phantom{(n\overline{m})}}_{\rho}$$

Here, k is Boltzmann's constant, $\overline{m}$ is the mean molecular mass, n is the number density or number of molecules per unit volume, and $\rho = n\overline{m}$ is the mass density. The universal gas constant R $(8.314 \, \text{J K}^{-1} \, \text{mol}^{-1})$ is related to a specific gas constant (different for each atmosphere) by $\overline{R} = R/\overline{M} = K/\overline{m}$, where $\overline{M}$ (kg mol^{-1}) is the mean molar mass. Dalton's law states that the total pressure is the sum of partial pressures p_i, for each species i, $p = \sum p_i$. Applied to eqn [2], the mean molecular mass is

$$\overline{m} = \frac{\sum_i n_i m_i}{n} = \frac{\overline{M}}{N_A} \quad [3]$$

where m_i is the mass of the ith molecule and N_A is Avogadro's number. On Mars, for example, using the data of Table 2, the mean molar mass $\overline{M} = 0.0435 \, \text{kg mol}^{-1}$ and $\overline{R} = R/\overline{M} = 191 \, \text{J kg}^{-1} \text{K}^{-1}$. For dry air on Earth, $\overline{M} = 0.029 \, \text{kg mol}^{-1}$ and $\overline{R} = R/\overline{M} = 287 \, \text{J K}^{-1} \, \text{kg}^{-1}$.

We usually describe atmospheric composition with the volume mixing ratio f_i, for species i, which is also the mole fraction. Less commonly, we use a mass mixing ratio μ_i, which is the mass of a particular gas divided by the total mass of a gas mixture sample. For an ideal gas,

$$f_i = \frac{p_i}{p} = \frac{V_i}{V} = \frac{n_i}{n}, \quad \mu_i = \frac{\rho_i}{\rho}\frac{m_i}{\overline{m}}\frac{p_i}{p} = \frac{m_i}{\overline{m}}f_i \quad [4]$$

In all atmospheres, high total pressure at low altitudes pushes upward against the weight of overlying air, so that pressure declines with altitude. Air settles into hydrostatic equilibrium. This equilibrium assumes no vertical motion – a good approximation over large horizontal scales (e.g., a few kilometers on the Earth) that average out updrafts and downdrafts. A column of air with unit area cross section and small height Δz has a mass $\rho\Delta z$, so that the pressure change going up in height Δz is $\Delta p = -(\rho\Delta z)g = $ force/(unit area), where g is the gravitational acceleration. Written in calculus form, we get the hydrostatic equation relating pressure, density, and altitude:

$$\frac{\partial p}{\partial z} = -\rho(z)g(z), \quad p(z) = \int_z^\infty \rho(z)g(z)\mathrm{d}z \quad [5]$$

For an ideal gas, the air density is $\rho = p/\overline{R}T$ (eqn [2]), so that we can rewrite eqn [5] as

$$\frac{\partial p}{\partial z} = \left(\frac{-g(z)}{\overline{R}(z)T(z)}\right)p \Rightarrow \frac{\partial p}{p} = -\left(\frac{\partial z}{H}\right) \Rightarrow p$$

$$= p_s \exp\left(-\int_0^z \left(\frac{\mathrm{d}z}{H}\right)\right) \Rightarrow p \approx p_s \exp\left(-\frac{z}{H}\right)_{\text{isothermal}} \quad [6]$$

Here, p_s is the surface pressure and we introduce a vertical length scale called the scale height,

$$H = \overline{R}T/g = kT/\overline{m}g \quad [7]$$

If we make the approximation that the temperature, gravity, and specific gas constant are constant with height, the integral of eqn [6] can be evaluated to give the exponential shown in the last expression. Thus, we see the meaning of the scale height: the vertical distance over which pressure drops by a factor of $1/e = 1/(2.7183) \approx 1/3$. In an isothermal atmosphere, density also drops by $1/e$ over the same height, but the density scale height will be slightly different if there is any temperature change with altitude. In the solar system, $H \approx 5$–20 km because the ratio $\overline{T}/\overline{m}g$ in $H = kT/\overline{m}g$ is similar given that smaller T (and larger g for Jupiter) compensates for small $\overline{m}$ in H_2-rich giant planets.
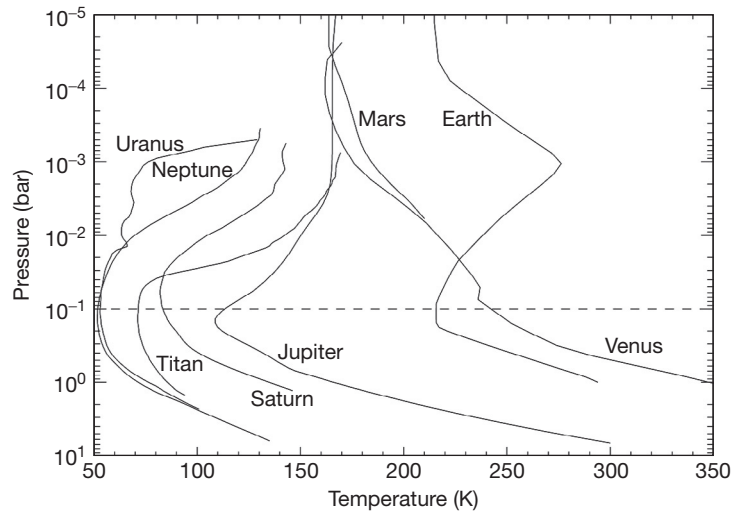
Figure 2 Temperature–pressure profiles for planetary atmospheres in the solar system. The dashed line at 0.1 bar indicates that planets with stratospheric temperature inversions have tropopause minima near this pressure level. (Drawn by the author.)

The surface pressure measures an atmosphere's mass because pressure is the weight of a column of air per unit area. Ignoring lateral forces in the real 3-D spherical geometry (which are a minor correction), we have

$$p_s = M_{col}g \Rightarrow M_{col} = \frac{p_s}{g} \qquad [8]$$

where M_{col} is the column mass. For example, $M_{col} = (610\ Pa)/(3.72\ m\ s^{-2}) = 164\ kg\ m^{-2}$ on Mars, $10^4\ kg\ m^{-2}$ on Earth, and $2 \times 10^5\ kg\ m^{-2}$ on Titan. Equation [8] can also be applied to the column mass above some reference pressure level for giant planets.

The hydrostatic equation combined with number density gives us another way to describe atmosphere composition, namely, column abundance N_c, which is the number of molecules above a unit area. For example, the typical abundance of terrestrial ozone is $N_{O3} \approx 8 \times 10^{18}$ molecules cm^{-2}. At altitude z, the column abundance $N_c(z)$ is defined by

$$N_c(z) = \int_z^{\infty} n(z)dz \qquad [9]$$

The column mass is $N_c(z)\overline{m}$, so the pressure at altitude z, by eqn [8], is $p(z) = N_c(z)\overline{m}g$. Using this, we obtain an expression for the column abundance in terms of scale height H:

$$N_c(z) = \frac{p(z)}{\overline{m}g} = \frac{n(z)kT(z)}{\overline{m}g} \Rightarrow N_c(z) = n(z)H(z) \qquad [10]$$

In some planetary literature, column abundance is expressed as 'cm-atm' or 'cm-amagat,' which are equivalent. These units are the depth in centimeters that would be produced if a gas in a column of air were all extracted and compressed to 1 atm (101325 Pa) pressure and 0 °C; they are given by the normalization $N_c(z)/n_0$, where $N_c(z)$ is in units of molecules cm^{-2} and $n_0 = 2.687 \times 10^{19}$ molecules cm^{-3} is the Loschmidt number, the number density of an ideal gas at 1 atm and 273.15 K. Ozone column abundance is also expressed with the Dobson unit (DU), which is the depth in thousandths of centimeters of a column of ozone taken to 1 atm and 0 °C, that is, DUs are $1000N_{O3}/n_0$. The Earth's ozone column is typically 300 DU (0.3 cm-atm) compared with a maximum of 6 DU on Mars.

10.13.2.4 Convection and Stability

Atmospheric temperatures vary with altitude (Figures 1 and 2) primarily because of radiation and convection, although large-scale atmospheric motion also plays a role (Section 10.13.5).

In lower tropospheres, warm air rises and cold air sinks so that heat is transferred upward by convection. Air expands and becomes buoyant, that is, less dense than surroundings, through (i) radiative heating, (ii) contact with a planetary surface warmed by sunlight, (iii) exothermic condensation of substances such as water vapor in the Earth's atmosphere (see Chapter 10.11), and (iv) heating from the interior of a planet, which is significant on giant planets but not usually on rocky ones.

Convection commences when the lapse rate exceeds a certain threshold. The lapse rate is denoted $\Gamma = -(dT/dz)$ and usually given in $K\ km^{-1}$. The minus sign is a convention to make Γ positive for typical tropospheric conditions. Convection is very efficient in transporting heat upward to the upper troposphere. There, the overlying atmosphere is relatively transparent to thermal IR and energy is radiated to space. Also, in the upper troposphere, the lapse rate is no longer steep and convection ceases. In this way, a state of radiative–convective equilibrium is achieved, in which outgoing IR radiation from the warm planet balances the energy of incoming sunlight and sets a characteristic radiative–convective temperature profile (see Section 10.13.3.4).

The adiabatic lapse rate is the threshold lapse rate for convection. If the actual lapse rate is bigger or smaller, the atmosphere convects or it does not. Adiabatic means no exchange of energy with surroundings. So if a vertically displaced air parcel expands or contracts adiabatically to adjust to its surrounding pressure, the temperature change as a function of height is readily calculable. Applying conservation of energy to the parcel, we have

$$\underbrace{dq}_{\text{heat added/kg (zero for adiabatic)}} = \underbrace{c_v dT}_{\text{change in internal heat/kg}} + \underbrace{p\,d\alpha}_{\text{work done/kg}}$$

$$[11]$$

Here, dq is heat input per unit mass (zero if adiabatic) and c_v is the specific heat at constant volume. Work is 'force × incremental distance' or 'pressure (p) × incremental volume change.' Because we are dealing with energy per unit mass, we define volume per unit mass as $\alpha = 1/\text{density} = 1/\rho$, so that work is $p\,d\alpha$. Since $\alpha = \overline{R}T/p$ from eqn [2], the product rule of differentiation gives us $d\alpha = (\overline{R}/p)\,dT - (\overline{R}T/p^2)\,dp$. Substituting in eqn [11], we have

$$dq = c_v\,dT + \not{p}\left[\frac{\overline{R}}{\not{p}}dT - \frac{\overline{R}T}{p^{\not{2}}}dp\right] = (c_v + \overline{R})dT - \left(\frac{\overline{R}T}{p}\right)dp$$

$$\Rightarrow dq = c_p\,dT + g\,dz$$

[12]

In the middle expression, we have inserted $c_p = c_v + \overline{R}$ from kinetic theory, which relates specific heat at constant pressure (c_p) to specific heat at constant volume. We also substituted $-g\,dz$ for $(\overline{R}T/p)\,dp$ using the first expression in eqn [5], the hydrostatic equation. For adiabatic changes, $dq = 0$. Thus, from the last expression in eqn [12], we obtain the adiabatic lapse rate for dry air:

$$\Gamma_a = -\left(\frac{dT}{dz}\right) = \frac{g}{c_p}$$

[13]

This simple but fundamental equation gives the temperature change with altitude of a dry parcel of air moving up and down through an atmosphere in hydrostatic equilibrium. Table 3 gives the specific heat capacities, gravitational accelerations, and lapse rates Γ_a of various planetary atmospheres.

Comparison of the ambient lapse rate Γ with Γ_a indicates susceptibility to convection. When $\Gamma < \Gamma_a$, a parcel that rises adiabatically cools more than the gentler ambient decrease of temperature with height. This cold, dense parcel sinks back downward, so the atmospheric profile is convectively stable. Conversely, when $\Gamma > \Gamma_a$, a parcel that rises adiabatically is warmer than surroundings, and the parcel continues to rise. The resulting rapid mixing by convection of such unstable atmospheres tends to adjust the temperature profile toward the adiabatic one. Thus, we find planetary atmospheres typically with $\Gamma \leq \Gamma_a$ (ignoring local circumstances such as thunderstorms) (Table 3).

Our analysis is incomplete because condensable species and aerosols strongly affect temperature profiles. For example, in the Earth's troposphere, the condensation of water vapor releases heat making Γ smaller than the adiabatic value. Condensation of sulfuric acid on Venus has a similar thermodynamic effect. We discuss a saturated adiabatic lapse rate (SALR) in Section 10.13.2.5. For deep atmospheres, such as on Venus, one should also take account of the temperature dependence of specific heat capacity c_p so that $\Gamma_a = \Gamma_a(T)$.

A shorthand description of the stability of temperature gradients uses potential temperature θ, which is the temperature that a parcel of air would have if it were taken to a reference pressure p_{ref} (e.g., 10^5 Pa for Earth) dry adiabatically. Potential temperature is an alternative thermodynamic variable to temperature and, from its definition, is constant with altitude z if the lapse rate is adiabatic. Otherwise, an increase of θ with z indicates convective stability, while negative $\partial\theta/\partial z$ indicates instability. Using the adiabatic version of eqn [12] with $dq = 0$, we define θ as follows:

$$\frac{dT}{T} = \left(\frac{\overline{R}}{c_p}\right)\frac{dp}{p} = \kappa\frac{dp}{p}; \quad \text{integrate } (\theta, T), \ (p_{ref}, p)$$

$$\Rightarrow \ln\left(\frac{T}{\theta}\right) = \kappa\ln\left(\frac{p}{p_{ref}}\right) \Rightarrow \theta = T\left(\frac{p_{ref}}{p}\right)^{\kappa}$$

[14]

where $\kappa = \overline{R}/c_p$. The final expression in eqn [14] is Poisson's (adiabatic state) equation. We use eqn [14] later in Section 10.13.3.4, and potential temperature comes up again in Section 10.13.5.

In convectively stable atmospheres, a buoyancy force causes vertically displaced parcels to return to their original altitude, but overshooting creates oscillations at an angular frequency called the Brunt–Väisälä frequency, N_B. Large-scale oscillations of air create buoyancy waves (also called gravity waves) that are important in the turbulence of upper atmospheres (Section 10.13.5.7). The Brunt–Väisälä frequency can be derived by considering an adiabatic air parcel of volume V displaced upward δz from an altitude where the temperature is T to a place where the environmental temperature is T_{env}. The parcel cools adiabatically to a new temperature $T_p = T - \Gamma_a\delta z$, while the environment cools less at the ambient lapse rate as $T_{env} = T - \Gamma\delta z$. The difference in density between the parcel

Table 3   Thermodynamic and physical properties of various planetary atmospheres

Body	Main gases	Molar mass, M ($g\,mol^{-1}$)	Specific gas constant $\overline{R}$ ($J\,kg^{-1}\,K^{-1}$)	Gravity g ($m\,s^{-2}$)	Specific heat capacity c_p ($J\,kg^{-1}\,K^{-1}$)	$\Gamma_a = g/c_p$ troposphere ($K\,km^{-1}$)	Mean Γ observed ($K\,km^{-1}$)
Venus	CO_2, N_2	43.5	189	8.901	930	9.5	~8.0
Earth	N_2, O_2	28.97	287	9.81	1004	9.8	~6
Mars	CO_2, N_2	43.5	191	3.72	850	4.4	~2.5
Jupiter	H_2, He	2.22	3745	24.25	10,988	2.1–2.45[a]	1.9
Saturn	H_2, He	2.14	3892	10.0	10,658	0.7–1.1[a]	0.85
Titan	N_2, CH_4	28.67	290	1.36	1044	1.3	1.0–1.4
Uranus	H_2, He	2.3	3615	8.80	8643	0.7–1.1[a]	0.75
Neptune	H_2, He	2.3	3615	11.1	8643	0.85–1.34[a]	0.95
Hot Jupiter HD209458b	H_2, He	2.0	4160	18.5	14 300	1.3	~0.2 (model)[b]

Γ_a is the tropospheric adiabatic lapse rate, while Γ is the observed tropospheric lapse rate.
[a]On giant planets, g varies from equator to pole.
[b]Menou and Rauscher (2009).

(ρ_P) and air (ρ_e) drives a buoyancy force, which we can write as Newton's second law:

$$\underbrace{(\cancel{V}\rho_p)}_{mass}\underbrace{\frac{d^2(\delta z)}{dt^2}}_{acceleration} = \underbrace{-g(\rho_p - \rho_e)\cancel{V}}_{buoyancy\ force} \quad \Rightarrow \frac{d^2(\delta z)}{dt^2} = g\left(\frac{\rho_e}{\rho_p} - 1\right)$$

$$= g\left(\frac{T_{env}}{T_p} - 1\right)$$

[15]

Substituting for temperatures T_p and T_{env}, we get

$$\frac{d^2(\delta z)}{dt^2} = g\left(\frac{T - \Gamma_a \delta z}{T - \Gamma \delta z} - 1\right) = g\left(\frac{\Gamma \delta z - \Gamma_a \delta z}{T - \Gamma \delta z}\right) \approx g\left(\frac{\Gamma - \Gamma_a}{T - \cancel{\Gamma \delta z}}\right)\delta z$$

$$\Rightarrow \ddot{\delta z} + \frac{g}{T}(\Gamma_a - \Gamma)\delta z = 0$$

[16]

In the last expression of eqn [16], we recognize simple harmonic motion, that is, the '$\ddot{x} + \omega^2 x = 0$' of elementary physics. Thus, the square of the angular (Brunt–Väisälä) frequency of oscillation is

$$N_B{}^2 \equiv \frac{g}{T}(\Gamma_a - \Gamma) \equiv \frac{g}{T}\left(\frac{dT}{dz} + \frac{g}{c_p}\right) \equiv \frac{g}{T}S$$

[17]

Here, $S(\text{K km}^{-1})$ is static stability, which measures the difference between the adiabatic lapse rate (eqn [13]) and actual lapse rate $(-dT/dz)$ and is usually positive. Equation [17] makes intuitive sense: the more stable the atmosphere, the higher the oscillation frequency, like stiffening an oscillating spring.

The effect of buoyancy oscillations can be observed. Vertical deflection of horizontal air flow over an obstacle such as a mountain on Earth or a large crater rim on Mars sometimes causes oscillations where the air swings up and down beyond the obstacle at a frequency $\sim N_B/2\pi$, forming a standing buoyancy wave. At the cold crests of the waves, moisture can condense into a series of parallel clouds called lee wave clouds, given that they form in the lee of the obstacle. Roughly speaking, the distance between parallel clouds has wavelength, $\lambda = (\text{horizontal wind velocity}/\text{frequency}) = u/(N_B/2\pi)$, which obviously can change with altitude-dependent u and N_B. Approximate terrestrial values of $N_B = 0.01\ \text{s}^{-1}$ and $u = 10\ \text{m s}^{-1}$ give $\lambda \sim 6\ \text{km}$, consistent with satellite imagery of lee wave cloud spacing of 3–20 km.

10.13.2.5 Condensables and the Clausius–Clapeyron Equation

Gases that condense – condensables – affect atmospheres through release or uptake of heat when they change into a liquid or solid from the vapor phase, and vice versa. Condensables include H_2SO_4 ($SO_3 + H_2O$) on Venus, H_2O on Earth, H_2O and CO_2 on Mars, H_2O and NH_3 on Jupiter and Saturn, and CH_4 on Titan, Uranus and Neptune, and HCN on Titan. Some condensables also form rain (e.g., CH_4 on Titan), snow (e.g., CO_2 in Mars' polar atmosphere), and clouds (e.g., CH_4 on Titan, Uranus, and Neptune).

The key concept governing condensable behavior is saturation vapor pressure (SVP), which is the vapor pressure exerted in equilibrium with a liquid or solid condensed phase. The curve of SVP versus temperature for a particular substance defines the transition between vapor and condensed phases
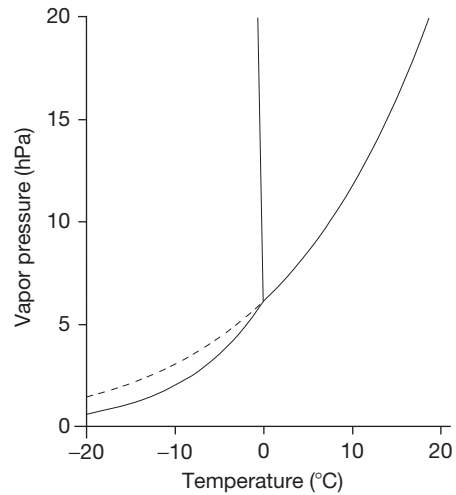

Figure 3 The saturation vapor pressure (SVP) curve between the vapor phase and condensed phase (liquid or ice) for water. The dashed line is the SVP with supercooled water. (Drawn by the author.)

(Figure 3). The Clausius–Clapeyron equation defines this SVP curve as a unique function of temperature. On Earth, we use a Clausius–Clapeyron equation for water, but analogous equations apply for other condensables. When noncondensable gases are part of a gas mixture, the vapor pressure of the condensable gas is a partial pressure, and if that partial pressure reaches SVP, then the solid or liquid phase forms.

The Clausius–Clapeyron equation comes from thermodynamics. Two phases are in equilibrium along the SVP versus T line, so the Gibbs free energy change of the phase transition is zero everywhere along the line. If e_s is the SVP, it can be shown by considering Gibbs free energy that the slope of e_s versus temperature T is given by (e.g., Atkins and De Paula, 2010)

$$\frac{de_s}{dT} = \frac{\delta s}{\delta \alpha} = \frac{\text{entropy gained per kg from condensed to vapor}}{\text{volume increase per kg from condensed to vapor}}$$

$$= \frac{l_c}{T\delta\alpha} = \frac{l_c}{T(\alpha_{vapor} - \alpha_{condensed})} \approx \frac{l_c}{T\alpha_{vapor}}$$

[18]

where α is specific volume ($\alpha = 1/\rho$), which, in the last step, we reasonably assumed, is far larger than for the vapor than for condensed phase, that is, $\alpha_{vapor} \gg \alpha_{condensed}$. We also substituted $l_c = T\delta s$, where l_c is the latent heat or enthalpy, which is heat absorbed (or released) when a unit mass changes from one phase to another at constant temperature and pressure. For different phase transitions, this quantity can be 'latent heat of vaporization' for liquid–vapor, or latent heat of fusion for ice–liquid, or latent heat of sublimation for ice–vapor. We can define a specific gas constant for the condensable species vapor as $R_c = R/M_c = k/m_c$, where M_c and m_c are its molar mass and molecular mass, respectively. By substituting for $\alpha_{vapor} = R_cT/e_s$ from the ideal gas law, we obtain the Clausius–Clapeyron equation:

$$\frac{de_s}{dT} = \frac{l_c e_s}{R_c T^2} \Rightarrow \frac{d(\ln e_s)}{dT} = \frac{l_c}{R_c T^2} \Rightarrow e_s(T)$$

$$= e_s(T_0)\exp\left(\int_{T_0}^{T}\frac{l_c}{R_c}\frac{dT}{T^2}\right) \approx e_s(T_0)\exp\left[\frac{l_c}{R_c}\left(\frac{1}{T_0} - \frac{1}{T}\right)\right]$$

[19]

Here, the last step makes the approximation that l_c does not change with temperature. Because exponents are additive,

eqn [19] shows $e_s \propto \exp(-m_c l_c/kT)$. Thus, SVP is a Boltzmann equation, which makes sense: the numerator $m_c l_c$ is the energy to free a molecule from its neighbors, while the denominator kT is the average molecular energy. For water vapor above liquid water, we use $T_0 = 273.15$ K, $e_s(T_0) = 611$ Pa, $R_c = 461$ J K^{-1} kg^{-1}, and latent heat of vaporization $l_c = 2.5 \times 10^6$ J kg^{-1}, finding that SVP roughly doubles for every 10 K temperature rise.

On some bodies, SVP is essential for understanding the bulk atmospheric gas. On Mars, for example, CO_2 condenses at the cold poles. A temperature of 148 K corresponds to an SVP of 6 mbar ($\sim$600 Pa) for CO_2, which is a typical air pressure on the surface of Mars (Leighton and Murray, 1966). Consequently, Mars's CO_2 ice caps are buffered at a temperature near 148 K. On Triton and Pluto, the atmospheric pressure is essentially the SVP of N_2 over N_2 ice at temperatures of 38 and $\sim$40 K, respectively (Brown and Ziegler, 1979; Lellouch et al., 2011; Zalucha et al., 2011).

The presence of even a minor condensable can change the lapse rate considerably, as water vapor does on Earth. Once condensation starts in a cooled, vertically displaced parcel of air, further condensation (into liquid or ice) reduces the rate of cooling by release of latent heat. An SALR, or moist adiabat, denoted Γ_{sa}, occurs when chilled moist air is held at saturation by the warming associated with continual condensation of vapor. This lapse rate is called the pseudoadiabatic lapse rate if condensates are assumed to fall out of the parcel because then the process is not reversible and adiabatic. However, saturated and pseudoadiabats tend to be similar because condensation products carry relatively little heat out of a parcel of air. The SALR can be derived as a function of temperature and saturation mass mixing ratio $\mu_{cms} = (m_c/\overline{m})f_c = \epsilon(e_s/p)$, where f_c is the volume mixing ratio of the condensable, p is the total pressure, and ϵ is the ratio of molecular masses. In this way, the SALR can be expressed as a modification of the adiabatic lapse rate, that is, $\Gamma_{sa} = \Gamma_a \times f(T, \mu_{cms})$ (e.g., see Andrews (2010), pp. 37–39). Formulations of the SALR for major constituent condensation are also possible (Ingersoll, 1969; Kasting, 1988, 1991).

Under saturated conditions, static stability is controlled by comparing the actual lapse rate to the saturated lapse rate, Γ_{sa}. Air is stable if $\Gamma < \Gamma_{sa}$. For example, on Earth, $\Gamma_{sa} \approx 4$ K km^{-1} in warm humid air near the ground, $\Gamma_{sa} \approx 6$–7 K km^{-1} in the middle troposphere, and Γ_{sa} is close to dry adiabatic in the cold, dry upper troposphere. In the Earth's tropics, observations show that moist convection controls static stability up to $\sim$0.4 bar (Zelinka and Hartmann, 2011).

A further nuance applies to giant planets, where the weight of saturated air parcels is greater than the dry atmosphere unlike the case for water-saturated parcels on Earth or methane-saturated parcels on Titan that tend to be buoyant. Ammonia and water on Jupiter and Saturn have greater molecular mass (17 and 18 g mol^{-1}, respectively) than the hydrogen–helium dry atmospheres (2.22 and 2.14 g mol^{-1}, respectively), and the same situation applies to methane on Uranus and Neptune. If the abundance of a condensable species drops faster in the environment with altitude than in a rising air parcel, the parcel will tend to be heavy relative to the environment and sink back downward. Consequently, convection on giant planets is favored when the relative humidity in the environment is high and

disfavored by a steep compositional gradient in the environment due to condensation. Temperature profiles on Uranus and Neptune are superadiabatic where methane condenses, which suggests that convection may be inhibited there (Guillot, 1995).

SVP also gives us a first-order understanding of clouds. Clouds will form on average where the mean pressure–temperature conditions reach the SVP for various condensables (Sanchez-Lavega et al., 2004) (**Figure 4**).

10.13.3 Radiation

10.13.3.1 Planetary Energy Balance, Blackbody Radiation, and the Greenhouse Effect

Physical and chemical processes in planetary atmospheres are driven by sources of free energy, meaning energy that can do useful work. For most planets, light from the parent star dominates free energy sources, although some giant planets have an internal energy flux that leaks to the exterior and is significant compared to the energy flux received from the parent star.

Consequently, for planetary atmospheres, the solar flux at the top of the atmosphere is a key parameter. Satellites measure the Earth's solar constant as $S_0 = 1360.8 \pm 0.5$ W m^{-2} (Kopp and Lean, 2011), consistent with ground-based inferences (Chapman et al., 2012). As a result, the solar flux at the top of the atmosphere averaged over the area of the whole Earth and over time is $S_0/4 \approx 340$ W m^{-2}. We divide S_0 by 2 to account for glancing angles on a spherical planet, and we divide it by 2 again because only one side of the Earth is in daylight. Alternatively, another way to understand the factor of $\frac{1}{4}$ is that the solar flux intercepted by a planet of radius R is equivalent to that on a projected disk of area πR^2. So, the $\frac{1}{4}$ factor represents the ratio of received flux on a disk to the whole planetary area $(\pi R^2/4\pi R^2)$ to get a global average in W m^{-2}.

A fraction of sunlight's incident power is reflected and scattered back to space, which, over all wavelengths, is called the Bond albedo A (or planetary albedo). For the solar system planets with atmospheres, A ranges from 0.25 for Mars to 0.76 for Venus (Moroz et al., 1985), the giant planets have $A \approx 0.3$, while for Earth, A is 0.3 (Trenberth et al., 2009). Thus, the solar flux absorbed by the Earth's surface and atmosphere is $(1-A) \times (S_0/4) = (1-0.3) \times (1361$ W m$^{-2}/4) \approx 238$ W m^{-2}.

An essential concept for understanding what happens to the energy on planets is blackbody radiation. All objects emit a spectrum of electromagnetic radiation based on their temperature (e.g., a molten lava emits visible light plus radiation extending into the IR), and for practical purposes, blackbody radiation can be simply considered as an idealized spectrum that depends only on the temperature of the emitting object. Temperature determines the flux of emitted radiation as a function of wavelength, and when the flux is summed over all wavelengths, the total flux depends only on temperature also. Historically, the blackbody concept originated in considering radiation within a closed cavity that had walls that perfectly absorbed and emitted radiation at all wavelengths. At equilibrium, the spectrum was found to be uniquely related to the cavity wall temperature T by the Planck function, $B(T)$:
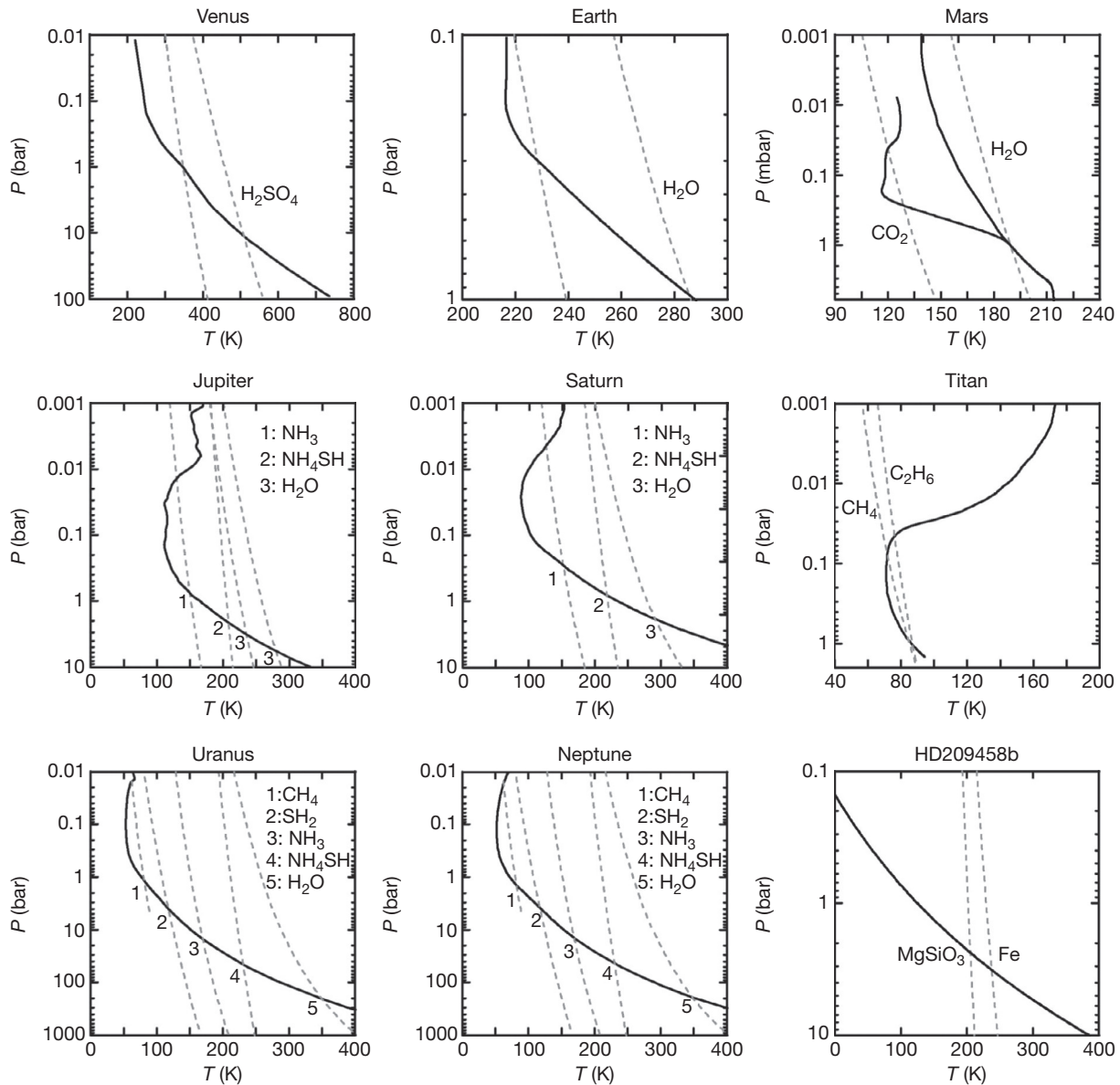
Figure 4 Use of the vapor pressure and saturation vapor pressure (SVP) for various condensables to predict cloud formation in solar system atmospheres and hot Jupiter HD209458b. The solid line is the vertical profile of pressure (p) versus temperature (T). For Mars, an annual average p-T profile is shown as well as a colder profile. The dashed lines are the saturation vapor pressure (SVP) curves for various condensable species, as indicated, assuming a fixed volume mixing ratio of condensable. It is assumed that particles condense when the partial pressure (e) reaches the saturation vapor pressure (e_s), that is, where $e = f_c p(T) e_s(T)$, where f_c is the volume mixing ratio of the condensable. Thus, the base of clouds is marked where a dashed line crosses the solid pressure–temperature profile. Below this level, the phase is vapor because the ambient air is too hot. Various mixing ratios are assumed to calculate the dashed curves as follows: Venus 2 ppm and 2000 ppm H_2SO_4 (where liquid clouds form); the Earth 250 ppm and 1.5% H_2O, giving rise to ice and liquid clouds, respectively; Mars 0.95 CO_2 and 300 ppm H_2O giving ice clouds; Jupiter 200 ppm NH_3, 36 pppm NH_4SH, 50 ppm H_2O, 0.17% H_2O giving solid phase clouds except for the higher water level; Saturn 200 ppm NH_3, 36 pppm NH_4SH, 0.17% H_2O, giving solid particles; Titan 5% CH_4, 10 ppm C_2H_6, giving solid particles; Uranus and Neptune 2% CH_4, 37 ppm SH_2, 200 ppm NH_3, 36 pppm NH_4SH, 0.17% H_2O, giving solid particles; and HD209458b 75 ppm $MgSiO_3$ and 68 ppm Fe, giving solid particles. Reprinted from Sanchez-Lavega A, Perez-Hoyos S, and Hueso R (2004) Clouds in planetary atmospheres: A useful application of the Clausius–Clapeyron equation. *American Journal of Physics* 72: 767–774.

$$B_v \, dv = \frac{2hv^3}{c^2} \frac{dv}{(e^{hv/kT} - 1)}, \quad B_\lambda \, d\lambda = \frac{2hc^2}{\lambda^5} \frac{d\lambda}{(e^{hc/\lambda kT} - 1)},$$

B_v in $Wm^{-2} Hz^{-1} sr^{-1}$; B_λ in $Wm^{-2} m^{-1} sr^{-1}$

$$B_{\tilde{v}} \, d\tilde{v} = 2hc^2 \frac{\tilde{v}^3 \, d\tilde{v}}{(e^{hc\tilde{v}/kT} - 1)} \qquad [20]$$

$B_{\tilde{v}}$ in $Wm^{-2} (cm^{-1})^{-1} sr^{-1}$

Here, $h = 6.626 \times 10^{-34}$ J s is Planck's constant and c is the speed of light, which is related to the frequency (v) and wavelength (λ) of radiation by $c = v\lambda$. The third expression in eqn [20] is in terms of wavenumber $\tilde{v} = 1/\lambda$, as used by some spectroscopists. Thus, each form of the Planck function in the preceding text applies when the spectrum is specified in units of frequency (Hz), wavelength (m), or wavenumber (usually cm^{-1}), respectively. In eqn [20], blackbody radiation $B_v(T)$ is a

radiance (or intensity), which is the power (W) per unit frequency (or wavelength or wave number) interval crossing unit area (m^{-2}) in unit solid angle (steradian^{-1} or sr^{-1}) in a given direction.

A flux density or irradiance (often shortened to just 'flux') has units of $Wm^{-2} Hz^{-1}$ (or $Wm^{-2} m^{-1}$ or $Wm^{-2} cm^{-1}$) and is the intensity integrated over all directions. In spherical polar coordinates, an elemental solid angle is $\sin\theta d\theta d\phi$ where θ is the angle from the polar axis and ϕ is the azimuthal angle. If the intensity B_v is isotropic (i.e., independent of θ), the flux over an entire hemisphere is π times B_v, as follows:

$$F_v = \int_0^{\phi=2\pi}\int_0^{\theta=2\pi} B_v \cos\theta \underbrace{\sin\theta\, d\theta}_{x} d\phi = 2\pi\int_0^{x=1} B_v x\, dx$$

$$= 2\pi B_v \left[\frac{x^2}{2}\right]_0^1 = \pi B_v \qquad [21]$$

The flux over all frequencies ($W\,m^{-2}$) is found by substituting for B_v (eqn [20]) in eqn [21] and integrating

$$F = \int_0^\infty \pi B_v\, dv = \frac{2\pi h}{c^2}\int_0^\infty \frac{v^2 dv}{(e^{hv/kT}-1)}$$

$$= \frac{2\pi k^4 T^4}{c^2 h^3}\underbrace{\int_0^\infty \frac{x^3 dx}{(e^x-1)}}_{\text{standard integral}=\pi^4/15} = \left(\frac{2\pi^5 k^4}{15 c^2 h^3}\right)T^4 \Rightarrow F = \sigma T^4 \quad [22]$$

Here, we substituted $x = hv/kT$ to obtain a standard integral. The final expression in eqn [22] is the Stefan–Boltzmann law with the Stefan–Boltzmann constant $\sigma = 5.67 \times 10^{-8}\,W\,m^{-2}\,K^{-4}$.

Blackbodies are ideal absorbers and emitters, and because planets are made of materials that absorb IR radiation strongly and reach thermal equilibrium, the spectrum that planets emit can be represented by a blackbody. Essentially, a planet absorbs visible sunlight, warms up, and radiates like a blackbody in the IR. When outgoing radiation balances incoming radiation along with an additional internal heat flux F_i (as occurs on the giant planets), the planet achieves an effective temperature T_e, that is, the equivalent blackbody temperature that characterizes the total flux output:

$$\underbrace{(1-A)\frac{S_p}{4}}_{\text{absorbed solar radiation}} + \underbrace{F_i}_{\text{internal heat flux}} = \underbrace{\sigma T_e^4}_{\text{outgoing IR radiation}},$$

$$\text{or } (1-A)\frac{S_p}{4} = \underbrace{\sigma T_{eq}^4}_{\text{outgoing IR radiation}} \quad \text{if } F_i \ll (1-A)\frac{S_p}{4} \quad [23]$$

Here, S_p is the solar flux at the orbital distance of the planet from the Sun. When the internal heat flux is negligible, the effective temperature is called the equilibrium temperature, T_{eq}, because there is equilibrium between incoming sunlight and outgoing IR. On Jupiter, F_i is $\sim 5.4\,W\,m^{-2}$ compared with $8.1\,W\,m^{-2}$ of absorbed sunlight (Hanel et al., 1981). For giant planets, sources of internal energy include gravitational energy released from formation and contraction as well as subsequent internal differentiation. However, unlike the other gas giants, Uranus has little internal heat flow ($42 \pm 47\,mW\,m^{-2}$ (Pearl

et al., 1990)), which is puzzling. For the Earth, $F_i \sim 0.09\,W\,m^2$ can be neglected, $S_p = 1361\,W\,m^{-2}$, and Bond albedo $A = 0.3$. Solving eqn [23] gives equilibrium temperature $T_{eq} = 255\,K$, which is also the Earth's effective temperature. Clearly, this temperature is not achieved at the surface, which has a mean temperature of 288 K. For planets with atmospheres, the difference between the surface temperature and effective temperature arises because of the greenhouse effect described in the succeeding text.

An idealized atmospheric level where Earth achieves its effective temperature can be estimated. The Earth's average tropospheric lapse rate is $\sim 6\,K\,km^{-1}$, so given the surface temperature of 288 K, the air temperature will be at 255 K at $\sim 5\,km$ altitude. This altitude is called the emission level, although it is somewhat fictitious because in reality, the atmosphere radiates to space from different levels as a function of wavelength, depending upon the IR transparency of the overlying air at that wavelength. Nonetheless, the Earth cannot buck conservation of energy, and in equilibrium, it must radiate a total flux back to space equivalent to a 255 K blackbody of the Stefan–Boltzmann law.

The greenhouse effect is when an atmosphere warms up and provides a flux of thermal IR radiation to the surface (or lower layers of giant planets) that adds to the shortwave solar flux. The surface of a rocky planet with an atmosphere is warmer than it would be without an atmosphere because the surface receives energy from both the Sun and the heated atmosphere. For specificity, the fraction of the total flux reaching the surface due to IR from the atmosphere is about 99.9%, 2/3, 1/3, and 9/10 for Venus, Earth, Mars, and Titan, respectively (Courtin et al., 1992). For rocky planets, the difference between T_{eq} and surface temperature T_s is another way to express the size of the greenhouse effect:

$$\Delta T_g \equiv T_s - T_{eq} \qquad [24]$$

For the Earth, $\Delta T_g = 288 - 255 = 33\,K$. Of course, this definition assumes that the albedo would be the same where the air removed – which it certainly would not – so ΔT_g should be viewed judiciously as a useful metric, a way to express the flux difference of about $150\,W\,m^{-2}$ between blackbodies at 255 and 288 K. Of course, slowly rotating airless bodies can have large day–night temperature differences, and so, the mean temperature will be different from the equilibrium temperature, as is well known (Pierrehumbert, 2010).

There are various greenhouse gases. In the Earth's modern clear sky atmosphere, water vapor contributes $\sim 60\%$ of ΔT_g, CO $\sim 25\%$, and ozone $\sim 8\%$, with the rest from CH_4, N_2O, anthropogenic chlorofluorocarbons (CFCs), and other trace gases (Karl and Trenberth, 2003; Stephens and Tjemkes, 1993). Importantly, water vapor condenses and exits the atmosphere as rain or snow, whereas the Earth's other main greenhouse gas, CO_2, does not condense. H_2O is effectively 'a slave' to the forcing by the concentration of CO_2. By forcing, we mean a persistent disturbance to the climate system that changes the energy balance. If CO_2 levels goes up, more water vapor enters a warmer atmosphere and increases the greenhouse effect. Thus, the climatic role of water vapor is a feedback rather than a forcing (Lacis et al., 2010, 2013). The bulk background gases that absorb very little IR, such as N_2 and O_2, are themselves

critical for the greenhouse effect because collisions of greenhouse gases (CO_2, H_2O, etc.) with N_2 or O_2 take away or add energy to the greenhouse gas molecules, which allows them to absorb over a much wider range of photon wavelengths. This process of pressure broadening (see Section 10.13.3.5) is fundamental to the greenhouse effect in thick atmospheres. On other bodies, rather than just trace gases, the bulk atmospheric gases are greenhouse gases. On all the giant planets, H_2 is the main source of IR opacity (see Section 10.13.3.5), on Titan, N_2, H_2, and CH_4 are important (McKay et al., 1991; Samuelson et al., 1981), while CO_2 is the key greenhouse gas on Venus (Bullock and Grinspoon, 2001; Titov et al., 2007) and Mars.

Clouds can cool a planet because of their contribution to the albedo, but they can also warm through adding to the greenhouse effect. For example, on Earth, icy cirrus clouds contribute to greenhouse warming since they are largely transparent to solar radiation but opaque to thermal IR, while low-lying marine stratus predominantly contributes to shortwave albedo. If we take clouds into account in our apportioning of the greenhouse effect on Earth, water vapor is responsible for ~50%, clouds ~25%, CO_2 ~20%, and other gases the remainder (Schmidt et al., 2010). Regarding their cooling effect, clouds contribute about half of the Earth's albedo of 0.3. According to satellite measurements, clouds reduce the Earth's absorbed radiation by -48 W m^{-2}, but enhance the greenhouse effect by $+30 \text{ W m}^{-2}$. So, overall, clouds cool the Earth by -18 W m^2 (Ramanathan and Inamdar, 2006). A hypothetical Earth without clouds would be far warmer (Goldblatt et al., 2013).

Like water vapor, clouds are a feedback and change in response to levels of CO_2 and other greenhouse gases. Feedbacks can alter the mean temperature of a planet in positive feedback (like the aforementioned water vapor feedback) or stabilize it in negative feedback. Another important positive feedback is the ice-albedo feedback. An increase in surface temperature causes a decrease in albedo from diminished snow and ice cover, which causes further warming, or the other way, cooling increases albedo with more snow and ice, causing further cooling. The ice-albedo feedback is crucial for understanding the Earth's ice ages during the last few million years (Lorius et al., 1990). Negative feedbacks include an increase in outgoing thermal IR as a planet warms up, operating on short timescales of weeks. Over geologic timescales, geochemical cycles act as negative feedbacks on the Earth's climate. The important one for Earth is the carbonate–silicate negative feedback, which acts over a timescale of ~0.5 My (Berner, 2004; Walker et al., 1981). If the climate warms, greater rainfall and temperatures consume atmospheric CO_2 in weathering reactions on the continents, which cools the Earth. If the climate cools, the consumption of CO_2 from dry air is slowed, and CO_2 accumulates due to volcanic emissions, which increases the greenhouse effect. On long times, negative feedbacks have evidently 'won' overall because the Earth has remained habitable since at least 3.5 Ga (Buick, 2007).

One further importance of blackbody theory is that it tells us the wavelength where most of the radiative energy is emitted from planets and stars. The Planck function is maximal where $\partial B_\lambda / \partial \lambda = 0$, which gives Wien's law:

$$\lambda_{\max} T = 2.897 \times 10^{-3} \text{ meters} \bullet K \qquad [25]$$

The Sun behaves like a blackbody because the ions and electrons inside the Sun are in thermal equilibrium. So, solar radiation has an effective temperature of 5780 K. Wien's law indicates peak emission at $\lambda_{\max} = (0.0029 \text{ m K})/(5780 \text{ K}) = 0.5 \,\mu\text{m}$, in the visible. The Earth is roughly 20 times cooler than the Sun's surface, and so, its Wien peak is 20 times larger at ~10 μm. Given typical temperatures, planets generally have their Wien peak at thermal IR wavelengths, which is where many atmospheric gases and aerosol particles absorb strongly.

Several atmospheres have windows, which are spectral intervals that are relatively transparent to thermal IR compared to high opacity at other wavelengths. A window can be a key means for a planet to radiate IR energy to space and cool. On Titan, a window at 16.5–25 μm is close to Titan's Wien peak of 31 μm. H_2, which is a minor constituent (~0.1%), absorbs weakly in this window (McKay et al., 1989). On Earth, the key atmospheric window of 8–12 μm encompasses the Wien peak at ~10 μm. Again, absorption by a minor constituent, water vapor, modulates the outgoing IR flux through the window. On Venus, dense CO_2 and clouds leaves only a few narrow windows in the near-IR. The significant ones are 1–1.2 μm in which only H_2O absorbs, 1.7 μm where CO and HCl absorb, and 2.2–2.5 μm where CO and SO_2 are seen (Crisp and Titov, 1997; Titov et al., 2007). These are wavelengths to peer relatively deep into Venus' atmosphere, which is otherwise opaque.

10.13.3.2 Radiative Transfer: Shortwave and Infrared

Atmospheres like the Earth's are transparent to incoming solar radiation but not entirely. The ozone in the Earth's stratosphere absorbs solar UV (0.2–0.4 μm) in the Hartley and Huggins bands, and ozone in both the stratosphere and troposphere absorbs visible light in the 0.4–0.85 μm Chappuis band. The Earth's tropospheric water vapor absorbs solar near-IR (1–4 μm region). A more extreme case is Titan's stratospheric methane and haze of aerosols, which absorb in the UV, visible, and near-IR (for methane) to such an extent that the reduction of solar flux reaching Titan's surface is called an antigreenhouse effect (McKay et al., 1989, 1991). Temporary antigreenhouse effects are also possible from debris raised in asteroid impacts (Pollack et al., 1983) or, on Earth, smoke created in nuclear war (Robock et al., 2007; Turco et al., 1983).

Radiative transfer restricted to the visible and UV is simpler than in the IR because the Planck function (eqn [20]) indicates that we can neglect visible or UV emission at temperatures typical of planetary surfaces and atmospheres. This is not true for IR calculations. The starting point in radiative transfer is the extinction law (or Beer–Lambert–Bouguer law). Experiments show that the loss of intensity of a beam of light of frequency v passing through a substance depends linearly on the incident intensity I_v and the elemental mass of absorbing or scattering material expressed as $\rho_a \, ds$, where ρ_a is the density of the absorber or scatterer (kg m^{-3}) and ds is the elemental path length:

$$dI_v = -k_v I_v \rho_a ds \Rightarrow I_v = I_{v0} \exp\left(-\int_0^s k_v \rho_a ds'\right) = I_{v0} e^{-\tau_v} \qquad [26]$$

Here, the proportionality constant k_v is the mass extinction coefficient (m^2 kg^{-1}) or opacity. In eqn [26], I_{v0} is the intensity at distance $s = 0$ and τ_v is a dimensionless optical path or

optical thickness along the beam direction. We usually define our optical path as increasing from the top of the atmosphere downward. In this geometry, we call τ_v the optical depth. In the case of a pencil beam inclined at zenith angle θ (from the vertical), the elemental path along the beam ds is related to that along the vertical path dz by geometry as $\cos\theta = dz/ds$. Replacing ds in eqn [26] by $dz/\cos\theta$ gives

$$I_v = I_{v0}e^{-\tau_v/\cos\theta} \Rightarrow \text{transmissivity } T_v = e^{-\tau_v/\cos\theta} \quad [27]$$

Here, the transmissivity (or transmittance) T_v is the ratio of light getting through (I_v) to the incident intensity (I_{v0}).

The visible optical depth can be large in planetary atmospheres. On Mars, the broadband visible optical depth in global dust storms reaches ~5 (Colburn et al., 1989; Kahn et al., 1992), which means that direct-beam sunlight is attenuated by a factor of $e^{-5} \approx 1/148$. On Titan's surface at 0.5 μm visible wavelength, the extinction optical depth is ~10 due to atmospheric haze (Tomasko and West, 2009). However, these surfaces are not dark because the total flux at the ground is the sum of a direct flux from the Sun's direction and a diffuse flux from the whole sky. The diffuse flux includes all scattered solar radiation from the sky, including scattered light from clouds or particles that is not in the direct beam. On Mars, for example, much light scattered by dust out of the direct solar beam reaches the ground diffusely (Haberle et al., 1993a). On Earth, when the sky is covered by dense cloud and the Sun cannot be seen, the ground is similarly well illuminated by a diffuse flux.

The extinction coefficient k_v considered in the preceding text is the sum of absorption and scattering due to gases or aerosols. We define the ratio of scattering to extinction as single scattering albedo ω_0,

$$k_v = \underbrace{a_v}_{\text{absorption coefficient}} + \underbrace{s_v}_{\text{scattering coefficent}}, \quad \omega_0 = \frac{s_v}{a_v + s_v} \quad [28]$$

The single scattering albedo is 1 for purely scattering media and <0.5 for strongly absorbing media. It is one of the three key parameters used to characterize optical properties of aerosols or cloud particles. The second is a volume absorption (or scattering) coefficient defined as $Q_{as}A_{xs}n$, where Q_{as} is a dimensionless absorption or scattering efficiency (when absorption and scattering are combined, Q_{as} can be redefined as an extinction efficiency), A_{xs} is the geometric cross section, and n is number density. Thus, we would write $dI_v = -I_vQ_{as}nA_{xs}ds$ in eqn [26]. For terrestrial cloud droplets, $Q_{as} \sim 2$ in the visible. The third parameter is the asymmetry factor g_s, a function that indicates whether scattering is isotropic ($g_s = 0$) or scatters in the forward ($0 < g_s \leq 1$) or backward ($-1 \leq g_s < 0$) direction. These parameters are used in models of scattering; for example, see Petty (2006).

Absorption of photons warms aerosols, causing them to heat atmospheres during daytime (e.g., dust on Mars (Pollack et al., 1979) or black carbon on Earth (Ramanathan and Carmichael, 2008)), while for gases, absorption can excite a molecule or atom into vibration or rotation or both. At high pressures, collisions generally occur before an excited atom or molecule undergoes radiative decay and emits a photon in a random direction, with the result that vibrational or rotational energy is converted into KE and heat, called thermalization or quenching. Absorption of EUV photons in the upper

atmosphere can instead create ions in photoionization or break molecules in photodissociation.

In contrast to absorption, scattering is when radiation is redirected out of the original direction of propagation as a result of interaction with aerosols or when radiative decay of a molecule emits a photon in a random direction, attenuating the direct beam. The type of scattering can be diagnosed from the size of a scatterer using a dimensionless size parameter, where r_p is the scatterer radius and λ is the wavelength of radiation,

$$x = \frac{2\pi r_p}{\lambda} \quad [29]$$

For gas molecules or particles with $x \ll 1$, the scattering of solar radiation is Rayleigh scattering, which is isotropic with a scattering efficiency $Q_s \propto \lambda^{-4}$, a strong wavelength dependence that causes the Earth's blue sky when convolved with the solar spectrum. Aerosols (dust, smoke, and cloud droplets) with $0.1 < x < 50$ scatter according to Mie scattering (for spherical particles), typically with forward scattering. Mie theory gives the electromagnetic field around a dielectric particle. Photons can be scattered into the beam and scattered out of the beam in multiple scattering by aerosols. Finally, for particles with $x > 50$, there is just geometric scattering, where $Q_s \approx 2$ and the scattering cross section grows in proportion to the cross-sectional area πr_p^2.

To deduce information about the atmospheric structure and composition, we frequently view an IR spectrum from a planet remotely. On Earth, satellite measurements show that our planet does not have the smooth idealized curve of the Planck function but has big 'dips' in the spectrum compared to a blackbody curve at ~320 K surface temperature (in the case of Figure 5(a)) because of absorption by key greenhouse gases. The bottom of the dips indicates the effective temperature of the emission where photons are emitted not from the surface but a cooler atmospheric level, for example, the bottom of the CO_2 band at 15 μm emits at about the tropopause temperature, while water vapor at 20 μm emits from around the mid-troposphere (Figure 5(b)). The area under the Planck curves gives the total power emitted, which is reduced by the area of the dips. Thus, in order to maintain equilibrium between solar flux received and planetary flux emitted, the surface temperature (which is seen in the atmospheric window at 8–12 μm) increases above a 255 K blackbody curve. Effectively, Figure 5(a) visualizes the Earth's greenhouse effect.

To make a quantitative sense of remote measurements such as those in Figure 5(a), we use the physics of IR radiative transfer. If we consider a monochromatic beam of radiance I_v [W m^{-2} Hz^{-1} sr^{-1}] passing through an elemental path ds, then the intensity change will be that emitted into the beam minus that extinguished by absorption or scattering:

$$dI_v(s) = \underbrace{(k_v\rho_a ds)J_v}_{\text{light scattered in or emitted}} - \underbrace{(k_v\rho_a ds)I_v}_{\text{extinction}} \Rightarrow \frac{dI_v}{k_v\rho_a ds} = J_v - I_v \quad [30]$$

Here, ρ_a is the density of the absorbing or scattering gas and J_v [W m^{-2} Hz^{-1} sr^{-1}] is a source function, which accounts for thermal emission or scattering into the beam. The term labeled 'extinction' uses the extinction law, eqn [26]. The final expression in eqn [30] is the general radiative transfer equation with
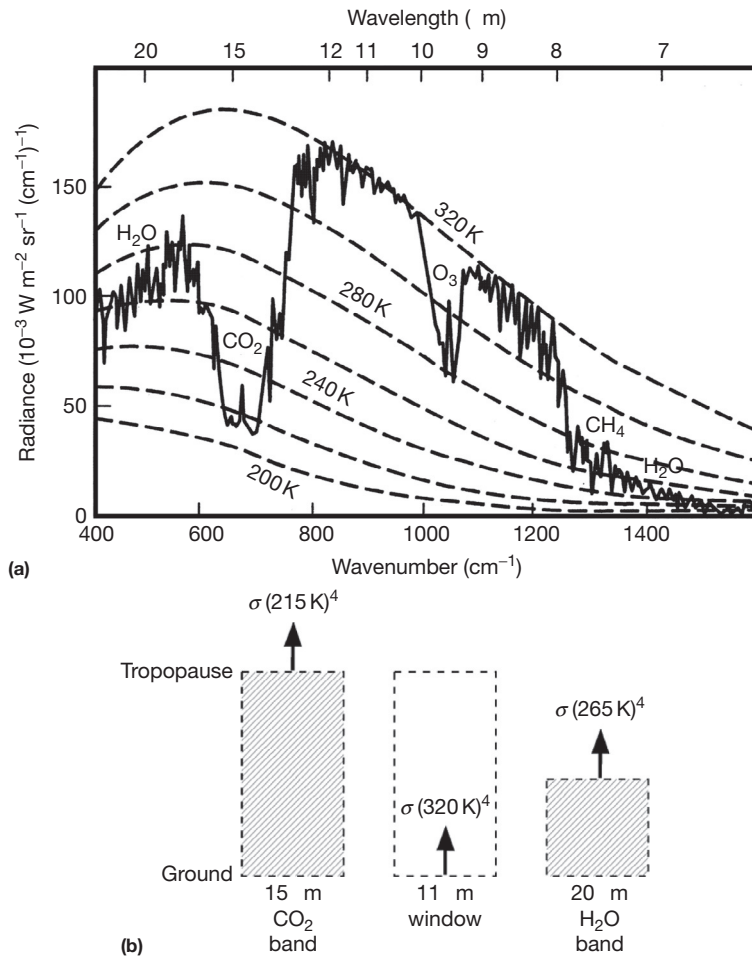
Figure 5 (a) The Planck function for noon over a vegetated region of the Niger Valley in N. Africa where the surface temperature is 320 K. Dashed lines show blackbody curves for particular temperatures (Adapted from Hanel RA, Conrath BJ, Kunde VG, et al. (1972) The Nimbus 4 infrared spectroscopy. Experiment, I: calibrated thermal emission spectra. *Journal of Geophysical Research* 77: 2629–2641). (b) A schematic diagram showing the meaning of parts of the curve in (a). The arrows indicate the layers in the atmosphere where blackbody fluxes originate, according to the Stefan–Boltzmann law. (Drawn by the author.)

no particular coordinate system or assumption about whether the source function behaves like a blackbody or not.

Next, we impose a coordinate system and assume that the medium is a blackbody, that is, a purely absorbing, non-scattering medium in thermal equilibrium with source function $J_v = B_v =$ the Planck function and k_v the mass absorption coefficient. Minus signs are confusing in radiative transfer due to different geometric conventions, so let us be clear that we now define our IR optical depth as measured downward along a path s, that is, τ is zero at an observer at $s = \infty$ and increases backward along the beam to some value τ inside the atmosphere. Thus,

$$\tau = \int_s^\infty k_v \rho_a ds = \int_{\tau=\tau}^{\tau=0} -d\tau, \quad \text{or} \quad \text{if } s \text{ is altitude:}$$

$$\tau = \int_z^\infty k_v \rho_a dz = \int_{\tau=\tau}^{\tau=0} -d\tau \qquad [31]$$

With these assumptions, the equation of radiative transfer becomes

$$\frac{dI_v(s)}{d\tau_v(s_1, s)} = I_v(s) - B_v(s) \qquad [32]$$

where the elemental optical path $d\tau$ is between distance s and some distance s_1. This is sometimes called Schwarzschild's equation after Karl Schwarzschild who first considered such a radiative transfer equation for the Sun's atmosphere in 1914. With a little work, a solution to eqn [32] can be found by multiplying by an integrating factor, $e^{-\tau_v(s_1, s)}$, integrating between 0 and s_1, and rewriting as

$$I_v(s_1) = I_{v0} e^{-\tau_v(s_1, 0)} + \int_0^{s_1} B_v(s) e^{-\tau_v(s_1, 0)} k_v \rho_a ds \qquad [33]$$

The first term is just the exponential attenuation of the emission from $s = 0$ to $s = s_1$. The second is the sum of the contributions from each point s along the path 0 to s_1, each exponentially attenuated by the path length to the observer.

Another useful form of the radiative transfer equation makes the plane-parallel approximation, that is, where pressure, temperature, and composition are assumed to be functions of height only. Then, if a beam of radiance I_v passes upward

through a layer of depth dz at an angle θ to the vertical, geometry gives $dz = ds \cos \theta = (ds)\mu$, defining the cosine of zenith angle as $\mu = \cos \theta$. Given our definition of optical depth (eqn [31]), the equation for radiative transfer in a plane-parallel atmosphere is a slight modification of eqn [32], as follows, where we return to generality by using J_v:

$$\mu \frac{dI_v}{d\tau_v} = I_v - J_v \qquad [34]$$

If we imagine looking down on a planet from some level in the atmosphere, we integrate eqn [34] from that level where the optical depth is τ to the surface where $\tau = \tau_*$. Given τ as a limit of integration, we use a dummy variable $\tau' - \tau$ in the integral for path lengths. To obtain the upward intensity at any level where the optical depth is τ, we multiply by an integrating factor $e^{-(\tau' - \tau)/\mu}$ and solve. Assuming that a v (frequency) subscript on τ is implicit, the solution for upward intensity is

$$I_v(\tau)^{\uparrow} = I_v(\tau_*)e^{-(\tau_* - \tau)/\mu} + \int_{\tau}^{\tau_*} J_v(\tau')e^{-(\tau' - \tau)/\mu}\frac{d\tau'}{\mu} \quad (1 \geq \mu > 0)$$

$$[35]$$

where the arrow superscript indicates upward. If we are looking down from space, we simply put $\tau = 0$ in the limit of integration, and the intensity observed at the satellite instrument is

$$I_v(\tau = 0)^{\uparrow} = \underbrace{I_v(\tau_*)e^{-\tau_*/\mu}}_{\text{surface contribution}} + \underbrace{\int_0^{\tau_*} J_v(\tau')e^{-\tau'/\mu}\frac{d\tau'}{\mu}}_{\text{contributions along the path}} \qquad [36]$$

Here, the first term is the extinction along the path from the ground to the spacecraft where $I_v(\tau_*)$ is the upward intensity at the ground. The second term is the upward emission contribution from points along the path to the spacecraft. Here, $J_v(\tau')$ corresponds to emission in the upward direction. The same expression can also be written in altitude coordinates but is more complicated:

$$I_v(z)^{\uparrow} = I_v(z = 0)e^{-\frac{1}{\mu}\int_0^z k_v(z')\rho_a(z')dz'}$$

$$+ \int_0^z k_v(z')\rho_a(z')J_v(z')e^{-\frac{1}{\mu}\int_0^z k_v\rho_a dz''}\frac{dz'}{\mu} \qquad [37]$$

We derive a hemispheric monochromatic flux F_v from the measured intensity I_v at a particular frequency v by integrating over a hemisphere. Then, we derive a total flux (W m^{-2}) by integrating over all frequencies. We will use eqn [37] in the succeeding text.

10.13.3.3 Optical Thickness and Thinness

Vertical sections of atmospheres are described as optically thick ($\tau_v \gg 1$) or optically thin ($\tau_v \ll 1$) to radiation of a particular frequency. 'Optically thick' just means opaque to a particular frequency or frequency band of radiation, and 'optically thin' means nearly transparent. This is a useful concept in looking at spectra such as **Figure 5(a)**. The IR photons can be thought of as 'escaping' from the level where the IR optical depth drops below ~ 1 and then passing up through overlying 'optically thin' or IR-transparent air to space. We can also apply the idea to incoming solar flux. Solar photons are mainly absorbed in the atmosphere near the level of unity optical depth for a

particular UV or visible wavelength. As a result, UV heating or ionization can occur at this level.

It is possible to justify the concept of absorption near $\tau_v \sim 1$ quantitatively for both solar and IR radiation. For solar radiation, we work with fluxes directly because of the typical lack of emission in atmospheres at solar frequencies. Within a planetary atmosphere at height z, the vertical component of direct flux crossing a surface parallel to the ground for a solar beam at zenith angle θ and frequency v can be deduced from the extinction law (eqn [27]) as

$$F_v = \mu F_{v\odot}e^{-\tau_v/\mu} \qquad [38]$$

The volume heating rate Q [W m^{-3} Hz^{-1}] is related to how this flux changes with altitude due to absorption by the expression, $Q = -(dF_{\text{net},v}/dz)$, where $F_{\text{net},v}$ is the net flux, that is, the upward minus the downward flux. With no upward solar flux, the heating rate is

$$Q = \frac{dF_v}{dz} = \frac{dF_v}{d\tau}\frac{d\tau_v}{dz} = \left(-\frac{1}{\mu}\mu F_{v\odot}e^{-\tau_v/\mu}\right)\underbrace{(-k_v\rho_v)}_{-k_v\rho_v} \quad Q \Rightarrow$$

$$= (k_v\rho_v F_{v\odot})e^{-\tau_v/\mu} \qquad [39]$$

Initially, the value of Q in eqn [39] increases downward as the term $k_v\rho_v$ in the curved brackets increases because τ_v is small at the top of the atmosphere and the exponential factor is near 1. Eventually, the optical depth becomes significant, so the term $\exp(-\tau_v/\mu)$ begins to dominate over the downward increase of $k_v\rho_v$, and Q begins to decrease exponentially downward toward zero. We deduce that Q has a single maximum at some altitude in between.

We find the maximum in Q by differentiating w.r.t. z, using the product rule and setting $dQ/dz = 0$

$$\frac{dQ}{dz} = 0 = \left(k_v\rho_v\right)\left(\cancel{F_{v\odot}e^{-\tau_v/}}\frac{(k_v\rho_v)}{\mu}\right) + \cancel{F_{v\odot}e^{-\tau_v/}}\frac{d(k_v\rho_v)}{dz}$$

$$[40]$$

$$\Rightarrow -\frac{d(k_v\rho_v)}{dz} = \frac{(k_v\rho_v)^2}{\mu} \Rightarrow \frac{d^2\tau_v}{dz^2} = \frac{1}{\mu}\left(\frac{d\tau_v}{dz}\right)^2$$

In the last step, we use $d\tau_v/dz = -k_v\rho_v$ from the definition of optical depth (eqn [31]). Because the density of absorbing gases usually drops exponentially with increasing height and the absorption coefficient is either constant or an approximate power law relationship with pressure, optical depth should vary approximately exponentially with altitude, that is, $\tau_v = \tau_{v0} \exp (z/H_\tau)$ where H_τ is a scale height for the optical depth. If this expression for τ_v is inserted into eqn [40], after a little manipulation, an important result is obtained that $dQ/dz = 0$ occurs where

$$\tau_v \sec \theta = 1, \quad \text{or} \quad \tau_v = 1 \quad \text{when zenith angle } \theta = 0 \qquad [41]$$

Thus, at any frequency, the maximum volume heating rate Q, or related effect such as dissociation or ionization, occurs where the optical depth is unity for normal incidence radiation. The altitude is higher by factor $\sec \theta$ for solar radiation incident at zenith angle θ. Also, the characteristic width of activity is $\sim H_\tau$. Such a vertical structure is called a 'Chapman layer'.

A similar insight about the importance of unity optical depth applies in the thermal IR for atmospheres that are

optically thick at depth, that is, when we cannot see the surface emission looking downward from space. In our expression for upward intensity from an atmosphere (eqn [37]), we neglect the first term due to surface radiation, extend the integral to the whole atmosphere, and assume blackbody emission. Then,

$$I_v(\infty)\uparrow \quad \sec\theta \int_0^\infty k_v\rho_a B_v \exp\left[-\sec\theta \int_z^\infty k_v\rho_a \mathrm{d}z'\right]\mathrm{d}z$$
$$\Rightarrow I_v(\infty)\uparrow \quad \sec\theta \int_0^\infty B_v W_v \mathrm{d}z \qquad [42]$$

where W_v is a weighting function, defined by

$$W_v(z) \equiv k_v(z)\rho_a(z)\exp\left[-\sec\theta\int_z^\infty k_v(z')\rho_a(z')\mathrm{d}z'\right] \qquad [43]$$

Equation [42] says that the radiance to space is a weighted vertical integral of the Planck function. The weighting function W_v is mathematically similar to heating rate Q in eqn [39]. Just like Q, function W_v is zero at the bottom of the atmosphere where the exponential reaches zero, W_v is zero at the top of the atmosphere where density is zero, and W_v has a maximum in between. As a result, the monochromatic IR radiance comes from a layer with characteristic thickness that is a scale height in optical depth or smaller and centered where optical depth has exactly the same $\tau_v \sim 1$ condition as eqn [41]. For frequencies with large $k_v\rho_a$ that are highly absorbing, the $\tau_v \sim 1$ peak of the weighting function W_v will be high up (large z), given that τ_v is the integral of $k_v\rho_a$ from z to ∞. This is seen in a planetary IR spectrum such as **Figure 5(a)** in dips where greenhouse gases absorb. The dependence of $I_v(\infty)\uparrow$ on gas composition and wavelength in eqn [42] is also how we deduce the temperature and chemical structure of planetary atmospheres using remote sensing, for example, from orbiters around other planets or ground-based telescopes.

10.13.3.4 Radiative–Convective Equilibrium

Combining the theory of convection (Section 10.13.2.4) and radiation (Sections 10.13.3.1–10.13.3.3) allows us to understand the average vertical structure of planetary atmospheres quantitatively given that it is primarily controlled by these processes.

A hypothetical atmospheric structure determined only by radiation balance (ignoring convection) will generate an unrealistic temperature profile in an IR-opaque troposphere with a steep temperature gradient that is actually unstable to convection. Conceptually, a temperature profile for purely radiative transfer for a stratosphere and upper troposphere has to be joined to a convective profile below with both continuities of temperature and flux. How do we calculate this? For analytic calculations, three approximations are made, as follows:

- The first is a gray approximation, where the thermal opacity of the atmosphere is assumed to be independent of wavelength and represented by a single, broadband value. 'Gray opacity' should be viewed as a fitting parameter to match an observed thermal structure. It rarely makes sense to laboriously compute gray opacities from spectral averaging, and it is a misconception to consider gray opacities as 'real' properties of atmospheres, given that the real opacity is wavelength-sensitive. Instead, a gray optical property gives

a characterization of an atmosphere that is useful for semi-quantitative comparison of planetary atmospheres.
- The second is that the diffuse approximation is implemented. This replaces radiances I and B in Schwarzschild's radiative transfer equation with fluxes, with the optical depth scaled by a factor D, called the diffusivity factor to account for the integration of the radiances over a hemisphere. A value of $D = 1.66$ is close to numerical results (Armstrong, 1968; Rodgers and Walshaw, 1966) and equivalent to assuming an average zenith angle of 53°, that is, $1/\mu = \sec\theta = 1.66$, in eqn [34]. Others set $D = 3/2$ (Goody and Yung, 1989; Weaver and Ramanathan, 1995) or $D = 2$.
- The third simplification is to handle thermal IR with a two-stream approximation, in which upward (F^+) and downward (F^-) fluxes are treated separately.

Radiative–convective equations are easiest to formulate with optical depth τ as the vertical coordinate but can be converted into physical space using a relationship between τ and pressure. In a plane-parallel atmosphere, Schwarzschild's equation (eqn [34]) for the upwelling and downwelling thermal radiative fluxes (F^+ and F^-, respectively) can be written as

$$\frac{\mathrm{d}F^+}{\mathrm{d}\tau} = D(F^+ - \pi B), \quad \frac{\mathrm{d}F^-}{\mathrm{d}\tau} = -D(F^- - \pi B);$$
$$\text{where } \pi B(\tau) = \sigma T^4(\tau) \qquad [44]$$

Equation [44] allows calculation of upwelling and downwelling thermal fluxes if $T(\tau)$ is specified. The net thermal flux is $F_{\text{net}} = F^+ - F^-$. Subtracting $\mathrm{d}F^-/\mathrm{d}\tau$ from $\mathrm{d}F^*/\mathrm{d}\tau$ in eqn [44], we get

$$\frac{\mathrm{d}F_{\text{net}}}{\mathrm{d}\tau} = D(F^+ + F^- - 2\pi B) \qquad [45]$$

and differentiating w. r. t. τ gives

$$\frac{\mathrm{d}^2 F_{\text{net}}}{\mathrm{d}\tau^2} = D\left(\underbrace{\frac{\mathrm{d}(F^+ + F^-)}{\mathrm{d}\tau}}_{DF_{\text{net}}} - 2\pi\frac{\mathrm{d}B}{\mathrm{d}\tau}\right) \Rightarrow \frac{\mathrm{d}^2 F_{\text{net}}}{\mathrm{d}\tau^2} - D^2 F_{\text{net}} = -2\pi D\frac{\mathrm{d}B}{\mathrm{d}\tau}$$

$$[46]$$

In the last step, addition of $\mathrm{d}F^-/\mathrm{d}\tau$ and $\mathrm{d}F^+/\mathrm{d}\tau$ from eqn [44] gives $\mathrm{d}(F^+ + F^-)/\mathrm{d}\tau = DF_{\text{net}}$. Equation [46] can be solved for blackbody radiance $B(\tau)$ and the atmospheric temperature profile using the Stefan–Boltzmann law if $F_{\text{net}}(\tau)$ and a boundary condition are known.

Boundary conditions involve the solar flux. In the solar system, atmospheres absorb solar radiation in the troposphere or at the surface and partly in stratospheres. The latter often leads to stratospheric temperature inversions (Figure 2), while absorption in troposphere can stabilize upper troposphere against convection, as happens on Titan. Exponential attenuation is a reasonable approximation for solar radiation, so the net absorbed stellar flux $F_{\text{net}}^\odot$ can be written as (Robinson and Catling, 2012)

$$F_{\text{net}}^\odot(\tau) = \underbrace{F_{\text{net}}^\odot e^{-k_{\text{tropo}}\tau}}_{\text{tropospheric (and surface) solar absorption}} + \underbrace{F_{\text{strato}}^\odot e^{-k_{\text{stratio}}\tau}}_{\text{stratospheric solar absorption}}$$

$$[47]$$

Here, $F_{\text{strato}}^\odot$ and $F_{\text{tropo}}^\odot$ are the top-of-atmosphere net absorbed stellar fluxes in the stratosphere and troposphere (including

the surface for planets with surfaces), respectively. Parameters $k_{strato} = \tau_{sws}/\tau$ and $k_{tropo} = \tau_{swt}/\tau$ control the attenuation of solar flux in two channels, where τ_{sws} and τ_{swt} are shortwave optical depths and τ is the gray thermal IR optical depth. At the top of the atmosphere, where $\tau = 0$, the net absorbed stellar flux must be (eqn [23])

$$F_{net}^{\odot}(\tau = 0) = (1 - A)\frac{F^{\odot}}{4} \qquad [48]$$

where A is the planet's Bond albedo and $F^{\odot}$ is the solar flux incident at the top of the atmosphere. The overall energy balance at any atmospheric level is between the net thermal flux with the absorbed stellar flux and any internal energy flux, F_i from a planet's interior (relevant for giant planets):

$$F_{net}(\tau) = F_{net}^{\odot}(\tau) + F_i \qquad [49]$$

By combining eqn [47] with eqn [49] and inserting into eqn [46], we obtain

$$\frac{d\sigma T^4}{d\tau} = \frac{1}{2D}\left[\left(D^2 - k_{tropo}^2\right)F_{tropo}^{\odot}e^{-k_{tropo}\tau}\right.$$
$$\left. + \left(D^2 - k_{strato}^2\right)F_{strato}^{\odot}e^{-k_{strato}\tau} + D^2 F_i\right] \qquad [50]$$

which integrates to

$$\sigma T^4(\tau) = \sigma T^4(0) + \frac{1}{2D}\left[\frac{D^2 - k_{tropo}^2}{k_{tropo}}\left(1 - e^{-k_{tropo}\tau}\right)F_{tropo}^{\odot}\right.$$
$$\left. + \frac{D^2 - k_{strato}^2}{k_{strato}}\left(1 - e^{-k_{strato}\tau}\right)F_{strato}^{\odot} + D^2 F_i\tau\right] \qquad [51]$$

The flux at the top of the atmosphere in this equation ($\sigma T^4(0)$) can be eliminated by applying the boundary condition that there is no downwelling thermal radiation at the top of the atmosphere where $\tau = 0$. We first use the definition $F_{net} = F^+ - F^-$ to rewrite eqn [45] as

$$\frac{dF_{net}}{d\tau} = D\left(F_{net} + 2F^- - 2\sigma T^4\right) \qquad [52]$$

and, second, we solve for σT^4 using eqns [49] and [47]:

$$\sigma T^4(\tau) = F^-(\tau)$$
$$+ \frac{1}{2}\left[\frac{D + k_{tropo}}{D}F_{tropo}^{\odot}e^{-k_{tropo}\tau} + \frac{D + k_{strato}}{D}F_{strato}^{\odot}e^{-k_{strato}\tau} + F_i\right]$$
$$\qquad [53]$$

Third, inserting $\tau = 0$, and noting that $F^-(0)$ is zero, gives $\sigma T^4(0)$. Inserting $\sigma T^4(0)$ into eqn [51] gives a final expression for the temperature profile in the radiative part of a gray atmosphere that sits above a radiative–convective boundary and extends into the stratosphere:

$$\sigma T^4(\tau) = \frac{F_{strato}^{\odot}}{2}\left[1 + \frac{D}{k_{strato}} + \left(\frac{k_{strato}}{D} - \frac{D}{k_{strato}}\right)e^{-k_{strato}\tau}\right]$$
$$+ \frac{F_{tropo}^{\odot}}{2}\left[1 + \frac{D}{k_{tropo}} + \left(\frac{k_{tropo}}{D} - \frac{D}{k_{tropo}}\right)e^{-k_{tropo}\tau}\right] + \frac{F_i}{2}(1 + D\tau)$$
$$\qquad [54]$$

If there are no internal heat ($F_i = 0$) and no solar attenuation (the limit $k_{strato} = k_{tropo} \to 0$, applying l'Hôpital's

rule), eqn [54] reduces to $\sigma T^4(\tau) = (F_{net}^{\odot}(0)/2)(1 + D\tau)$, which is a common form for simple radiative models in textbooks (e.g., Andrews (2010), p. 85; Goody and Yung (1989), p. 392). Using $\sigma T^4(\tau)$ in eqn [54], the downwelling flux can also be deduced from eqn [53] and the upwelling flux from a similar expression.

We can now ask: what is required for an atmosphere to have a strong stratospheric temperature inversion and thus a well-developed tropopause minimum? The minimum occurs in the radiative regime, and we can simplify eqn [54] by omitting terms in tropospheric shortwave attenuation, that is, $k_{tropo} \ll 1$, which is the case for real atmospheres. Then, setting the derivative w.r.t. τ of the resulting expression to zero, the optical depth of the tropopause minimum is (Robinson and Catling, 2014)

$$\tau_{tp} = \underbrace{\frac{1}{k_{strato}}}_{-1/100} \ln\left[\underbrace{\frac{F_{strato}^{\odot}}{F_{tropo}^{\odot} + F_i}}_{\sim 1/10}\underbrace{\left(\frac{k_{strato}^2}{D^2} - 1\right)}_{\sim 10^3}\right] \qquad [55]$$
$$\underbrace{}_{\sim 5}$$

The numbers given under parts of eqn [55] are typical averages for the Earth, Titan, and the giant planets, which all have stratospheres and tropopause minima (Table 4). Using these numbers, the gray IR optical depth where the tropopause minimum occurs is $\tau_{tp} \sim 0.05$. This optical depth depends on $F_{strato}^{\odot}/(F_{tropo}^{\odot} + F_i)$, which is the ratio of the stratospheric absorbed flux relative to that from below and $k_{stratio}$, which is the ratio of shortwave optical depth to IR optical depth in the stratosphere. Equation [55] only makes mathematical sense if

$$k_{strato}^2 > D^2\left[1 + \left(F_{tropo}^{\odot} + F_i\right)/F_{strato}^{\odot}\right] \qquad [56]$$

which sets a threshold condition on k_{strato} for a tropopause minimum or, alternatively, the condition for a stratospheric temperature inversion. It tells us that to have a stratospheric inversion, an atmosphere has to have a large k_{strato}, that is, a strong shortwave absorber with a shortwave optical depth that dominates over the IR opacity; otherwise, cooling to space by the IR-active molecules cancels shortwave heating of a stratosphere. Typical flux ratios in the planets of the solar system in eqn [56] mean that k_{strato} must be $\sim 10^2$ for a well-developed tropopause minimum.

The condition for a stratospheric inversion (eqn [56]) is satisfied by some planets but not by others depending on stratospheric composition and the balance of shortwave absorption to IR cooling (Table 5). The Earth's stratospheric ozone absorbs strongly in the UV, so k_{strato} is large and heating is not overwhelmed by emission by CO_2 at 15 μm, water vapor, or ozone at 9.6 μm. Consequently, the Earth has a stratospheric inversion. In contrast, CO_2 in the atmospheres of Mars and Venus does not absorb strongly in the visible or solar near-IR; instead, in the upper atmosphere, the 15 μm band of CO_2 radiates heat to space efficiently. Thus, k_{strato} is too small for stratospheric inversions in the global average on Mars and Venus. On the giant planets, dark stratospheric aerosols absorb in the UV and visible, while methane has many

Table 4 Solar absorption and infrared properties of gray radiative–convective parameters for the Earth, Titan, and the giant planets

Parameter	World					
	Earth	Jupiter	Saturn	Titan	Uranus	Neptune
P_{ref} [bar]	1	1	1	1.5	1	1
T_0 [K]	288	166	135	94	76	72
α_c	0.6	0.85	0.94	0.77	0.83	0.87
$F_{strato}^{\odot}$ [W m^{-2}]	7	1.3	0.41	1.49	0.24	0.09
$F_{tropo}^{\odot}$ [W m^{-2}]	233	7.0	2.04	1.12	0.41	0.18
F_i [W m^{-2}]	Minor, 0.087	5.4	2.01	Minor	Minor, 0.042 ± 0.047	0.43
k_{strato}	90	90	180	120	220	580
k_{tropo}	0.16	0.06	0.03	0.20	0.08	0.20
τ_{rc}	0.15	0.34	0.44	4.4	0.62	0.41
τ_0	1.9	6.3	9.2	5.6^a	8.7	3.0
τ_{tp}	0.050	0.064	0.040	0.077	0.042	0.017
p_{tp} [bar] (model)	0.16	0.10	0.066	0.18	0.070	0.075
p_{tp} [bar] (observed)	0.16	0.14	0.08	0.2	0.11	0.1

^{a}For Titan, $\tau_0 = 2.5$ at $p = 1$ bar.

Parameters inferred from measurements include a tropospheric reference pressure (P_{ref}) and temperature (T_{ref}), an empirical adjustment factor applied to the dry adiabat to account for volatile condensation (α_c) (eqn [59]), an internal energy flux (F_i), and the solar flux absorbed in the stratosphere ($F_{strato}^{\odot}$) and troposphere ($F_{tropo}^{\odot}$). For rocky bodies, $F_{tropo}^{\odot}$ includes surface absorption. For example, the Earth has $F_{strato}^{\odot} + F_{tropo}^{\odot} = 240$ W/m^2, the global mean absorbed solar flux. Parameters that control solar energy attenuation in the stratosphere and troposphere are $K_{strato} = \tau_{sws}/\tau$ and $K_{tropo} = \tau_{swt}/\tau$, where τ_{sws} and τ_{swt} are shortwave optical depths and τ is the gray thermal IR optical depth at any atmospheric level (eqn [47]). The gray IR optical depths at the reference pressure, radiative–convective boundary, and tropopause are τ_0, τ_{rc} and τ_{tp}, respectively. A comparison of τ_0 values shows that IR optical depth is somewhat larger on the giant planets than the Earth or Titan. Also, Titan has the largest fraction of solar radiation absorbed in its stratosphere.

Source: Robinson TD and Catling DC (2014) Common 0.1 bar tropopause in thick atmospheres set by pressure-dependent infrared transparency *Nature Geoscience* 7: 12–15.

Table 5 Molecules that dominate stratospheric shortwave heating and infrared cooling in atmospheres of the solar system

Planet	Stratospheric heating	Stratospheric cooling
Oxidizing stratospheres		
Venus	Unknown absorber (UV), CO_2, sulfur-bearing aerosols	CO_2, sulfur-bearing aerosols
Earth	Ozone	CO_2, water vapor, ozone
Mars	CO_2	CO_2
Reducing stratospheres		
Jupiter	Aerosols (UV/vis), CH_4 (NIR)	H_2–H_2 and H_2–He CIA continuum, acetylene (C_2H_2), ethane (C_2H_6), methane
Saturn	Aerosols (UV/vis), CH_4 (NIR)	H_2–H_2 and H_2–He CIA continuum, acetylene (C_2H_2), ethane (C_2H_6), methane
Titan	Haze, CH_4 (NIR)	Acetylene (C_2H_2), ethane (C_2H_6), haze
Uranus	Aerosols (UV/vis), CH_4 (NIR)	H_2–H_2 and H_2–He CIA continuum, acetylene (C_2H_2), ethane (C_2H_6), methane
Neptune	Aerosols (UV/vis), CH_4 (NIR)	H_2–H_2 and H_2–He CIA continuum, acetylene (C_2H_2), ethane (C_2H_6), methane

CIA, collision-induced absorption.

absorption bands in solar near-IR. A collision-induced absorption (CIA) continuum of H_2–H_2 and H_2–He and thermal IR emission bands of acetylene (C_2H_2, 13.7 µm) and ethane (C_2H_6, 12.1 µm) and methane (7.6 µm) cool these stratospheres inefficiently (Yelle et al., 2001; Zhang et al., 2013). Overall, k_{strato} is large, and all the giant planets have stratospheric inversions. On Titan, a thick stratospheric haze absorbs visible and UV radiation, along with stratospheric absorption in the near-IR by methane. The results are a large k_{strato} and a pronounced stratospheric inversion.

The aforementioned is radiation only; the other part of the radiative–convective problem to consider is the convective regime. Equation [14] describes a dry adiabat, which we can rewrite as temperature as a function of pressure,

$$T = T_{ref}\left(\frac{p}{p_{ref}}\right)^{\overline{R}/c_p} \Rightarrow T = T_{ref}\left(\frac{p}{p_{ref}}\right)^{(c_p - c_v)/c_p} \Rightarrow T = T_{ref}\left(\frac{p}{p_{ref}}\right)^{(\gamma-1)/\gamma}$$ [57]

Here, T_{ref} is a reference temperature at a reference pressure p_{ref} (e.g., 1 bar), while γ is the ratio of specific heats c_p/c_v. Kinetic theory relates γ to the degrees of freedom, N_{dof}, for the primary atmospheric constituent(s), where

$$\gamma = 1 + \frac{2}{N_{dof}}$$ [58]

For atmospheres of linear diatomic gases, such as N_2–O_2 (Earth), H_2 (giant planets), or N_2 (Titan), the molecules have

3 translational and 2 rotational degrees of freedom, so that $N_{dof} = 5$ and $\gamma = 7/5 = 1.4$. For CO_2-dominated atmospheres (Venus and Mars), there are 3 translational, 2 rotational, and ~ 0.3 vibrational degrees of freedom, so $N_{dof} = 6.3$ and $\gamma = 1.3$ (Bent, 1965). With these γ values, a tropospheric temperature T is proportional to $p^{0.3}$ and $p^{0.2}$ for diatomic and triatomic planetary atmospheres, respectively. However, no observed troposphere follows a dry adiabat because condensables release latent heat and lower the lapse rate. Following Robinson and Catling (2012), a semiempirical approximation adjusts the convective tropospheric temperature structure as follows:

$$T = T_{ref} \left(\frac{p}{p_{ref}} \right)^{\alpha_c (\gamma - 1)/\gamma} \qquad [59]$$

where α_c is a dimensionless constant, ~ 0.6–0.9 for planets in the solar system, representing the average ratio of the observed lapse rate to dry adiabatic lapse rate in the planet's convective regime.

Equation [59] gives temperature as a function of pressure in the convective regime, whereas eqn [54] gives temperature as a function of optical depth in the radiative regime, so how is optical depth related to pressure? The gray differential optical depth, $d\tau$, across an elemental layer of vertical thickness dz is the sum of various contributions from N_a sources of opacity, such as absorbing gases:

$$d\tau = -\sum_{i=1}^{N_a} k_i \rho_i dz = -\sum_{i=1}^{N} k_i \underbrace{\mu_i \quad \rho}_{\mu_i \rho} dz \Rightarrow d\tau = \sum_{i=1}^{N} k_i \mu_i \frac{dp}{g}$$

$$= \sum_{i=1}^{N} k_i(p_{ref}) \mu_i(p_{ref}) \left(\frac{p}{p_{ref}} \right)^{a_i + b_i} \frac{dp}{g} \qquad [60]$$

Here, k_i is the mass absorption coefficient for absorber i, which generally depends on pressure and temperature, while $\rho_i = \mu_i \rho$ is the corresponding density of the ith absorber, where μ_i is the mass mixing ratio (eqn [4]). In the second step, we substitute for the hydrostatic eqn [5]. In the last step, we use the fact that the profiles of μ_i and k_i are generally power laws of pressure:

$$\mu_i(p) = \mu_i(p_{ref}) \left(\frac{p}{p_{ref}} \right)^{a_i}, \quad k_i(p) = k_i(p_{ref}) \left(\frac{p}{p_{ref}} \right)^{b_i} \qquad [61]$$

Water vapor is the main source of opacity in the Earth's atmosphere, whereas in other atmospheres, gases have similar pressure dependence of opacity and mass mixing ratio, such as N_2 and CH_4 on Titan. Furthermore, the sum over $k_i \mu_i$ in eqn [60] could be replaced with a single weighted-mean absorption coefficient k. Thus, we can integrate and normalize eqn [60] to get a power law dependence of optical depth on pressure, where the power is $n_p = a + b + 1$,

$$dt \propto \left(\frac{p}{p_{ref}} \right)^{a+b} dp \Rightarrow \tau = \tau_0 \left(\frac{p}{p_{ref}} \right)^{a+b+1}, \text{ or } \tau = \tau_0 \left(\frac{p}{p_{ref}} \right)^{n_p} \qquad [62]$$

Here, τ_0 is the gray IR optical depth at reference pressure p_{ref}, such as 1 bar. In troposphere and lower stratospheres, often a well-mixed gas ($a = 0$) with an absorption coefficient linearly dependent on pressure ($b = 1$) occurs, such as H_2 in giant-planet atmospheres. In that case, $n_p = 2$. The Earth's

atmosphere is complicated, with a 8–12 μm window, a steep ($n_p = 4$–5) τ–p scaling for the 6.3 μm water absorption band and water bands beyond about 20 μm, and an $n_p = 2$ scaling for the 15 μm CO_2 band. But it turns out that $n_p = 2$ is a good approximation for troposphere and lower stratosphere for all the planets with thick atmospheres in the solar system, validated by comparison of numerical calculations (Robinson and Catling, 2012, 2014).

An $n_p = 2$ power law in eqn [62] also has a physical basis. The primary absorption processes that cause IR opacity in thick troposphere are pressure broadening and CIA (see Section 10.13.3.5). Because both processes rely on collisions, they tend to have an absorption coefficient $k_i \propto p$, so by integration of $d\tau \propto p$, it follows that $\tau \propto p^2$.

With an opacity–pressure power law scaling of eqn [62], we can rewrite our tropospheric convective profile with opacity as the vertical coordinate instead of pressure:

$$T = T_{ref} \left(\frac{\tau}{\tau_0} \right)^{\alpha_c (\gamma - 1)/n_p \gamma} = T_{ref} \left(\frac{\tau}{\tau_0} \right)^{\beta/n_p} \qquad [63]$$

This equation can be inserted into Schwarzschild's differential equation that describes the upwelling thermal radiative flux (eqn [44]) to give a differential equation in $dF^+/d\tau$, which can be solved (see the Appendix of Robinson and Catling (2012)) to give an analytic solution for the convective upwelling flux below the radiative–convective boundary in a gray troposphere:

$$F^+(\tau) = \underbrace{\sigma T_{ref}^4 e^{-D(\tau_0 - \tau)}}_{\text{attenuated upwelling flux from } \tau_0 \text{ level}}$$

$$+ \underbrace{\frac{\sigma T_{ref}^4 e^{D\tau}}{(D\tau_0)^{4\beta/n_p}} \left(\Gamma_u \left(1 + \frac{4\beta}{n_p}, D\tau \right) - \Gamma_u \left(1 + \frac{4\beta}{n_p}, D\tau_0 \right) \right)}_{\text{flux contribution from atmosphere above the reference level}}$$

$$[64]$$

Here, Γ_u is an upper incomplete gamma function, which is a mathematical function defined by

$$\Gamma_u(a, x) \equiv \int_x^\infty t^{a-1} e^{-t} dt \qquad [65]$$

Although this looks complicated, from a practical perspective, the incomplete gamma function is evaluated as simply as a sine or cosine in computer programs, such as MATLAB, IDL, or Python. Thus, the thermal flux in eqn [64] can be instantly computed as a function of optical depth, if input parameters (n_p, β) and variables (T_0, τ_0) are specified.

In the preceding text, we have written analytic equations that govern radiative–convective equilibrium in planetary atmospheres with the gray approximation. The temperature follows a convective profile according to eqn [63] up to a radiative–convective boundary, where the temperature then obeys eqn [54] according to radiative equilibrium. There will be a tropopause temperature minimum above the radiative–convective boundary at an IR optical depth given by eqn [55] if the stratospheric shortwave absorption is large compared to IR opacity, that is, the condition of large k_{strato} in eqn [56]. Figure 6(a) is a schematic profile

that shows a purely radiative–convective equilibrium for an atmosphere without a stratospheric shortwave absorber. The temperature asymptotes to an isothermal stratosphere with a so-called skin temperature. The skin temperature is given by eqn [53] with $\tau = 0$, no downward thermal flux, and no solar atmospheric absorption. If we also neglect the internal heat flux, we get

$$\sigma T_{skin}^4 = \frac{F_{tropo}^{\circ} + F_{strato}^{\circ} + F_i'}{2} \Rightarrow T_{skin}^4 = \frac{(\text{absorbed solar flux})}{2\sigma}$$

$$= \frac{\sigma T_e^4}{2\sigma} \qquad \Rightarrow T_{skin} = \frac{T_e}{2^{1/4}}$$
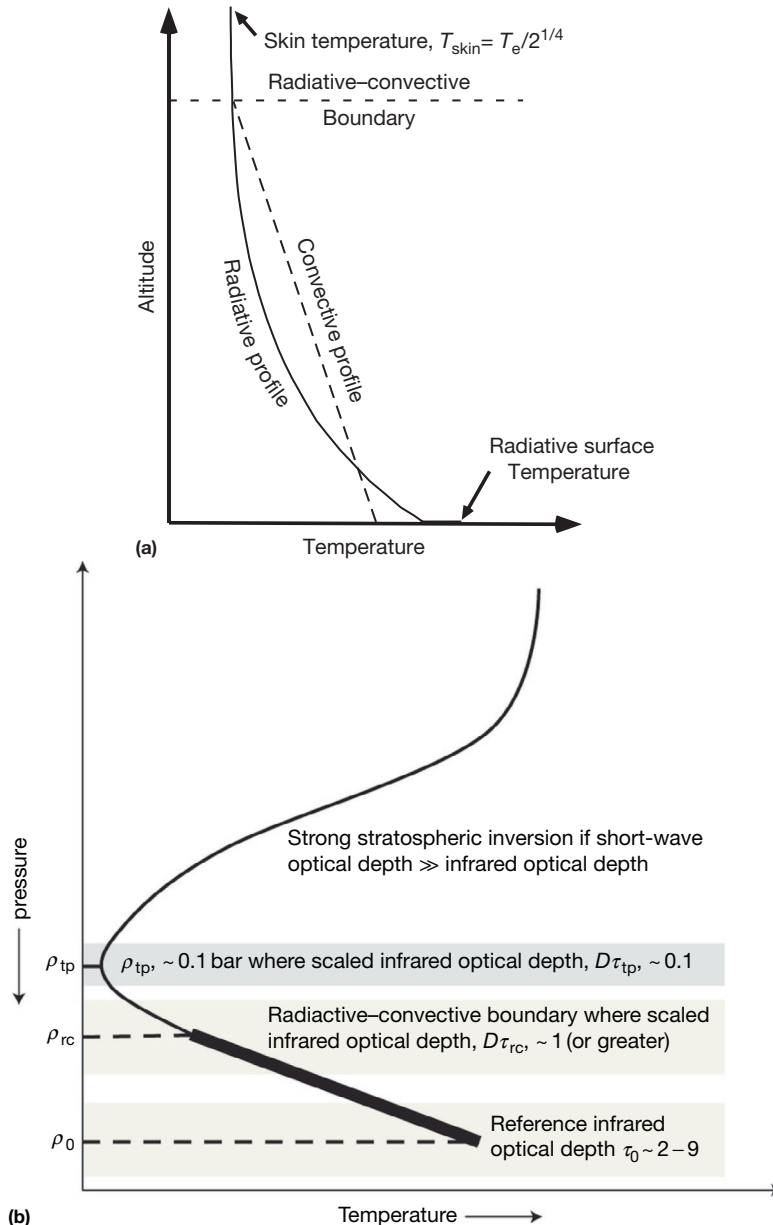
[66]

Figure 6   (a) A schematic profile of a radiative–convective equilibrium for an atmosphere without a shortwave absorber. A purely radiative profile (solid line) is unphysical. It is unstable to convection and has a discontinuity at the surface, so turbulence ensues and an adiabatic (i.e., convective) profile (dashed line) is established. The convective profile intersects the radiative profile at a level called a radiative–convective boundary with continuity of net flux and temperature. Without a stratospheric inversion, there is no tropopause minimum. In the absence of significant internal heat from the planet, the temperature asymptotes at altitude to a skin temperature that is a simple function of the effective temperature T_e, as shown. In our solar system, this schematic radiative–convective profile is roughly representative of the global mean profile of Venus. (b) A more general radiative–convective equilibrium profile where a strong shortwave stratospheric absorber is present. The conditions for the stratospheric inversion, tropopause minimum, and typical IR optical depths are shown (applicable for the Earth, Titan, and the giant planets). D is the diffusivity factor (see text). Reproduced from Robinson TD and Catling DC (2014) Common 0.1 bar tropopause in thick atmospheres set by pressure-dependent infrared transparency. *Nature Geoscience* 7: 12–15.

where T_e is the effective temperature. Thus, the skin temperature of an Earth-like world without the properties that give it a stratospheric inversion would be $255\ K/2^{1/4}$, which is 214 K. Although simple, the skin temperature actually gives a rough estimate for the tropopause minimum temperature; on Earth, the observed global mean tropopause temperature is 208 K (Han et al., 2011). **Figure 6(b)** shows a schematic for the more general case for an atmosphere with a stratospheric inversion.

Of course, gray radiation is an approximation, and numerical nongray calculations are required to replicate the details of atmospheres, for example, Goody and Yung (1989), p. 404–407; Thomas and Stamnes (1999), p. 450–453; and Satoh (2004), p. 380–383. Such models were first pioneered for the Earth by Manabe and coworkers (**Figure 7**) (Manabe and Strickler, 1964; Manabe and Wetherald, 1967). Since then, radiative and radiative–convective models have been applied to Venus (Bullock and Grinspoon, 2001; Crisp, 1986, 1989; Meadows and Crisp, 1996), Mars (Kasting, 1991; Marinova et al., 2005), Jupiter and Saturn (Appleby and Hogan, 1984), Uranus and Neptune (Appleby, 1986), Titan (McKay et al., 1991, 1999), and exoplanets (Heng et al., 2012; Robinson and Catling, 2012).

10.13.3.5 Absorption and Emission by Atmospheric Gases

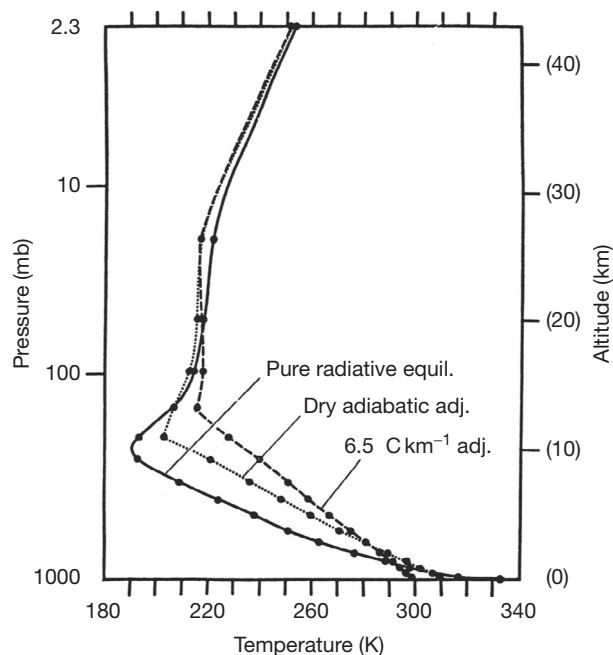In the previous subsection, we implicitly assumed that some gases absorb or scatter radiation at certain wavelengths

Figure 7 Results from radiative transfer modeling for the Earth that includes the effects of stratospheric ozone that causes a temperature inversion above a tropopause minimum. Three models are shown: purely radiative equilibrium, radiative–convective equilibrium with a dry adiabat, and radiative–convective equilibrium with a typical adiabat modified by water vapor. Reprinted from Manabe S and Strickler RF (1964) Thermal equilibrium of the atmosphere with a convective adjustment. *Journal of Atmospheric Sciences* 21: 361–385, with permission from the American Meteorological Society.

(described as optically *or* radiatively active gases), whereas others do not (optically inactive). Why this is so involves an understanding of molecular spectroscopy.

In a spectrum from a planetary atmosphere, we see discrete lines, groups of lines called bands, windows of weak spectral absorption, and a continuum of smoother varying absorption. Our starting point recognizes that the total internal energy of a gas molecule can be written as

$$E_{total} = E_{electronic} + E_{vibrational} + E_{rotational} + E_{translational} \qquad [67]$$

where $E_{electronic}$ is the energy associated electron orbits and other terms represent vibrational energy, rotational KE, and translational KE, respectively. Molecular collisions depend on temperature through $E_{translational}$ and redistribute energy between the various forms (if the air is dense enough) to establish local thermodynamic equilibrium where a local volume behaves like a blackbody. This was the assumption in the radiative transfer discussed in **Sections 10.13.3.3** and **10.13.3.4**.

A photon can be absorbed if its energy is close to a quantized energy jump within a molecule or it can be scattered by changing phase or direction. Transitions in rotational speed require less energy than vibrational ones, while electronic transitions require the most. Planck's law for photon energy, $E = h\nu = hc/\lambda$, indicates that types of transition correspond to general wavelength ranges (**Table 6**). However, absorption often occurs as combinations of transitions, such as rotational and vibrational.

An electric dipole moment due to separated positive charge and negative charge determines whether a molecule undergoes certain rotational or vibrational transitions. For example, the slight positive charge on hydrogen relative to oxygen in H_2O produces an electric dipole moment. The electric field in electromagnetic radiation torques the electric dipole and induces rotation. Isolated homoatomic molecules such as H_2 do not possess electric dipoles but dipoles can be induced by collisions. CH_4 and CO_2 also have no electric dipoles, but their bonds can bend, allowing a temporary electric dipole with associated rotational–vibrational transitions.

Some molecules possess a magnetic dipole moment. The magnetic field in an electromagnetic wave can torque a molecule with a magnetic dipole moment into rotation, analogous to a torqued needle on a compass. Many molecules do not have significant magnetic moments because electrons of opposite spin pair up. O_2 notably has two unpaired electrons and a magnetic dipole, which allows rotational bands in the microwave. In fact, satellite sensing of microwave emission from O_2 measures the Earth's atmospheric temperature over broad altitudes according to instrument weighting functions like those discussed in **Section 10.13.3.2** (Shine et al., 2008; Yang et al., 2013).

Table 6   Typical wavelength ranges of molecular transitions

Dominant transition	Wavelength range	Band
Electronic	$<1\ \mu m$	X-ray to UV to visible
Vibration	$1–20\ \mu m$	Near-IR to far-IR
Rotation	$>20\ \mu m$	Far-IR to microwave[a]

[a]H_2 can have rotational transitions at shorter wavelengths in warm, dense atmospheres (Wordsworth and Pierrehumbert, 2013).
IR, infrared; UV, ultraviolet.

For IR opacity and climate, the most important transitions are vibrational and rotational, so we discuss these next.

10.13.3.5.1   Rotational transitions

Rotating molecules have a rotational frequency that is quantized analogous to a household fan spinning at set speeds. A molecule's rotational KE is $^{1}/_{2}I\omega^2$, where I is the moment of inertia. In general, there are three principal moments of inertia about three axes of symmetry through the center of mass of a molecule, denoted l_A, l_B, and l_C from smallest to largest. However, in many simple molecules, some moments of inertia are equivalent or zero. For example, the axis through the atoms of CO_2, a linear molecule ($O=C=O$), has $l_A \approx 0$, while the moments of inertia around two perpendicular axes are equal and can be designated as l. In quantum theory, the quantized total rotational angular momentum L, associated with a so-called linear rotor such as CO_2, is

$$L = \frac{h}{2\pi}\sqrt{J(J+1)} \tag{68}$$

where $J = 0, 1, 2, \ldots$ is the rotational quantum number. The rotational KE for number J is

$$E_J = \frac{1}{2}I\omega^2 = \frac{(I\omega)^2}{2I} = \frac{L^2}{2I} = \frac{h^2}{8\pi^2 I}(J(J+1)) = hB(J(J+1)) \quad \text{where } B$$

$$= \frac{h}{8\pi^2 I} = \text{rotational constant}$$

Only transitions between adjacent states J and $J+1$ are allowed, giving an energy change,

$$\Delta E = hB[(J+1)(J+2) - J(J+1)] = hB[J^2 + 3J + 2 - J^2 - J]$$

$$= 2hB(J+1)$$

Thus, the photon frequency needed to cause a rotational transition in a linear rotor is

$$\nu = \frac{\Delta E}{h} = 2B(J+1) \tag{69}$$

Consequently, a pure rotational absorption spectrum has a series of lines separated by frequency differences $\Delta\nu = 2B$. As a molecule rotates with increasing J, centrifugal force causes bonds to stretch, which requires a more complex treatment. Also, similar expressions can be derived for more molecules with many moments of inertia.

10.13.3.5.2   Vibrational transitions

Molecular bonds behave like springs, so a diatomic molecule has a classical simple harmonic resonant frequency ν_0. In quantum mechanics, however, the oscillation frequency and associated energy levels of a diatomic molecule are quantized as

$$\nu = \left(v + \frac{1}{2}\right)\nu_0, \quad E_v = h\nu_0\left(v + \frac{1}{2}\right)$$

where the letter 'vee,' $v = 0, 1, 2,\ldots$, is a vibrational quantum number. The $v = 0$ state has a finite zero point energy, $E_0 = h\nu_0/2$, and a transition from this state to the next highest, or vice versa, is the fundamental, which typically produces the strongest line because at atmospheric temperatures and pressures, most molecules are in the ground state. Large displacements of atoms in molecules corresponding to $\Delta v = \pm 2, \pm 3, \ldots$ produce less intense overtones.

The frequency of combined vibrational and rotational transitions is slightly lower or higher than the pure vibration. Consequently, rotational–vibrational spectra have lines on either side of a pure vibrational frequency. The *P branch* is the low-frequency side corresponding to changes $\Delta J = -1$, while the *R branch* is the higher-frequency side with $\Delta J = +1$. The central frequency line with $\Delta J = 0$ is called the *Q branch*, which may not exist if quantum mechanics requires $\Delta J \neq 0$. Lines in the *P* and *R* branches are labeled according to the initial rotational quantum number J, that is, R(0), R(1),..., and P(0), P(1), etc. Superposed $\Delta J = -2$ or $+2$ electric quadrupole transitions can also occur. Instead of a PQR branch structure, there are the *O branch* ($\Delta J = -2$) and *S branch* ($\Delta J = +2$). Giant-planet atmospheres have electric quadrupole absorption lines of H_2 in the far-IR, for example.

Vibrational bands of CO_2 are important on Venus, Earth, and Mars. The bending of CO_2 produces a 15 µm rotation–vibration band – actually a PQR branch structure but individual lines are hidden by pressure broadening (see the succeeding text). The 4.3 µm asymmetrical stretch CO_2 band is important on Venus for absorbing a large amount of outgoing IR at depth because of Venus's high temperature. A vibration–rotation band of methane at 7.6 µm contributes IR opacity in the Earth's atmosphere but appears in emission in spectra of the giant planets and Titan due to warm CH_4-containing stratospheres.

10.13.3.5.3   Collision-induced absorption

Homoatomic molecules such as H_2 or N_2 lack permanent electric dipoles, but collisions at high-pressure distort the electronic structure and produce a temporary electric dipole, allowing vibrational and rotational transitions (Trafton, 1966; Trafton et al., 1998). CIA in various pairs of molecules creates significant IR continuum opacity in several planetary atmospheres: H_2–H_2 and H_2–He on the giant planets, N_2–N_2 and N_2–CH_4 in Titan's atmosphere (McKay et al., 1989), and CO_2–CO_2 on Venus (Moskalenko et al., 1979) or the early Earth (Kasting and Ackerman, 1986; Wordsworth et al., 2010). As first noted by Sagan (1977) H_2–N_2 and H_2–CO_2 CIA may have been important on prebiotic Earth (Wordsworth and Pierrehumbert, 2013) and early Mars (Ramirez et al., 2014). At Earth-like temperatures, H_2 is a strong greenhouse gas because its small moment of inertia causes widely spaced rotational energy levels (eqn [69]) that absorb across the thermal IR.

10.13.3.5.4   Broadening

Broadening processes are critical for planetary climates because otherwise, IR absorption lines would be delta-functions with negligible climatic effect. The three processes are the following:

- *Natural broadening*, in which a finite time for absorption or emission causes energy and frequencies to spread by Heisenberg's uncertainty principle. Apart from the UV, this broadening is tiny compared to the other two processes in the succeeding text.
- *Doppler broadening*, where random motion of molecules relative to the radiation source causes absorption and emission at frequencies that are Doppler-shifted relative to the

rest position of a line. This broadening tends to dominate in upper stratospheres and higher.

- *Pressure (or collisional) broadening*, where collisions add or remove energy during radiative transitions allowing emission or absorption over a broader range of photon energies. Pressure broadening is a key source of IR opacity in tropospheres (Section 10.13.3.4).

Pressure broadening produces a characteristic line shape called the *Lorenz profile* allowing absorption and emission far from the line center (Petty, 2006). A key property is that pressure-broadened lines have a width linearly proportional to pressure (i.e., the mass absorption coefficient relationship $k_v \propto p$, as assumed in Section 10.13.3.4 for tropospheres) unlike Doppler broadened lines, but both Doppler line broadening and pressure line broadening depend on temperature.

10.13.3.5.5   *Continuum*

A CIA continuum for giant planets and Titan was mentioned in the preceding text. For Earth, weak continuum absorption from 12.5 to 8 µm is mainly due to water vapor with absorption coefficient proportional to the square of the water vapor density. This absorption may be caused by the distant wings of very many lines in the far-IR or by dimers ($H_2O \cdot H_2O$), trimers, and polymers of H_2O molecules, but the problem is not fully resolved. At shorter wavelengths, continuum absorption arises from well-known processes, including photoionization and photodissociation.

10.13.3.5.6   *Numerical radiative transfer*

Although gray models like those in Section 10.13.3.4 are indispensable for intuitive understanding, numerical radiative transfer calculations are needed for realism, which deal with hundreds of lines that often overlap. Line-by-line calculations explicitly sum the effects of all the contributions of individual lines. This accurate method is very computationally demanding for climate models. Consequently, two more practical approaches have been developed (Goody and Yung, 1989; Liou, 2002; Petty, 2006; Thomas and Stamnes, 1999; Vardavas and Taylor, 2007):

- *Band models* use an analytic form for the positions and strengths of lines. Over a spectral interval, lines can be represented by a mean line strength and spread in a random distribution or by some other spacing that is amenable to analytic formulation.
- The *correlated k-distribution method* is a statistical representation of the apparently haphazard variation of absorption coefficients k_v over spectral interval Δv with a smooth cumulative probability function of the occurrence of k_v. Within Δv, the Planck function can be considered a function of temperature without frequency dependence. The order in which the k_v's are summed then does not matter. In this way, integration can be done using bigger spectral intervals than in the detailed line-by-line spectrum.

Line-by-line calculations validate the aforementioned two methods and constrain the region of parameter space where the inherent assumptions are valid.

10.13.4   **Photochemistry**

10.13.4.1   **Basic Principles of Chemical Kinetics**

Clearly, through molecular properties like those discussed in the preceding text, atmospheric composition sets and controls planetary climates and atmospheric structures. But what sets composition? The concentration of any gas is determined by chemical kinetics, that is, a competition between source and sink fluxes, which depends on reaction rates. In general, atmospheres are never in chemical equilibrium because of the free energy from sunlight (or starlight for exoplanets), as well as interior or tidal energy fluxes. However, giant-planet atmospheres that convect air to pressurized, hot interiors, where reactions are efficient, are far closer to chemical equilibrium than shallower atmospheres on rocky planets such as the Earth or Mars. One can think of chemical equilibrium as telling you what 'should happen' if everything fully reacted, whereas kinetics determines what actually happens according to the speed of reactions. Thus, the starting point for atmospheric chemistry is to consider reaction rates. Then, we consider other principles before discussing specific planetary atmospheres.

A general two body reaction can be written as

$$bB + cC \rightarrow gG + hH \qquad [70]$$

The number of reactions per unit volume and unit time is given by the reaction rate,

$$R_r = k_r n_B{}^m n_c{}^n \qquad [71]$$

where n_i is number density (molecules cm^{-3}) of species i. Here, the exponents are related to the order of the reaction $m + n$ and are determined experimentally. A rate coefficient or rate constant k_r is established in the lab by mixing reactants and measuring reaction rates. The units of k_r depend on the order of the reaction and the concentration units. If $m = 1$ and $n = 0$, the reaction would be first order with k_r in units of s^{-1}; if $m = n = 1$, the reaction would be second order with k_r in units of cm^3 molecule^{-1} s^{-1}; and so on. The rates of change of species are related:

$$\frac{dn_B}{dt} = -b \times \text{rate} = -bR_r, \quad \frac{dn_G}{dt} = gR_r, \text{ etc., so}$$
$$-\frac{1}{b}\frac{dn_B}{dt} = -\frac{1}{c}\frac{dn_C}{dt} = \frac{1}{g}\frac{dn_G}{dt} = \frac{1}{h}\frac{dn_H}{dt} \qquad [72]$$

We can consider an example, oxidation of methane by a hydroxyl (OH) species:

$$OH + CH_4 \rightarrow CH_3 + H_2O \qquad [73]$$
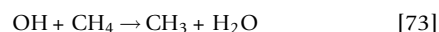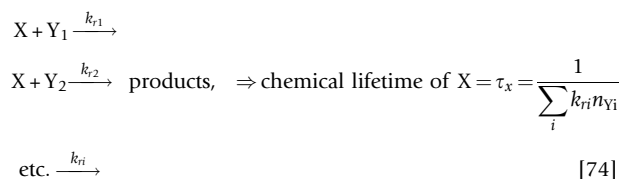
The Earth's troposphere has concentrations $n_{OH} \sim 8 \times 10^5$ molecules cm^{-3} and $n_{CH_4} \sim 4.3 \times 10^{13}$ molecules cm^{-3}, while an average tropospheric rate constant for eqn [73] is $k_{r\,CH_4} = 3.6 \times 10^{-15}$ cm^3 molecule^{-1} s^{-1}. The units indicate a first-order reaction. By applying eqn [71], we can estimate the chemical lifetime of CH_4, that is, the average time a CH_4 molecule spends in the atmosphere before destruction:

$$\tau_{CH_4} = \frac{n_{CH_4}}{\text{destruction rate}} = \frac{n_{CH_4}}{k_{r\,CH_4} n_{OH} n_{CH_4}}$$
$$= \frac{1}{(3.6 \times 10^{s-15} \text{cm}^{-3} \text{molecules}^{-1})(8 \times 10^5 \text{cm}^{-3})}$$
$$\sim 12 \text{ years}$$

Thus, methane would be removed rapidly without resupply. Methane attains a nonnegligible abundance of ~ 1.8 ppmv in the Earth's present atmosphere because of a significant source flux: ~ 80–90% is from the Earth's microbial biosphere, and the rest is from geothermal sources (Kirschke et al., 2013). On Mars – with another oxidizing atmosphere – the lifetime of methane is ~ 300 years (Lefevre and Forget, 2009; Zahnle et al., 2011), so methane sources are very limited or nonexistent given in situ measurements of <1 ppbv CH_4 (Webster et al., 2013).

Generally, we deduce that a lifetime is related to chemical sinks as follows:

$$X + Y_1 \xrightarrow{k_{r1}}$$

$$X + Y_2 \xrightarrow{k_{r2}} \text{ products, } \Rightarrow \text{chemical lifetime of } X = \tau_x = \frac{1}{\sum_i k_{ri} n_{Yi}}$$

$$\text{etc. } \xrightarrow{k_{ri}} \tag{74}$$

Three-body (termolecular) reactions are also important in planetary atmospheres, for example, the formation of ozone (O_3) in the Earth's stratosphere from $O + O_2 + $ a third body. When two gases, A and B, combine, bond formation releases energy that must be removed to prevent the *adduct* (the form AB) from splitting. A third body 'M' takes away the energy, where 'M' represents any atmospheric gas, usually the most abundant one:

$$A + B + M \rightarrow AB + M \tag{75}$$

Because a third body is needed, termolecular reactions are pressure-dependent up to a high-pressure limit, where the exact concentration of M no longer matters. Also, termolecular reactions are usually faster at lower temperatures because the molecules approach each other at slower speeds.

More generally, rate constants have an Arrhenius dependence on thermal energy kT, as
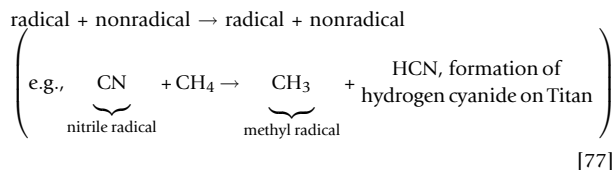
$$k_r = A \exp(-E_a/kT) \tag{76}$$

where a pre-exponential factor A and activation energy E_a are determined experimentally. A few useful rules are the following: (i) Reactions between molecules and radicals (species with unpaired electrons, see Section 10.13.4.2) usually have positive E_a so that k_r increases with temperature. (ii) Fast reactions between two radicals generally have negative activation energy E_a so that k_r decreases with temperature. (iii) Reactions between nonradical molecules are normally very slow unless they react on particle surfaces. (iv) Favored reactions tend to be exothermic.

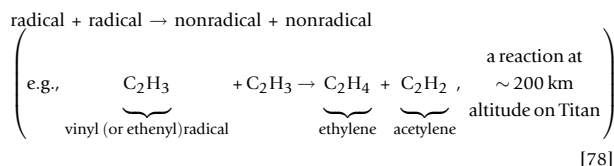### 10.13.4.2   Why Free Radicals Are So Important

Appreciably fast atmospheric reactions, with few exceptions, involve at least one radical species. A free radical has an unpaired electron in its outer shell (e.g., atomic chlorine, Cl) and reacts strongly to obtain more stable bonding. An exception is ground-state atomic oxygen (O), a biradical that has eight electrons of which two are unpaired. Some literature indicates radicals with dots, for example, $HO\cdot$.

Photochemistry is initiated by the Sun, loosely analogous to the spark plugs of an engine. Photons break up molecules
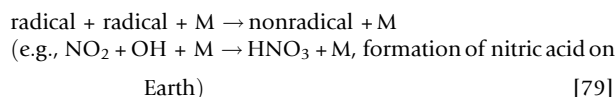
(Section 10.13.4.3), creating radicals that transmit the free energy. Reactions of radicals with nonradical molecules make further radicals because electrons do not pair up, that is,

radical + nonradical $\rightarrow$ radical + nonradical

$$\left(\text{e.g., } \underbrace{CN}_{\text{nitrile radical}} + CH_4 \rightarrow \underbrace{CH_3}_{\text{methyl radical}} + \begin{array}{l} \text{HCN, formation of} \\ \text{hydrogen cyanide on Titan} \end{array} \right) \tag{77}$$

However, radical–radical reactions remove radicals in two ways: disproportionation into nonradicals

radical + radical $\rightarrow$ nonradical + nonradical

$$\left(\text{e.g., } \underbrace{C_2H_3}_{\text{vinyl (or ethenyl) radical}} + C_2H_3 \rightarrow \underbrace{C_2H_4}_{\text{ethylene}} + \underbrace{C_2H_2}_{\text{acetylene}}, \begin{array}{l} \text{a reaction at} \\ \sim 200 \text{ km} \\ \text{altitude on Titan} \end{array} \right) \tag{78}$$

and recombination with the formation of a single molecule

radical + radical + M $\rightarrow$ nonradical + M
(e.g., $NO_2 + OH + M \rightarrow HNO_3 + M$, formation of nitric acid on

$$\text{Earth}) \tag{79}$$

By removing radicals, a chain of photochemical reactions initiated by sunlight is terminated. The net effect of all reactions is polymerization in reducing atmospheres, which can produce particles of hydrocarbons, sulfur, phosphorus, and so on, depending on the gas mixture, while in oxidizing atmospheres, the outcome is analogous to combustion, for example, full oxidation of CH_4 to water and CO_2 or oxidation of sulfur gases to sulfate aerosols (Hu et al., 2012, 2013).

Certain gas species can also be lost to planetary surfaces. 'Dry deposition' is interception with the surface and loss without the aid of precipitation, although the surface could be wet or dry. 'Wet deposition' is when raindrops, snow, or cloud or fog particles scavenge gases to the surface. For example, nitric acid formed in eqn [79] is dry-deposited onto the driest desert on Earth, the Atacama Desert (Catling et al., 2010; Michalski et al., 2004), whereas elsewhere, it usually dissolves in rain that falls to the surface. Deposition is how atmospheric chemistry can alter the geochemistry of a planetary surface. For example, the surface of Mars has accumulated sulfate salts that formed in its atmosphere from the oxidation of volcanic sulfur (Settle, 1979; Smith et al., 2014).

10.13.4.3   Photolysis

If species A is photolyzed, its number density n_A (molecules cm^{-3}) declines with a photodissociation rate,

$$A + h\nu \rightarrow \text{products, } \text{rate} = \frac{\partial n_A}{\partial t} = -j_A n_A \tag{80}$$

where j_A is the photolysis rate (or photodissociation) coefficient (s^{-1}). The probability Ψ_i per second for a molecule i to absorb radiation is related to j_i, as follows:
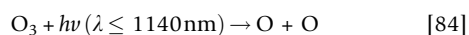
$$\Psi_i = \int_\lambda \sigma_{i\lambda} I_\lambda d\lambda \ \ s^{-1}, \ \ j_i = \int_\lambda q_{i\lambda} \sigma_{i\lambda} I_\lambda d\lambda \ \ s^{-1} \tag{81}$$

Here, $\sigma_{i\lambda}$ is the absorption cross section for species i (usually cm^2 molecule^{-1}), and $l_\lambda d\lambda$ is the photon flux crossing 1 cm^2 in spectral interval λ to $\lambda + d\lambda$. Absorption of a photon may sometimes lead to a different process (collisional deactivation, radiation, or breaking of a different bond), so $q_{i\lambda}$ is a dimensionless quantum yield for the photodissociation of interest.

### 10.13.4.4 Earth's Atmospheric Composition and Chemistry

With the principles in the preceding text, we can understand the Earth's atmosphere. The two key constituents responsible for its chemical character are very large amounts of O_2 and H_2O vapor compared with any other known atmosphere. The oxidizing chemistry caused by radicals associated with O_2 and H_2O is critical for radiative transfer because it renders the Earth's troposphere largely transparent to visible sunlight. At the same time, O_2 causes the creation of the ozone layer, shielding the Earth's surface from biologically harmful UV radiation with wavelengths less than about 300 nm.

In the stratosphere, the basic scheme for making O_3 from the O atoms of O_2 was deduced by Sydney Chapman in 1930 with the so-called Chapman reactions:

$$O_2 + h\nu (\lambda \leq 242\,nm) \quad O + O \quad \rightarrow \qquad [82]$$

$$O + O_2 + M \rightarrow O_3 + M \qquad [83]$$

$$O_3 + h\nu (\lambda \leq 1140\,nm) \rightarrow O + O \qquad [84]$$

$$O_3 + O \rightarrow 2O_2 \qquad [85]$$

Energy absorbed in ozone photolysis (eqn [84]) heats the stratosphere, causing its temperature inversion. O atoms derived from ozone photolysis cycle around to reform ozone via eqn [83]. But O_3 and O (the so-called odd oxygen species) return to stable O_2 molecules via eqn [85].

Chapman's scheme overpredicted the abundance of stratospheric O_3 compared to observations. In the 1970s, it was realized that minor constituents catalyze the removal of odd oxygen,

$$\begin{array}{c} X + O_3 \rightarrow XO + O_2 \\ \underline{XO + O \rightarrow X + O_2} \\ O_3 + O \rightarrow O_2 + O_2 \end{array} \qquad [86]$$
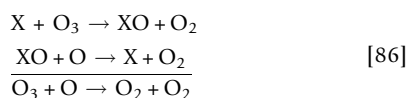
where X is a radical: NO, OH, Cl, Br, or H.

In the 1980s, it was further shown that heterogeneous reactions (gas–solid) on particles in polar stratospheres could deplete the ozone, as opposed to the homogeneous reactions (gas–gas) reactions such as eqns [82]–[86]. In Antarctica, an ozone hole of low ozone column abundance appears each southern spring. Chlorine radicals released from the UV decomposition of anthropogenic CFCs are responsible (Russell et al., 1996). It was deduced that heterogeneous reactions convert unreactive forms of chlorine, such as HCl and chlorine nitrate into Cl_2 on polar stratospheric cloud particles:

$$\underbrace{ClONO_2}_{\text{chlorine nitrate}} + HCl \rightarrow Cl_2 + \underbrace{HNO_3}_{\text{nitric acid}} \qquad [87]$$
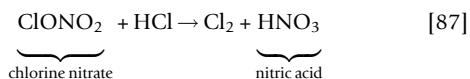
This reaction sequesters odd nitrogen ($NO_x = NO + NO_2$, pronounced 'nox') into unreactive nitric acid, which prevents NO_x from turning reactive chlorine back into unreactive chlorine nitrate via
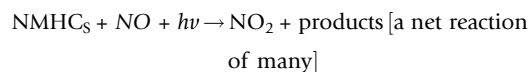
$$ClO + NO_2 + M \rightarrow ClONO_2 + M \qquad [88]$$

Nitric oxide (NO) is naturally present because biogenically produced nitrous oxide (N_2O) reacts with an energetic oxygen atom (denoted $O(^1D)$) to generate two NO radicals.

In Antarctica, springtime sunlight releases Cl_2 from particles, which photolyzes into Cl radicals, causing ozone depletion via eqn [86]. The process is encouraged by a springtime stratospheric vortex of eastward winds that prevents inflow of new odd nitrogen or ozone from lower latitudes. Unlike Antarctica, buoyancy waves associated with north–south mountain ranges disrupt the development of a coherent Arctic vortex, so the Arctic lacks an equivalent ozone hole.

One aspect of the Earth's stratosphere that bears some commonality to other oxidizing atmospheres (e.g., Venus and early Mars) is that sulfur gases (sulfur dioxide, SO_2, and carbonyl sulfide, OCS) are oxidized into sulfate aerosols that make a thin haze called the Junge layer (at $\sim$20–25 km altitude). The Junge layer scatters sunlight back to space and cools the Earth. The Junge layer is a photochemical haze of sulfates, analogous to Venus' clouds, although far thinner because the Earth's sulfur is mostly not gaseous but tied up in the form of sulfate and sulfide minerals on or below the Earth's surface. However, it is a general feature of oxidizing atmospheres with sulfur gases to produce sulfate hazes.

We now turn to the Earth's troposphere. All major gases (except Ar) in the Earth's atmosphere are mediated by biological cycles, including O_2, N_2, and CO_2. In addition, various trace gases have significant biological sources, such as CH_4 and bigger hydrocarbons, N_2O, OCS, dimethyl sulfide (CH_3SCH_3 and DMS), and carbon disulfide (CS_2).

A key factor for the Earth's tropospheric chemistry is the role of the dominant oxidizing radical, OH (Levy, 1971; Prinn, 2014). This species arises because of the presence of large amounts of water vapor and O_2, where the latter leads to the generation of tropospheric ozone ($\sim$10% of the ozone column abundance) in pathways involving NO_x. In the stratosphere, NO_x destroys ozone, but in the troposphere, NO_x makes ozone (Crutzen, 1979). To create ozone, O_2 and O need to be combined, so O atoms are required. These derive from NO_2, whose progenitor NO comes from lightning, soils, or transport from the stratosphere:

$$NMHC_S + NO + h\nu \rightarrow NO_2 + \text{products} \, [\text{a net reaction}$$
$$\text{of many}]$$

$$NO_2 + h\nu (\lambda \leq 410\,nm) \quad NO + O \rightarrow \qquad [89]$$

NMHCs are nonmethane reactive hydrocarbons (C_2–C_5 compounds plus isoprene (C_5H_8), e.g., butane (C_4H_{10}) and ethylene (C_2H_4)), which have biogenic sources such as marine plankton and vegetation. The O atoms from eqn [89] react with O_2 to form ozone (eqn [83]). Oxidation of methane and carbon monoxide, catalyzed by NO_x, can also produce ozone. Then, ozone photolysis with relatively energetic photons generates exited O atoms that react with water vapor to generate OH radicals:

$$O_3 + h\nu (\lambda \leq 310\,nm) \quad O_2 + O(^1D) \qquad [90]$$

$$H_2O + O(^1D) \rightarrow OH + OH \qquad [91]$$
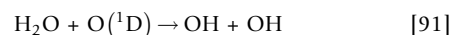
OH is the 'detergent of the atmosphere' because it helps oxidize sulfur-containing gases (SO_2, H_2S, DMS, etc.) into sulfates, removes hydrocarbon gases such as CH_4 and NMHCs by initiating their oxidation, and converts NO_x into nitric acid. Without significant OH, the Earth's atmosphere would accumulate hydrocarbons and sulfurous gases and be very different.
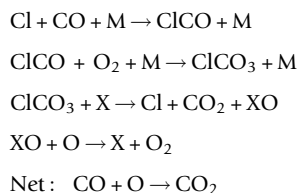
10.13.4.5 CO_2 Atmospheres: Venus and Mars

Venus and Mars both have CO_2-dominated atmospheres and so have some common behavior (Krasnopolsky and Lefevre, 2013). For example, CO_2 does not significantly decompose into CO by photolysis on either planet because catalytic reactions recombine CO_2 from CO and O. Also, both planets have cold thermospheres caused by CO_2 radiative cooling, but Venus' thermosphere is colder, which is counterintuitive given Venus' location. Photochemistry lies behind this situation.

Of course, the recombination of CO_2 relies on radicals. On Mars, OH radicals (derived from water vapor or hydrogen peroxide photolysis) catalyze the recombination of CO and O in cycles (McElroy and Donahue, 1972; Parkinson and Hunten, 1972), for example,

$$OH + CO \rightarrow CO_2 + H$$
$$H + O_2 + M \rightarrow HO_2 + M$$
$$HO_2 + O \rightarrow OH + O_2$$
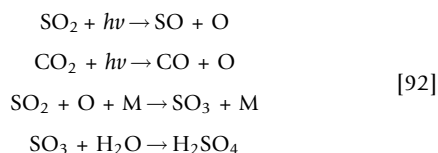$$Net: CO + O \rightarrow CO_2$$
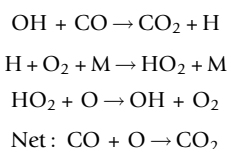
Unlike Mars, where the chemistry is largely restricted to C–O–H, seven principal elements are involved on Venus: O–C–S–H–Cl–N–F. Chlorine atoms (derived from HCl photolysis) play an important role in CO_2 recombination on Venus, along with various catalysts:

$$Cl + CO + M \rightarrow ClCO + M$$
$$ClCO + O_2 + M \rightarrow ClCO_3 + M$$
$$ClCO_3 + X \rightarrow Cl + CO_2 + XO$$
$$XO + O \rightarrow X + O_2$$
$$Net: CO + O \rightarrow CO_2$$

where X = H, Cl, O, SO, or SO_2.

A fundamental difference of Venus compared with Mars (and Earth) is a total cloud cover. Venus' clouds of sulfuric acid are photochemical, originating from the photolysis of SO_2 and CO_2:

$$
\begin{aligned}
SO_2 + hv &\rightarrow SO + O \\
CO_2 + hv &\rightarrow CO + O \\
SO_2 + O + M &\rightarrow SO_3 + M \\
SO_3 + H_2O &\rightarrow H_2SO_4
\end{aligned}
\qquad [92]
$$

Unlike the Earth's clouds that require updrafts and cooling for condensation, photochemical haze occurs globally on Venus, analogous to Titan's haze. Sulfur on Venus also disproportionates, that is, some gets oxidized, while the rest is reduced. Molecules of sulfur atoms and sulfane (sulfur–hydrogen) absorb visible and UV radiation and may be responsible for cloud coloring.

Venus' upper thermosphere is colder than Mar's ($\sim$250 K vs. $\sim$270 K) because O atoms are $\sim$10 times more abundant. There is a greater concentration of O atoms on Venus versus Mars because of more photodissociation of CO_2 and a smaller-scale height (eqn [7]) for the same temperature, given the dependence on gravitational acceleration (Krasnopolsky, 2011). On both planets, chemistry produces vibrationally excited CO_2 (denoted by an asterisk),
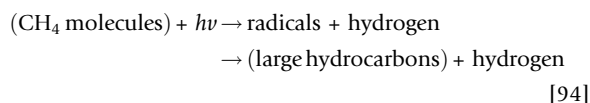
$$O + CO_2 \rightarrow CO_2{}^* + O \qquad [93]$$

which decays and radiates 15 μm photons through an optically thin path to space, causing cooling.

10.13.4.6 Reducing Atmospheres: Giant Planets and Titan

Much could be said about the photochemistry on Titan and the giant planets (e.g., Yung and Demore, 1999), but here, I focus on one general aspect – the fate of hydrogenated gases. Although Titan and the giant planets have reducing atmospheres, hydrogen escapes to space on Titan but not from the giant planets where H_2 is the major constituent. This changes the fate of carbon species on Titan compared to the giant planets and is also relevant for the processing of nitrogen, phosphorus, and sulfur species on the giant planets.

Methane is the most abundant carbon gas in the cold reducing atmospheres of the solar system (although CO is thermodynamically favored in hot Jupiters). Unlike the rapid conversion to CO_2 and water vapor that occurs in oxidizing atmospheres (Section 10.13.4.1), methane is destroyed when UV photons with wavelength of <145 nm break C–H bonds. The radicals that are released combine to make bigger hydrocarbons in the following overall schematic net reaction:

$$
\begin{aligned}
(CH_4\ molecules) + hv &\rightarrow radicals + hydrogen \\
&\rightarrow (large\ hydrocarbons) + hydrogen
\end{aligned}
\qquad [94]
$$

On Titan, for example, the lifetime of atmospheric methane against complete photolysis loss is 30–100 My (Yung et al., 1984). The hydrocarbons can be as simple as ethane (C_2H_6) or as complex as polyaromatic hydrocarbons, which are molecules consisting of linked benzene rings. On Titan, organic molecules also incorporate nitrogen to form nitriles (organics with C≡N groups) (Atreya et al., 2009). But on Titan, hydrogen escapes, so the organics accumulate on the surface as solids or liquids, and methane is destroyed (Figure 8(a)). However, on the giant planets, hydrogen does not escape and is the main gas. There, hydrocarbons eventually get mixed down to deep, hot ($\sim$1000 K) layers where they are hydrogenated and converted back into methane.

Similar cycles occur on the giant planets with nitrogen, phosphorus, and sulfur species. Ammonia (NH_3), phosphine (PH_3), and hydrogen sulfide (H_2S) are photolyzed to make hydrazine, elemental phosphorus, and sulfur-containing solids. However, sedimentation and mixing to depth cyclically reconstitute ammonia, phosphine, and hydrogen sulfide (Figure 8(b)).

10.13.5 Atmospheric Dynamics

10.13.5.1 Equations of Motion

Atmospheric dynamics concerns the study of atmospheric motions and their relationship to heating and forces (Holton, 2004; Houghton, 2002; Mak, 2011; Vallis, 2006). Winds are
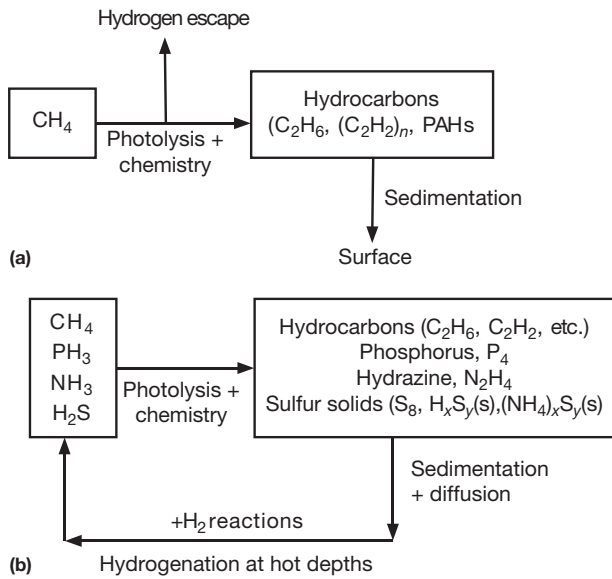
(a)

(b)

Figure 8 (a) Net hydrocarbon production on Titan, associated with the escape of hydrogen. PAHs are polyaromatic hydrocarbons. (b) The closed cycles of hydrogen-bearing species on giant planets. (Drawn by the author.)

critical for climate because they transport heat (e.g., from tropics to cold poles) and affect the formation of clouds by carrying condensables. Winds also redistribute non-condensables (e.g., O_3 in the Earth's stratosphere), modify surfaces (e.g., dunes on Mars or Titan), and can drive secondary circulations (e.g., ocean currents on Earth).

Atmospheric motions are usually considered from the perspective of an observer corotating with a planet. A rotating frame is accelerating, and in accelerating frames, apparent forces arise in the opposite direction to real accelerations. For example, scales in an upwardly accelerating elevator would incorrectly measure weight without accounting for a downward apparent force. In a rotating frame, centrifugal and Coriolis apparent forces arise. Centrifugal forces are known from everyday experience, but the Coriolis force is less familiar and, consequently, often illustrated by a ball thrown from the center of a merry-go-round to a catcher at its edge. If the merry-go-round does not rotate, the ball reaches the catcher in a straight line, but with counter-clockwise rotation, the catcher rotates around and the ball misses him; the ball appears to be deflected to the right of its motion from the viewpoint of the corotating catcher and thrower. The analogy is imperfect because the ball also experiences a radially outward centrifugal force. But the basic picture is analogous to looking down upon a planet spinning west to east: the Coriolis force acts to the right of motion (e.g., a wind vector) such as in the Earth's northern hemisphere. Viewed from below, the merry-go-round's rotation is clockwise and the Coriolis force acts to the left of the motion, akin to the effect on winds in the Earth's southern hemisphere.

Newton's second law for motion on a rotating planet (e.g., see Taylor, 2005) is

$$\underbrace{\mathbf{a}}_{\text{acceleration on co-rotating frame}} + \underbrace{(2\mathbf{\Omega}\times\mathbf{v})}_{\text{coriolis acceleration}} + \underbrace{[\mathbf{\Omega}\times(\mathbf{\Omega}\times\mathbf{r})]}_{\text{centripetal acceleration}}$$

$$= \underbrace{\frac{\mathbf{F}_g}{m}}_{\text{force of gravity}} + \underbrace{\frac{\mathbf{F}}{m}}_{\text{all other forces}}$$

[95]

where $\mathbf{\Omega}$ is the planet's angular velocity vector, the acceleration and velocity are measured by a corotating observer, and the last term includes pressure gradient forces, frictional forces, and external tidal forces caused by gravitational interaction with the Sun or parent star, from a moon, or from a planet being orbited if we are considering the atmosphere of a large moon. Usually, the centripetal acceleration is taken to the right-hand side, treated as 'centrifugal force per kg' and, combined with gravity to form an effective, measured gravity g. A modified g vector is valid because rotating planets deform into oblate surfaces as a result of the centrifugal force pulling outward at the equator. Simplifying eqn [95] by neglecting tidal torques, we get the usual basic form of the momentum equation in atmospheric dynamics,

$$\frac{d\mathbf{v}}{dt} = \underbrace{\frac{-1}{\rho}\nabla p}_{\text{pressure gradient force/kg}} - \underbrace{(2\mathbf{\Omega}\times\mathbf{v})}_{\text{Coriolis force/kg}} - g\mathbf{k} + \mathbf{F}_{\text{vise}} \quad [96]$$

where $\mathbf{F}_{\text{visc}}$ is the frictional or viscous force per unit mass, $\mathbf{v}$ is the wind vector, and $\mathbf{k}$ is an upward unit vector. It is possible that tidal forces should not be neglected for long-term climate models rather than weather models. But surprisingly little work has been done to examine this issue (Houben, 2013).

Equation [96] can be expanded into local Cartesian (x, y, z) coordinates on a sphere with equations in three velocity components (e.g., see Holton (2004), Chapter 2): a zonal wind u in the west to east or 'zonal' x direction, a meridional wind v in the south-to-north y direction, and a vertical wind w upward in the z direction, that is, $\mathbf{v} = u\mathbf{i} + v\mathbf{j} + w\mathbf{k}$. The resulting momentum equations simplify for large-scale motions, if we ignore friction and vertical motion (given that vertical winds are usually much smaller than horizontal ones) (e.g., see Andrews (2010) or Holton (2004)):

$$\text{Vertical (hydrostatic equation)}: \quad \frac{\partial p}{\partial z} = -g\rho \quad [97]$$

$$\text{Zonal momentum}: \quad \frac{du}{dt} - \underbrace{\left(f + \frac{u\tan\phi}{a}\right)}_{\text{Coriolis term Centrifugal term}} \mathbf{v} = -\frac{1}{\rho}\frac{\partial p}{\partial x} \quad [98]$$

$$\text{Meridional momentum}: \quad \frac{dv}{dt}$$
$$+ \underbrace{\left(f + \frac{u\tan\phi}{a}\right)}_{\text{Coriolis term Centrifugal term}} u = -\frac{1}{\rho}\frac{\partial p}{\partial y} \quad [99]$$

Here, a is the planetary radius at the local x, y, z origin, the latitude is ϕ, and f is the Coriolis parameter defined by

$$f = 2\Omega\sin\phi \quad [100]$$

where Ω is the planet's angular velocity. Specifically, $\Omega = 2\pi/\tau_d$ where τ_d is the rotation period (=a sidereal day), for example,

$\Omega = 2\pi/(86\,164\text{ s}) = 7.29 \times 10^{-5}$ rad s^{-1} for Earth. If put on the right-hand side, terms f_v and $-f_u$ are x and y components of the Coriolis force per kg that act to the right of the wind in Earth's northern hemisphere. Terms $-(u\tan\phi/a)v$ and $+(u\tan\phi/a)u$ are x and y components of cyclostrophic acceleration, which are important on slowly rotating planets (see **Section 10.13.5.2**).

In eqns [98] and [99], the derivatives in v and u are substantial *or* material derivatives. The dX/dt form is the (Lagrangian) rate of change of flow-field quantity X with respect to time following a fluid parcel, unlike dX/dt, the (Eulerian) rate of change at a fixed point. They are related by

$$\underbrace{\frac{\mathrm{d}X}{\mathrm{d}t}}_{\text{substantial derivative}} \equiv \underbrace{\frac{\partial X}{\partial t}}_{\text{local derivative}} + \underbrace{u\frac{\partial X}{\partial x} + v\frac{\partial X}{\partial y} + w\frac{\partial X}{\partial z}}_{\text{advective terms}}$$

$$= \frac{\partial X}{\partial t} + \mathbf{v}\cdot\nabla X \qquad [101]$$

Here, $\mathbf{v}$ is the velocity vector and we remind ourselves that $\mathbf{a}\cdot\mathbf{b} = a_1b_1 + a_2b_2 + a_3b_3$, while the gradient operator is $\nabla = \partial/\partial x + \partial/\partial y + \partial/\partial z$. For example, if 2-D spatial contours of temperature T are fixed in time ($\partial T/\partial t = 0$) and an observer moves eastward with velocity u in time. Δt between 250 and 270 K contours, then eqn [101] gives dT/d$t = u\nabla T = (\Delta x/\Delta t) \times (\Delta T/\Delta x) = 20$ K$/\Delta t$. Alternatively, if the 250 K contour moves with the wind speed and replaces the 270 K downstream contour, dT/d$t = 0$ because the local change $\partial T/\partial t$ (-20 K$/\Delta t$) is balanced by advection of temperature, $u\nabla T$. 'Advection' (Latin 'carry to') is the transport of an atmospheric property by the velocity field. The difference between advection and convection is that advection usually refers to the predominantly horizontal, large-scale atmospheric motions, while convection describes the mostly vertical, locally induced motions.

10.13.5.2 Balance Regimes: Geostrophic, Cyclostrophic, and Thermodynamic

10.13.5.2.1 Geostrophic balance
On planets that rotate fairly rapidly, such as Earth, Mars, and the giant planets, the Coriolis force is important. In the Earth's northern hemisphere (NH), the Coriolis force acting to the right of large-scale flow is frequently approximately balanced by low pressure to the left and high pressure to the right, that is, a pressure gradient force. Thus, on NH weather maps, winds blow counterclockwise around a 'low' cyclonic system or clockwise around a 'high' anticyclonic system. The balance of Coriolis and pressure gradient forces is called geostrophic balance. Because $f \gg u/\tan\phi$, eqns [98] and [99] provide this balance as

$$u_g = -\frac{1}{f\rho}\left(\frac{\partial p}{\partial y}\right)_z, \quad v_g = \frac{1}{f\rho}\left(\frac{\partial p}{\partial x}\right)_z \qquad [102]$$

The z subscript indicates a partial derivative evaluated along an altitude surface, while the g subscript denotes geostrophic winds. In deriving eqn [102], we assumed d(u or v)/d$t \ll f$ to eliminate d/dt terms. This condition is true if the dimensionless Rossby number (Ro), which is the ratio of the Lagrangian acceleration to Coriolis acceleration, is < 0.1 or so, where

$$\text{Rossby number, } Ro = \frac{\text{Relative acceleration}}{\text{Coriolis acceleration}} = \frac{U^2/L_h}{fU} = \frac{U}{fL_h} \qquad [103]$$

Equation [103] uses a scale analysis. The variables U and L_h are characteristic wind speeds and horizontal length scales, respectively. For example, Jupiter has $U \approx 100$ m s^{-1}, $L_h \approx 100\,000$ km $= 10^8$ m, and $f \approx 1.8 \times 10^{-4}$ s^{-1} at 45°N. Thus, $Ro \approx 0.01$, so rotation dominates and geostrophy applies. Similarly, $Ro \ll 1$ for other giant planets, Earth, and Mars. But at the equator, $\phi = 0$ and $f \to 0$, so Ro cannot be small. The result is that circulations on rotating planets are more symmetrical with latitude close to the equator but rotation affects flows strongly at higher latitudes, producing big eddies.

Geostrophy predicts that zonal winds should typically increase in speed with altitude. Usually, the distribution of sunlight creates a temperature decrease from equator to pole, so columns of air on average shrink toward the pole because they are cooler, which must create an increasing meridional pressure gradient at higher altitudes. Since $\partial p/\partial y$ grows with altitude, the zonal wind u_g will grow too by eqn [102]. This link between horizontal temperature gradients and the wind shear – that is, change of wind speed and direction with height – is captured in the thermal wind equation, which is derived from eqn [102] by substituting for $\rho = p/\overline{R}T$ from the ideal gas law (eqn [2]), differentiating w.r.t. z and then substituting the hydrostatic eqn [6]:

$$f\frac{\partial v_g}{\partial z} \approx \overline{R}T\frac{\partial}{\partial x}\left(\underbrace{\frac{1}{p}\left(\frac{\partial p}{\partial z}\right)}_{-g/\overline{R}T}\right) = \frac{-g\cancel{\overline{R}}T}{\cancel{\overline{R}}}\frac{\partial}{\partial x}\left(\frac{1}{T}\right) = \cancel{T}\left(\frac{g}{\cancel{T}}\frac{\partial T}{\partial x}\right)$$

$$= \frac{g}{T}\frac{\partial T}{\partial x}$$

An approximation sign is used for ignoring vertical variations in T. With analogous manipulation of the zonal geostrophic wind equation, the thermal wind equations in u_g and v_g are

$$f\frac{\partial u_g}{\partial z} \approx -\frac{g}{T}\frac{\partial T}{\partial y}, \quad f\frac{\partial v_g}{\partial z} \approx \frac{g}{T}\frac{\partial T}{\partial x} \qquad [104]$$

These equations (or slightly higher approximations) allow calculation of winds on other planets (e.g., Smith et al., 2001). After deriving temperatures from radiances measured by an orbital instrument, eqn [104] implies the geostrophic winds. Often, no surface wind is assumed as a boundary condition at the expense of some accuracy.

10.13.5.2.2 Cyclostrophic balance
The analysis in the preceding text applies to rapidly rotating planets, but for slowly rotating planets, the balance is different. For example, on Venus, $L_h \approx 1000$ km $= 10^6$ m, $U \approx 10$ m s^{-1}, and $f = 2\Omega\sin\phi = 2(2.98 \times 10^{-7}\text{ s}^{-1})(\sin\ 45) = 4.2 \times 10^{-7}\text{s}^{-1}$ at 45°N, so the $Ro \approx 10$ from eqn [103] and geostrophy is invalid. If the atmosphere itself rotates sufficiently rapidly over some altitude range, the substantial derivatives and f terms are negligible in eqns [98] and [99], and a cyclostrophic balance and a cyclostrophic thermal wind apply, as follows:

$$\underbrace{\frac{u^2\tan\phi}{a}}_{\textbf{(a)}\ \text{cyclostrophic balance}} = -\frac{1}{\rho}\frac{\partial p}{\partial y};$$

$$\underbrace{\frac{\tan\phi}{a}\frac{\partial(u^2)}{\partial z} \approx -\overline{R}T\frac{\partial}{\partial y}\left(\frac{1}{p}\frac{\partial p}{\partial z}\right) = -\frac{\cancel{\overline{R}}\cancel{T}g}{\cancel{\overline{R}}T\cancel{T}}\frac{\partial T}{\partial y} = -\frac{g}{T}\frac{\partial T}{\partial y}}_{\textbf{(b)}\ \text{cyclostrophic thermal wind equation}} \qquad [105]$$
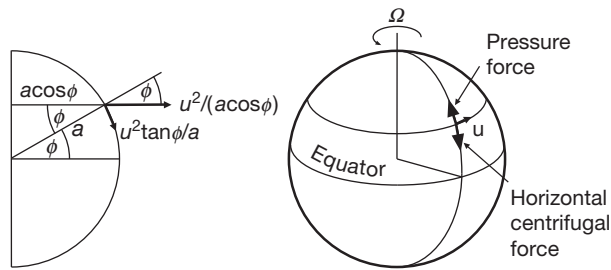
Figure 9 The geometry of cyclostrophic balance and the balance of forces on a slowly rotating planet such as Venus or Titan. Here, ϕ is latitude, a is planetary radius, $\mathbf{u}$ is the zonal wind vector, and Ω is a planetary rotation vector. (Drawn by author.)

Equation [105](a) is a balance between centrifugal force per unit mass and an equator-to-pole pressure gradient force (**Figure 9**). At latitude ϕ, the centrifugal acceleration due to the zonal wind is $u^2/(a\cos\phi)$, because $a\cos\phi$ is the distance to the rotation axis. On Venus and Titan, wind speeds increase with altitude consistent with a cyclostrophic thermal wind according to Pioneer Venus (Schubert, 1983; Seiff et al., 1980) and Huygens probe (Bird et al., 2005) measurements, respectively. Equation [105] should also apply to slowly rotating exoplanets.

10.13.5.2.3   Thermodynamic balance

Large-scale ascent and descent produce expansion and compression, which can change temperatures from those expected with simple radiative–convective equilibrium (**Section 10.13.3.4**). The physics derives from the first law of thermodynamics, written $dq = c_p dT - \alpha dp$, where $\alpha = 1/\rho$, from eqn [12]. Dividing by δt and c_p and taking the limit $\delta t \to 0$,

$$\underbrace{\frac{dT}{dt} - \frac{\alpha}{c_p}\left(\frac{dp}{dt}\right)}_{\approx -g\rho w} = \frac{Q}{c_p} \Rightarrow \underbrace{\frac{dT'}{dt}}_{\text{time variable component}} + \underbrace{w\left(\frac{\partial T}{\partial z} + \frac{g}{c_p}\right)}_{\text{workdone}}$$

$$= \underbrace{\frac{Q}{c_p}}_{\text{heat gain}} \Rightarrow \underbrace{w\left(\frac{\partial T}{\partial z} + \frac{g}{c_p}\right)}_{\text{static stability}} \approx \underbrace{\frac{Q}{c_p}}_{\text{heat gain}} \quad [106]$$

Here, $Q = dq/dt$ [J kg^{-1} s^{-1}] is the diabatic heating per kg caused by radiation, convection, or conduction. In the middle part of eqn [106], we used eqn [101] to define T' as the horizontal (x, y) and time variable component of temperature and T as a horizontal and time average temperature. Since the term in T' is usually small, we neglect it for the final expression, which is a thermodynamic energy equation. This describes a rate of temperature change (K s^{-1} or K day^{-1}) for a parcel of air with vertical velocity and diabatic heating. We can replace the diabatic heating term with a Newtonian cooling approximation, in which temperature relaxes back to an equilibrium reference temperature field described by T_{eqm} as $Q/c_p = -\alpha_N(T - T_{eq})$, where $\alpha_N = 1/\tau_{rad}$ where τ_{rad} is a radiative time constant. Recognizing static stability (eqn [17]) in eqn [106], we can write thermodynamic balance as

$$w(\Gamma_a - \Gamma) = -\alpha_N(T - T_{eqm}) \quad [107]$$

This equation indicates that heating or cooling from vertical motion is balanced by radiative relaxation back to an equilibrium temperature. The radiative time constant can be estimated as

$$\tau_{rad} = \frac{\text{heat change per m}^2}{\text{absorbed flux per m}^2} = \left(\frac{p_e c_p (\Delta T_e)}{g}\right) \Big/ \left(\frac{(1-A)S_p}{4}\right)$$

$$= \frac{4 p_e c_p (\Delta T_e)}{(1-A)S_p g} \quad [108]$$

where p_e is the pressure at the emission level, g is the gravitational acceleration, ΔT_e is the temperature change forced by the absorption of solar radiation ($\sim$2 K for Earth or 80 K for Mars), c_p is the specific heat capacity, A is the Bond albedo, and S_p is the top-of-atmosphere solar flux. This uses eqns [8] and [23].

We can see the effect of eqn [107] in latitude-averaged temperature structures of planetary atmospheres. Static stability $(\Gamma_a - \Gamma)$ is generally positive, so if we measure $T < T_{eqm}$, then w is positive and large-scale ascent produces temperatures colder than equilibrium from cooling by expansion. Conversely, if $T > T_{eqm}$, large-scale descent produces compressional warming. In Mars' equinox atmosphere (**Figure 10**), one's naive expectation of warmer tropics and colder poles is reversed at pressures below $\sim$0.5 mbar. Large-scale Hadley circulation cells (discussed in the succeeding text) produce descent and compressional warming at high latitudes and ascent and cooling at low latitudes.

10.13.5.3   Zonal Mean Meridional Circulation: Hadley Cells and Thermally Driven Jets

Jet streams or jets are significant features of the circulations of planetary atmospheres, defined as zonal wind maxima, whether eastward or westward. The style of atmospheric circulations is closely connected with jet stream structure, which varies greatly between planets. Jets can be single or multiple in each hemisphere. They may be strong or weak, meandering in latitude or straight. They are generally associated with transient eddies or waves whose zonal wave numbers (the number of complete waves around a latitude circle) vary between planets from wave number one on Venus to wave number >40 on Jupiter.

It is convenient to think of two types of jets: those driven directly by the equator-to-pole temperature gradient (thermally driven jets) and those driven indirectly by eddies (eddy-driven jets), respectively (Lee and Kim, 2003). In large-scale atmospheric dynamics, an eddy means a departure from a steady and uniform east–west flow, which results in variations in pressure with longitude. We consider thermally driven jets first.

The subtropical jet that occurs in the Earth's atmosphere at 30–40° latitude is thermally driven and associated with the descending branch of a large overturning of the tropical atmosphere called the Hadley circulation. This circulation is a large loop of airflow where air warms and rises in the tropics, cools and sinks at higher latitudes, and returns to the tropics near the surface to complete the loop, all under the influence of planetary rotation (**Figure 11**). George Hadley (1685–1786) invented the concept to explain tropical trade winds (Hadley, 1735). Equatorial-moving air is deflected by the Coriolis force toward the west and produces persistent westward tropical winds. In the subtropics, sinking causes high-pressure zones of dry air that also explain deserts such as the Sahara.

Hadley imagined a circulation symmetrical about the equator, but we know now that the Earth's Hadley circulation is
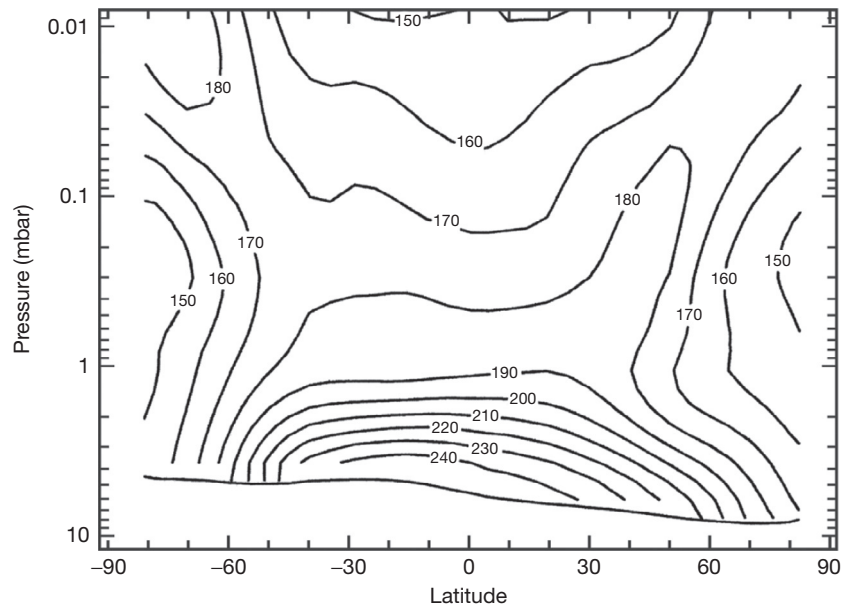
Figure 10 Contours of the zonal mean meridional temperatures (in K) at northern hemisphere autumnal equinox on Mars derived from measurements by the Thermal Emission Spectrometer (TES) instrument on NASA's Mars Global Surveyor orbiter. The solid line at the lower boundary of the temperature contours is the zonal mean atmospheric pressure at the surface. Adapted from Smith MD, Pearl JC, Conrath BJ, and Christensen PR (2001) Thermal Emission Spectrometer results: Mars atmospheric thermal structure and aerosol distribution. *Journal of Geophysical Research* 106: 23929–23945 with permission.

(a)
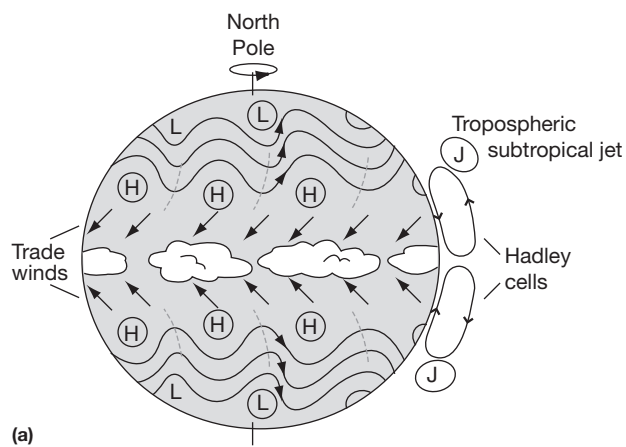
Figure 11 Idealized symmetrical Hadley cells on Earth. Moist air rises near the equator tropics causing a belt of clouds. The air aloft travels poleward, acquiring a fast zonal speed by conservation of angular momentum. This results in a subtropical jet near the descending branch of the Hadley cell. At the surface, air returns to complete the loop, causing westward trade winds in the tropics. In each hemisphere, a different circulation is found beyond the maximum latitudinal extend of the Hadley circulation. In midlatitudes, there are waves that are found in the eastward winds. (Adapted from Wallace JM and Hobbs PV (2006) *Atmospheric Science: An Introductory Survey*, 2nd edn. Burlington, MA: Elsevier Academic Press, International geophysics series. Used with permission.)

symmetrical in neither latitude nor longitude (Cook, 2004; Dima and Wallace, 2003; Lindzen and Hou, 1988). Rising air occurs as relatively small-scale convection associated with heavy rainfall in the intertropical convergence zone (ITCZ)

where low-level southwestward trade winds from the northern hemisphere converge with northwestward trade winds from the south. The ITCZ is generally located somewhat off the equator (Figure 12). The descending branches of the Hadley circulation are also not uniform in longitude. Subsidence takes place preferentially in high-pressure areas over the subtropical Atlantic, Pacific, and Indian Oceans.

Monsoons are associated with the Hadley circulation and exist on Earth and Mars. A monsoon is a seasonal reversal of winds associated with latitudinal movement of the ITCZ, and the monsoon behaves as an intensification of the Hadley circulation in particular longitude ranges (e.g., Schneider (2006)). On Earth, the ITCZ is offset from the equator because of planetary obliquity and the distribution of oceans and continents. Surface winds curve across the equator and turn from westward to eastward due to the Coriolis force and become a monsoon circulation. The Martian orbit has a relatively high eccentricity with more incoming solar radiation near the southern summer winter solstice, and there is asymmetrical topography between hemispheres, causing the Hadley circulation to be stronger than during southern winter solstice (Haberle et al., 1993b; Richardson and Wilson, 2002). The lower Hadley branch can be channeled by large-scale topography to form monsoon-like circulations (Joshi et al., 1994, 1995).

A key physical concept behind the Hadley circulation is conservation of angular momentum. In the simplest model, one assumes that angular momentum per unit mass is conserved in the upper branch of the Hadley circulation. At the equator, assuming no zonal wind, the angular momentum per unit mass is Ωa^2, where a is the planetary radius. If angular momentum per unit mass is conserved in transport of air parcels from the equator to latitude ϕ, a zonal wind u is acquired, as follows:
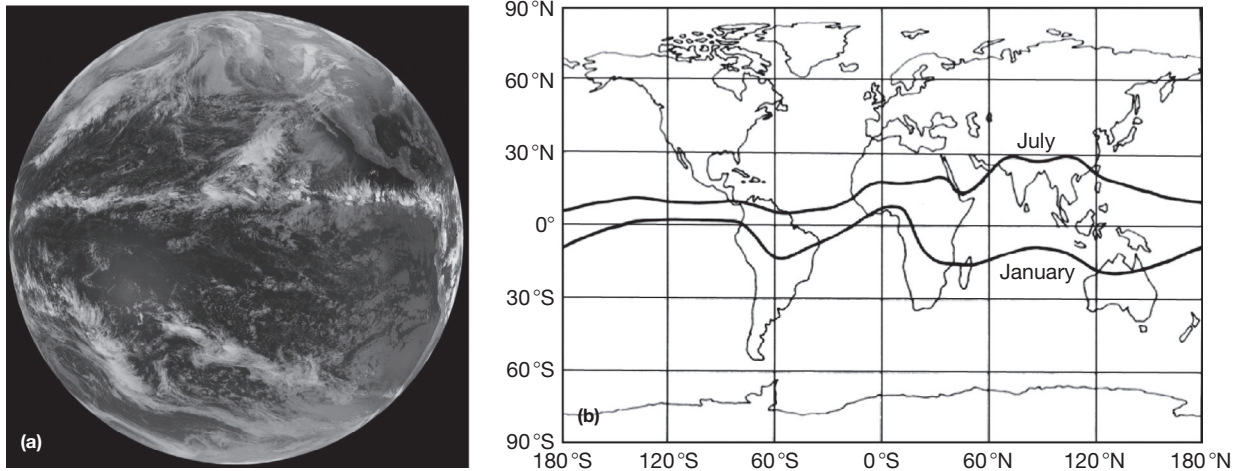
Figure 12   (a) The intertropical convergence zone (ITCZ) of the trade winds is visible on Earth as a band of cloud across the eastern Pacific from west to east (Courtesy: NOAA/NASA GOES project). (b) The latitude of the ITCZ changes seasonally and the annual average latitude of the ITCZ is north of the equator unlike an idealized symmetrical Hadley circulation.
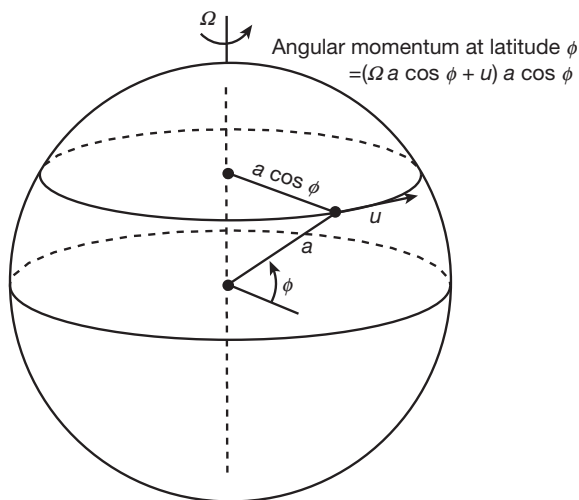

Figure 13   Zonal angular momentum acquired at latitude ϕ in poleward motion of air in the upper branch of the Hadley circulation helps in understanding the Hadley circulation. Rapid zonal wind speeds u are produced, which is responsible for a subtropical jet at the most poleward latitude to which the Hadley circulation extends. (Drawn by the author.)

$$\underbrace{\Omega a^2}_{\text{ang. momentum@equator}} = \underbrace{(\Omega a \cos\phi + u)a\cos\phi}_{\text{angular momentum@latitude }\phi} \Rightarrow u\cos\phi$$

$$= \Omega a \underbrace{(1 - \cos^2\phi)}_{\sin^2\phi} \Rightarrow u = (\Omega a)\frac{\sin^2\phi}{\cos\phi} \quad [109]$$

A point on the planet's surface at latitude ϕ moves with tangential velocity $\Omega a \cos\phi$, to which we add the zonal wind speed, u (Figure 13). The radius to the planetary rotation axis is $a \cos\phi$, so that angular momentum conservation is given by

the first equality, and we solve for u. Imagine air in the upper branch of the Hadley circulation carried from the equator, where $u = 0$, to latitude 30°. Equation [109] predicts $u = 134$ m s^{-1} at 30° Thus, we expect strong subtropical eastward winds at altitude.

The subtropical jet core in the upper branch of the Earth's Hadley circulation seasonally reaches $\sim$30–70 m s^{-1} – nowhere as high as predicted in the preceding text because eddies from the midlatitudes provide westward angular momentum that decelerates the upper branch of the Hadley cell (Schneider, 2006). Of course, friction causes slow surface winds, so that winds must increase with altitude near the jet. We can look at the thermal wind eqn [104] in 'reverse': a large wind shear must have a correspondingly big meridional temperature gradient $\partial T/\partial y$ in the vicinity of the jet, unlike the smooth variation of equilibrium temperature with latitude that we might expect. Large-scale ascent is associated with $T < T_{eqm}$ on the equatorial side of the jet. Conversely, large-scale descent occurs on the polar side where $T > T_{eqm}$.

If one assumes that heating and cooling balance across a Hadley cell, then it is possible to derive an equation for the maximum latitude ϕ_H for how far a Hadley cell extends, which varies as $\phi_H \propto g^{0.5}/(\Omega a)$ (Held and Hou, 1980). However, such a theory underpredicts the meridional mass transport (kg s^{-1}) of the Hadley circulation by an order of magnitude. Other models suggest that midlatitude eddies confine the Hadley circulation. Possibly, the Hadley circulation winds and temperatures become unstable, which prevents penetration into midlatitudes. Energy carried from the tropics is transferred from the Hadley cells to eddies and waves characteristic of midlatitudes. Using such ideas, Held (2000) derived a weaker dependence on rotation of $\phi_H \propto (g^{0.5}/(\Omega a))^{0.5}$. Earth-like general circulation model simulations confirm that the Hadley circulation contracts in latitude range with increasing rotation rate (Del Genio and Suozzo, 1987; Navarra and Boccaletti, 2002; Showman et al., 2013). With slow rotation, if the

$Ro \gtrsim 10$, a planet behaves as an 'all tropics' world because Hadley cells extend to high latitudes (Showman et al., 2013).

As slowly rotating bodies, Venus and Titan should have Hadley circulations extending to high latitude, but relatively little evidence proves this. On Venus, $\sim 20 \, W \, m^{-2}$ of sunlight reaches the surface (Titov et al., 2007), so the Hadley circulation must be weak. Surface wind markings from Magellan radar have an equatorward direction at higher latitudes and an east–west direction nearer the equator consistent with a large-scale Hadley circulation (Greeley et al., 1997). Venus absorbs $100 \, W \, m^{-2}$ near its cloud tops (~ 60–$70 \, km$), which should drive a second Hadley-like circulation above the clouds (Baker and Leovy, 1987). A strong temperature gradient and weak maximum in the zonal wind speed at $\sim 55°$ latitude in both hemispheres indicates this circulation's probable extent. On Titan, low-latitude dunes indicate eastward flow, opposite to the expected trade winds (Jaumann et al., 2009). Possibly, the dunes form during periods when equatorial zonal winds reverse and strengthen (Tokano, 2009, 2010) (see Chapter 10.12).

10.13.5.4 Eddy-Driven Jet Streams

In terrestrial midlatitudes, we find an eddy-driven polar jet stream associated with systematically structured eddies superimposed on the zonal mean flow. A familiar example of such eddies are traveling cyclones and anticyclones. There is also a stationary wave structure due to the distribution of oceans and continents. On the giant planets, multiple jets are probably eddy-driven also (Ingersoll, 1990; Williams, 1978) (Figure 14). On Mars and Venus, the single, primarily thermally driven jet in each hemisphere is also altered by large-scale stationary and transient eddies.

To understand eddy-driven jets, we introduce concepts of rotation in fluid dynamics. Rather than quantify spin in terms of velocity and distance to a center of rotation, vorticity is used, a single quantity that describes the spin of a fluid element at a point, equivalent to the curl of the wind vector, curl $\mathbf{v} = \nabla \times \mathbf{v}$. In 2-D flows, ignoring the velocity dependence on altitude and the vertical velocity, relative vorticity ζ is a measure of spin about a vertical axis on a planet's surface:

$$\zeta = \nabla_h \times \mathbf{v}_h = \left(\frac{\partial}{\partial x}, \frac{\partial}{\partial y} \right) \times (u, v) \Rightarrow \zeta = -\frac{\partial u}{\partial y} + \frac{\partial v}{\partial x} \quad [110]$$

The sign of ζ follows a right-hand rule: with fingers in the direction of curved flow, 'thumb up' is positive. Vorticity measures both change of velocity transverse to the flow (horizontal shear) and curvature of the flow. In solid-body rotation, relative vorticity is 2ω (where ω is angular velocity): a shear contribution of the change in tangential velocity with radius, $\partial V / \partial r = \partial(\omega \, r)/\partial r = \omega$, adds to curvature from the change in the tangential velocity with angle, $V(\partial(\text{angle})/\partial(\text{path})) = V(2\pi/2\pi r) = V/r = \omega$. Cyclonic relative vorticity is always in the same direction as the component of the planet's rotation, and a cyclonic vortex is always a low-pressure zone. In the Earth's northern hemisphere, cyclonic flow is counterclockwise but would be clockwise in the southern hemisphere. Anticyclonic relative vorticity is in the opposite direction to the component of planetary rotation.
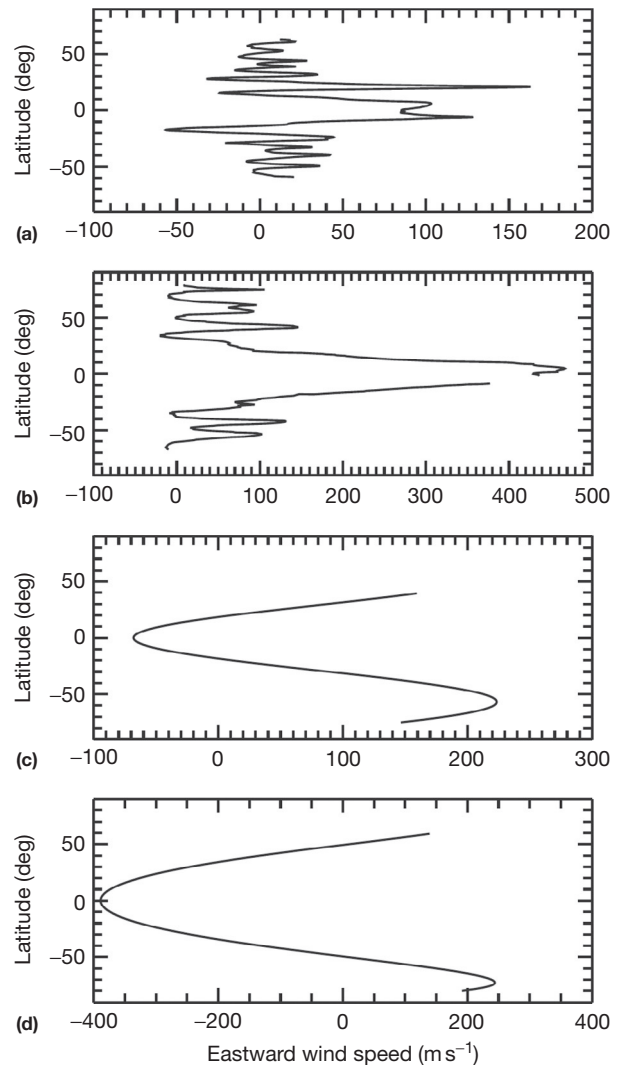

Figure 14 Jet streams on the giant planets are shown in zonal mean zonal winds from cloud tracking on (a) Jupiter, (b) Saturn, (c) Uranus, and (d) Neptune. The peaks, whether eastward or westward, correspond to jets. Jupiter and Saturn have 20 east–west jets, with a strong prograde jet over the equator, while Uranus and Neptune appear to have 3 broad jets, with strong retrograde jet over the equator. Adapted from Showman AP, Cho JYK, and Menou K (2010) Atmospheric circulation of extrasolar planets. In: Seager S (ed.) *Exoplanets*, pp. 471–516. Tucson, AZ: University of Arizona Press.

An element of fluid has a component of the planet's spin as well as any relative vorticity. The solid planet has a vorticity of 2Ω, and its vertical component of $2\Omega \sin \phi$ at latitude ϕ is the planetary vorticity, equivalent to the Coriolis parameter, f (eqn [100]). If we add relative vorticity (ζ) and planetary vorticity (f), we obtain the absolute vorticity η:

$$\eta = \zeta + f = \left(-\frac{\partial u}{\partial y} + \frac{\partial v}{\partial x} \right) + f \quad [111]$$

In adiabatic, inviscid flow in a thin homogeneous layer absolute vorticity, η, is conserved, that is, stays constant with time, if there is no friction or stirring. We denote the latter by a vorticity forcing term S_η:

(a) no friction or stirring $\dfrac{\mathrm{d}\eta}{\mathrm{d}t}=0$,

(b) with friction or stirring $\dfrac{\mathrm{d}\eta}{\mathrm{d}t}=S_\eta$ [112]

Here, the substantial derivative is $\mathrm{d}/\mathrm{d}t = \partial/\partial t + u\partial/\partial x + v\partial/\partial y$.

Equation [112](b) can be used to understand how jets are forced by eddies. A common technique in fluid dynamics is linearization in which variables are represented by mean values and perturbations and inserted into equations; then certain terms are eliminated to obtain equations that can be solved analytically. Consider a uniform zonal mean flow and an eddy fluctuation deviation that is primed, $u = \overline{u} + u'$, along with a small meridional perturbation $v = v'$. Primed variables represent parts that vary in longitude, associated with eddies. The average of the product of fluctuation components, for example, $\overline{u'v'}$, is the covariance and is nonzero only when u' and v' are correlated, that is, in phase. Thus, applying a perturbation to eqn [112](b), we have

$$\left(\frac{\partial}{\partial t} + (\overline{u} + u')\frac{\partial}{\partial x} + v'\frac{\partial}{\partial y}\right)(\overline{\eta} + \eta') = S_\eta'$$

$$\Rightarrow \left(\frac{\partial}{\partial t} + \overline{u}\frac{\partial}{\partial x}\right)\eta' + v'\frac{\partial}{\partial y}\overline{\eta} = S_\eta' \qquad [113]$$

Here, $\overline{\eta}$ has no dependence on t or x, and we eliminate small terms. If we multiply eqn [113] by η', take the zonal average, and delete terms with a zonal mean of zero, we get an

$$\underbrace{\overline{\eta'\frac{\partial\eta'}{\partial t}}}_{\frac{1}{2}\frac{\partial(\eta')^2}{\partial t}} + \cancel{\overline{\overline{u}\eta'\frac{\partial\eta'}{\partial x}}} + \overline{v'\eta'}\frac{\partial\overline{\eta}}{\partial y} = \overline{S_\eta'\eta'} \Rightarrow \underbrace{\overline{v'\eta'}}_{\substack{\text{poleward vorticity}\\\text{transport by eddies}}}$$

$$= \underbrace{-\frac{\overline{\partial(\eta')^2}/\partial t}{2\,\partial\overline{\eta}/\partial y}}_{\text{vorticity variance term}} + \underbrace{\frac{\overline{S_\eta'\eta'}}{\partial\overline{\eta}/\partial y}}_{\text{eddy forcing term}} \qquad [114]$$

Examine eqn [114]. Because f increases with latitude and $\partial f/\partial y$ is positive, the meridional gradient of absolute vorticity $\partial\overline{\eta}/\partial y$ is generally >0. So, the generation of vorticity variance by eddy stirring is associated with poleward flux of vorticity across some latitude circle ϕ_1 by the eddies represented by $\overline{v'\eta'}$ at latitude ϕ_1. This increases vorticity in the whole area of the planet poleward of ϕ_1.

It turns out that an increase of vorticity above latitude ϕ_1 can drive a prograde jet at ϕ_1 (here, the word prograde means in the same direction as the rotation of the planet, e.g., eastward for Earth; retrograde means the opposite direction). The vorticity (rotation at a point) is related to the circulation (rotation over an area) around a closed curve enclosing that area by Stokes' theorem. Writing down this theorem and applying it to the whole domical region (a spherical cap) north of latitude ϕ_1, we have

$$\underbrace{\Gamma_C}_{\text{circulation } [\mathrm{m^2s^{-1}}]} = \oint \underbrace{V_s}_{\text{velocity along arc } \mathrm{d}s}\mathrm{d}s = \iint_{\text{area A}} \eta\,\mathrm{d}A$$

$$\Rightarrow 2\pi(a\cos\phi_1)\overline{u}$$

$$= \int_{\lambda=0}^{2\pi}\int_{\phi=\phi_1}^{\pi/2} \eta a^2\cos\phi\,\mathrm{d}\phi\,\mathrm{d}\lambda$$

$$= 2\pi[\eta]a^2\int_{\phi=\phi_1}^{\pi/2}\cos\phi\,\mathrm{d}\phi \qquad [115]$$

The result means the following: a poleward vorticity flux by eddies that increases the average vorticity $[\eta]$ in the domical region poleward of ϕ_1 also increases the mean zonal wind $\overline{u}$ at ϕ_1.

Conversely, if eddies drift poleward to another latitude ϕ_2 where there is dissipation, then $\overline{S_\eta'\eta'}$ is negative. At latitude ϕ_2, the eddy vorticity flux will be equatorward (negative), and a retrograde jet will be forced via eqn [115]. Thus, if eddies propagate north or south, prograde and retrograde jets can be generated and multiple jets could form on rapidly rotating planets.

Another way to look at eddy-driven jets is to consider the north–south flux of momentum from the eddies. The northward eddy momentum across a latitude circle is $\rho v'$ (kg m^2 s^{-1}) so that the poleward flux of eastward eddy momentum is $\int\overline{u'(\rho v')}\mathrm{d}A$ where the overbar is a zonal average and $\mathrm{d}A$ is an element of area of an imaginary great wall around the latitude circle. If the northward eddy wind and eastward eddy wind are correlated, $\overline{u'v'} > 0$, and there is northward flux of zonal momentum per unit mass. Negative $\overline{u'v'}$ corresponds to a southward flux. From vector addition of the primed velocities, eddy wind component covariance corresponds to a tendency for tilted eddies. Where $\overline{u'v'} > 0$, there is SW to NE tilt of the eddies. Conversely, $\overline{u'v'} < 0$ corresponds to systematic NW to SE tilt. So, air parcels traveling along a SW–NE trajectory and then back feed momentum to an eastward jet to the north. More generally, if the shear of the zonal wind along a meridian, $\mathrm{d}\overline{u}/\mathrm{d}y$, and $\overline{u'v'}$ have the same sign, eddies accelerate jets. Eddies are said to transport momentum upgradient (Held, 1975; Thompson, 1971). This appears to be true on Jupiter (Salyk et al., 2006). On Earth, we find a departure from the symmetrical sinusoid form of waves and a systematic eastward tilt in eddies in midlatitudes so that southward motions have a smaller eastward component than northward motions (Starr, 1948), which causes net angular momentum transport (Figure 15).

10.13.5.5 Planetary Waves and Barotropic and Baroclinic Instabilities

Jets meander in latitude because of waves in the circulation. The most important class of waves in this regard are Rossby waves, which are oscillations that arise primarily in the horizontal because conservation of absolute vorticity acts to restore flows displaced meridionally to the latitude of origin. Consider an air parcel moving eastward with zero relative vorticity ($\zeta = 0$) that is perturbed northward, perhaps because of flow over topography. Planetary vorticity f increases northward
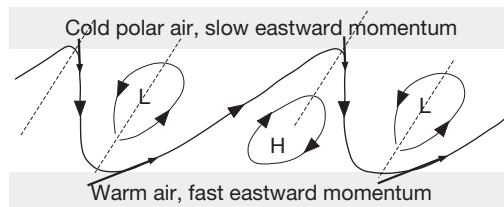

Figure 15 Tilts in the eastward winds cause momentum to be transported from the equator to poles. (These tilts were also drawn on **Figure 11** as dashed lines). (Drawn by the author.)

(eqn [100]), so relative vorticity ζ must become negative to keep absolute vorticity constant ($\eta = \zeta + f$). Remembering the right-hand grip rule, negative ζ is anticyclonic curvature (clockwise in the Earth's northern hemisphere), which sends the parcel southward, back to its initial latitude (**Figure 16**). Then, an overshoot beyond the initial latitude will induce cyclonic curvature and send the parcel back northward. The air parcel sinusoidally oscillates as it moves downstream making a Rossby wave. Meanders in the Earth's midlatitude jet stream with typical wave numbers of 4 to 6 are guided by Rossby waves. Low-pressure cyclones tend to form in the troughs of the waves, and high-pressure anticyclones tend to form in the crests. Similar Rossby waves have been observed on Mars in midlatitudes in spring and winter with wave numbers 1–2 (Hollingsworth and Barnes, 1996; Read and Lewis, 2003; Wilson et al., 2002).

The restoring effect due to the gradient in planetary vorticity (f) is called the beta effect where beta $= \beta = \partial f / \partial y$ is the meridional gradient of planetary vorticity. If we assume a zonal mean zonal wind and differentiate absolute vorticity η (eqn [111]) w.r.t. y, we get

$$\frac{\partial \eta}{\partial y} = \beta - \frac{\partial^2 \overline{u}}{\partial y^2}, \quad \text{where } \beta \equiv \frac{\partial f}{\partial y} = \underbrace{\frac{\partial(2\Omega \sin \phi)}{\partial y}}_{\delta y = a\delta\phi, \text{ spherical geometry}}$$

$$= \frac{1}{a}\frac{df}{d\phi} = \frac{2\Omega \cos \phi}{a} \qquad [116]$$

Usually, β is much larger than $-\partial^2 \overline{u} / \partial y^2$ so $\partial \eta / \partial y \approx \beta$ provides the restoring effect.

It is possible to derive sinusoidal functions in x, y, and t that represent Rossby waves. The procedure is to rewrite the vorticity eqn [113] in terms of a single variable, a stream function, ψ, which is a scalar field for a fluid flow with contour lines that are streamlines of the flow, defined as $u = -\partial \psi / \partial y$ and $v = -\partial \psi / \partial x$ (e.g., see Holton (2004), pp. 213–217). The Rossby wave solutions in ψ are found to have a dispersion relation, meaning how the eastward phase speed c of the Rossby wave varies with wavelength, as follows:

$$c = \frac{\omega}{k} = \overline{u} - \frac{\beta}{(k^2 + n^2)}$$

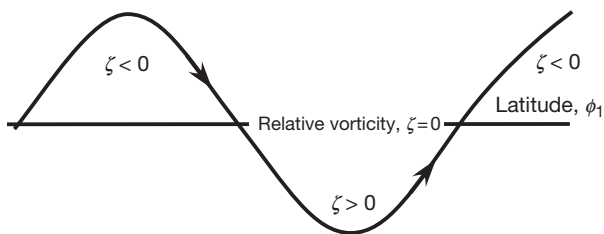$$= \text{phase speed relative to planet's surface} \qquad [117]$$

Figure 16 Illustration of the mechanism of Rossby waves in the *x-y* plane: a restoring effect caused by the gradient of absolute vorticity. A fluid parcel in the northern hemisphere moves eastward through the wave pattern. As it crosses latitude ϕ_1, the relative vorticity $\zeta = 0$. North of ϕ_1, conservation of absolute vorticity requires $\zeta < 0$, so the trajectory curves to the south anticyclonically. When it shoots over latitude ϕ_1, to conserve absolute vorticity $\zeta > 0$ and the trajectory curves northward cyclonically. (Drawn by the author.)

Here, $k = 2\pi / \lambda_x$ and $n = 2\pi / \lambda_y$ are zonal and meridional wave numbers, where λ_x and λ_y are zonal and meridional wavelengths, respectively. In the simple case where $n = 0$, the waves propagate eastward relative to the planet and westward relative to the zonal wind, at phase speeds that increase with increasing wavelength or smaller k. Setting $n = 0$ and $c = 0$ in eqn [117] gives $k^2 = \beta / \overline{u}$ for stationary waves with a west–east wavelength of $\lambda_x = 2\pi(\overline{u} / \beta)^{0.5}$. For example, in the Earth's middle troposphere at 45°N, $\beta \sim 1.6 \times 10^{-11}$ m^{-1} s^{-1}, the stationary wavelength is ~ 7000 km if $\overline{u} = 20$ m s^{-1}, and four such wavelengths would encircle the Earth.

Strictly horizontal flows with no temperature variations (parallel isobars and isotherms) are called barotropic and such flows are stable when $\beta - \partial^2 \overline{u} / \partial y^2 0$. However, if the second term – the curvature of the zonal wind profile with latitude – becomes bigger than β, then instability is produced called the barotropic instability or Rayleigh–Kuo instability. Then, growing unstable eddies derive their energy from the KE of the zonal mean flow. In prograde jets, the zonal wind decreases to the right of the flow where $\partial^2 \overline{u} / \partial y^2$ can be large. Barotropic instability produces unstable eddies that propagate to latitudes where they decay and accelerate retrograde zonal mean flow. Numerical simulations of jets forced by the eddies indicate a meridional length scale associated with this instability, characteristic of the width of the jets, called the Rhines radius, $r_{Rh} \sim (2U/\beta)^{1/2}$, where U is the typical speed of the jet (Rhines, 1975). On giant planets, vortices stop growing at this size in the meridional directional and stretch out east–west, around a circle of latitude. Thus, the number of bands on the face of a gas giant is roughly a semicircle meridian divided by the Rhines radius, $-(\pi a)/r_{Rh}$ (Menou et al., 2003).

In real atmospheres, we must consider vertical variations. General flows with vertical wind variations, nonzero vertical velocity, and horizontal temperature gradients (thus, mutually inclined isobars and isotherms) are called 'baroclinic.' Instead of vorticity, an analogous quantity, potential vorticity (PV), is introduced to allow for the vertical stretching or shrinking of fluid columns. Shrinking of the radius of a column of spinning fluid increases the spin rate, like an ice skater drawing in their arms. PV is conserved for a fluid element in the absence of mixing with other air parcels or frictional loss of KE and, in a constant density fluid, can be defined as

$$P_v = \frac{\eta}{h} = \frac{(f + \zeta)}{h} \, (\text{m}^{-1}\text{s}^{-1}) \qquad [118]$$

where h is the height of a short segment of a fluid column (e.g., Wallace and Hobbs, 2006, p. 289). Here, the word potential crops up again. In potential temperature (Section 10.13.2.4), we had a quantity remaining the same in adiabatic expansion, although the actual temperature changed. Potential vorticity is conserved for a fluid element, but the element's relative vorticity changes with changing latitude or column height. When density ρ varies with height, a more general version of PV is Ertel's potential vorticity Q_P:

$$Q_P = \frac{\eta}{\rho}\frac{\partial \theta}{\partial z} \qquad [119]$$

where θ is potential temperature and the sign of $\partial \theta / \partial z$ indicates static stability (Section 10.13.2.4). In adiabatic flow, if static stability $\partial \theta / \partial z$ increases, shrinking and horizontal expansion

of fluid columns causes the absolute vorticity n to decrease according to eqn [119], if Q_P stays constant. The converse also applies. Since Q_P involves potential temperature, it can be generated and dissipated by diabatic heating, stirring, or friction.

Ertel's PV can be calculated from temperature and pressure fields, but analytic approaches often use quasigeostrophic (QG) potential vorticity q_g, which is an approximate form of PV valid when the Ro is small and flows are approximately geostrophic. Equations based around QGPV are helpful in studying large-scale motions characteristic of atmospheric circulations. An equation analogous to eqn [113] can be derived but with absolute vorticity η replaced by QGPV, q_g, which again can be written in terms of a single stream function and solved to give 3-D planetary wave solutions (e.g., see Andrews, 2010). The key difference is that such waves have an amplitude perturbation ψ' that depends on height. Analogous to $^1/_2(\text{mass}) \times (\text{velocity})^2$, the wave KE density $\sim \rho\psi'^2$ is independent of height in the absence of dissipation. So, for this quantity to remain constant, the amplitude grows as $\psi' \sim \rho_0^{-0.5}$, where ρ_0 is the background density. Such a relationship is used in photochemical models of planetary atmospheres where turbulence (at least to certain altitudes) is often parameterized proportional to $\rho^{-0.5}$. The same $\rho^{-0.5}$ dependence also applies to the vertical amplitude growth of buoyancy waves (Section 10.13.5.7).

The meridional gradient of zonal mean QGPV is somewhat analogous to eqn [116] but has an extra term that depends on the vertical shear of the zonal mean zonal wind (e.g., see Salby (2012), p. 465, or Andrews (2010), p. 128 for derivation of QGPV equations):

$$\frac{\partial \overline{q}_g}{\partial \gamma} = \beta - \frac{\partial^2 \overline{u}}{\partial \gamma^2} + \left(\frac{1}{\rho_0}\right)\frac{\partial}{\partial z}\left[\left(\rho_0 \frac{f_0^2}{N_B^2}\right)\frac{\partial \overline{u}}{\partial z}\right] \qquad [120]$$

Here, f_0 is the value of the Coriolis parameter f at a reference latitude ($f = f_0 + \beta\gamma$), N_B is the Brunt–Väisälä frequency (Section 10.13.2.4), and ρ_0 is a height-dependent zonal and time-mean density, that is, $\rho_s \exp(-z/H)$, where H is density scale height and ρ_s a reference density. Just as barotropic instability was caused by a change of sign of $\partial\eta/\partial\gamma$ in eqn [116], so instability arises when $\partial\overline{q}_s/\partial\gamma$ changes sign. When the third term $(1/\rho_0)\partial/\partial z(\rho_0 B\partial\overline{u}/\partial z)$ dominates, a different kind of instability emerges. This is baroclinic instability, which is when flow is driven by the extraction of potential energy from a latitudinal temperature gradient, causing large-scale eddies. If we use the barometric law $\rho_0 = \rho_s \exp(-z/H)$ and differentiate the last term of eqn [120] w.r.t. z using the product rule, we see that this term depends on the vertical wind shear:

$$\left(\frac{1}{\rho_0}\right)\frac{\partial}{\partial z}\left[(\rho_0 B)\frac{\partial \overline{u}}{\partial z}\right] \approx \left(\frac{B}{\rho_0}\right)\left(-\left(\frac{\rho_0}{H}\right)\frac{\partial \overline{u}}{\partial z} + \rho_0 \frac{\partial^2 \overline{u}}{\partial z^2}\right) \propto -\left(\frac{1}{H}\right)\frac{\partial \overline{u}}{\partial z}$$

$$[121]$$

Thus, baroclinic instability is most commonly found near the regions of strong vertical shear of the mean zonal wind. On Earth, it occurs when $\partial\overline{u}/\partial z$ exceeds ~ 1 m s^{-1} km^{-1}. This threshold is small and less than the wind shear predicted from the thermal wind equation with a typical horizontal gradient induced by the spread of sunlight over midlatitudes. Consequently, baroclinic instability is generally predicted on

rapidly rotating rocky planets at the appropriate latitudes and occurs on Mars, making associated baroclinic waves (Banfield et al., 2004; Collins and James, 1995; Hinson et al., 2012; Read and Lewis, 2003; Wilson et al., 2002). The net thermal effect of 3-D baroclinic eddies is to transport warm low-latitude air poleward and up and cold high-latitude air equatorward and down. For this reason, the process has been called stantwise (or sloping) convection (Hide and Mason, 1975). As described in Section 10.13.5.4, eddies can drive jet streams. However, baroclinic instability should be less important on slowly rotating planets with small horizontal temperature gradients.

The horizontal length scale of the most unstable eddies produced by baroclinic instability is the Rossby radius of deformation:

$$r_{Ro} = \frac{N_B H}{f_0} \qquad [122]$$

where H is the scale height, N_B the Brunt–Vaisala frequency, and f_0 a reference Coriolis parameter. The Rossby radius can be understood as follows. Imagine air rising vertically through a height H and then spreading out perhaps when it reaches the tropopause. Initially, the spreading gas will not 'feel' the effects of the planetary rotation, but after a certain distance, its lateral spread will be converted to rotational motion around a core. This distance is roughly the Rossby radius. In the Earth's midlatitude troposphere, $r_{Ro} \sim 700$ km, using $f_0 \sim 10^4_-$ s^{-1}, $H \sim 7$ km, and $N_B \sim 10^2$ s^{-1}. Perhaps as a consequence, only one eddy-driven jet can fit in the Earth's midlatitudes (Schneider and Walker, 2006). On Jupiter, $r_{Ro} \sim [(0.003–0.02) \times 27]/[2 \times (2\pi/35730) \times \sin(45°)] \approx 325–2200$ km using a range of N_B values (Magalhaes et al., 2002; Shetty and Marcus, 2010), which is small compared to Jupiter's vast size.

10.13.5.6   Deep and Shallow Atmospheres on Giant Planets

The pattern of strong eastward jets at the equator on Jupiter and Saturn, with alternatively eastward and westward jets at higher latitudes is a puzzle of atmospheric dynamics. Historically, there have been two approaches to explain the jet structure (Vasavada and Showman, 2005):

(i) The observed wind systems are occurring in a shallow layer overlying a horizontally uniform but convective deep interior (Williams, 1978).

(ii) The observed winds somehow reflect the dynamic activity of an active deep atmosphere, and the jets probably represent very deeply rooted systems (Busse, 1976, 1983).

In the first scenario, shallow-layer models can produce eddies (Cho and Polvani, 1996; Huang and Robinson, 1998) – sometimes associated with the moist convection (Lian and Showman, 2010) – that force alternating zonal jets, though many models produce westward jets at the equator. In the second scenario, circulations extend deeply into the interior. The deep interior opacities of giant planets should lead to nearly adiabatic and convective conditions (Nutzman et al., 2009). The jets themselves could perhaps result from the surface manifestation of large circulating cells in systematic alignment with the jets. Galileo probe measurements of a vertical wind profile on Jupiter show nearly uniform strong zonal

winds to great depth from 5 to 20 bar, but consistent with temperature measurements interpreted in the light of the thermal wind equation, these measurements show decay of wind strength upward in the uppermost troposphere (Atkinson et al., 1997). This wind profile supports the deep circulation camp, but because the profile may not be representative, it does not prove it. The probe descended in a 'hot spot' of high IR emission at 5 μm, which emerges from deeper, unusually cloud-free parts of the troposphere (Ortiz et al., 1998).

On Uranus and Neptune (the ice giants), a broad band of strong retrograde winds exist at low latitudes with a single high-latitude prograde jet in each hemisphere (**Figure 14**). Moreover, Neptune's retrograde jet speed exceeds 500 m s^{-1}, the fastest in the solar system. It is unclear why there are such significant circulation differences between the gas giants and Uranus and Neptune. Possibly, convection is weaker on the ice giants and unable to drive the eddies needed for the kind of jet structure seen on the giant planets or only operates to drive prograde jets at high latitudes. Perhaps, a surprising result is that the jet speeds increase going outward in the solar system, which is counterintuitive if one assumes that incident sunlight is important. This puzzle has been called Suomi's paradox after Vern Suomi, who first pointed it out and is not resolved.

10.13.5.7   Buoyancy Waves and Thermal Tides

Besides planetary waves, another class of atmospheric waves that are very important for circulation are propagating buoyancy waves (also called internal gravity waves), which correspond to oscillations primarily in the vertical plane when the square of the Brunt–Väisälä frequency exceeds zero, $N_B^2 > 0$. Given that N_B^2 has the same sign as static stability (eqn [17]), this situation is common in atmospheres. As discussed in Section 10.13.2.4, the restoring force of the mean vertical buoyancy gradient acts on vertically displaced fluid parcels to cause oscillations. It is possible to derive a wave equation for buoyancy waves called the Taylor–Goldstein equation and find solutions (e.g., Holton, 2004, pp. 196–201; Nappo, 2002). In the x-z plane, wave perturbations in density, vertical velocity, pressure, and potential temperature vary as $\sim e^{(z/2H)} e^{i(kx - \omega t)}$, where the factor $\exp(z/2H)$ accounts for the vertical variation of atmospheric density, where H is the density scale height.

Such waves are generated mainly by flow over topography and large-scale flow associated with convective cells. Wave amplitude varies with density as $\rho^{-1/2}$, so amplitudes grow upward as density decreases, causing some waves to break aloft, in crude analogy to ocean waves breaking on a beach. Theory shows that buoyancy waves can also be absorbed at lower levels, the so-called critical levels, if the phase speed of the wave c equals the mean zonal wind, that is, $c = \overline{u}$ (Forbes, 2002; Nappo, 2002). Otherwise, the waves continue to propagate vertically and break well above these critical levels. Thus, for example, if an eastward jet exists at altitude, buoyancy waves propagating upward with eastward phase speeds will be absorbed and are said to be filtered out, whereas waves with westward or near-zero relative speed (the speed of the underlying surface) will penetrate higher, break, and dump their westward momentum (Forbes, 2002). The result is that these breaking waves diminish eastward zonal winds aloft, which is called closing off the winds – that is, a jet exists

below the breaking altitude and winds diminish upward from the core of a jet. This process is important for shaping jets in general, acts as a drag on the zonal mean flow, and makes upper atmospheres 'feel' the rotation of the underlying planet. Thermal wind balance (eqn [104]) applied to the effect of waves closing off the jets and declining wind speed with altitude is associated with a reverse equator-to-pole temperature gradient in the Earth's stratosphere. In turn, through thermodynamic balance (eqn [107]), this is connected with ascent and descent, where tropospheric air rises into the tropical stratosphere and subsides at the poles – the Brewer–Dobson circulation (Brewer, 1949; Dobson, 1956) – which carries stratospheric ozone from equator to poles.

An important and special class of large-scale buoyancy waves are atmospheric thermal tides, which are global oscillations in pressure and wind fields caused by the heating and cooling associated with the apparent motion of the Sun over a planet (Chapman and Lindzen, 1970). The wave periods are fractions of a solar day, so that the wave with a solar day length is a diurnal tide, while that with half a day length is a semidiurnal tide. Furthermore, the tides divide into migrating tides that move around the planet with the Sun's apparent motion and nonmigrating tides that do not, which are modes generated by migrating tides interacting with planet-scale topography.

A key theoretical result is that global-scale thermal tidal waves only propagate vertically if their angular frequency ω exceeds the Coriolis parameter, that is, $\omega > f$ (Lindzen, 1971). A diurnal tide with $\omega = \Omega$ cannot propagate vertically beyond 30° latitude because $f = 2\Omega \sin(30°) = \Omega$ at that latitude. Thus, on Earth and Mars, the diurnal tide acts as a buoyancy wave only between latitudes ±30° where it propagates vertically and its amplitude increases with height, whereas the semidiurnal tide is a global buoyancy wave from pole to pole with very large vertical wavelength ~ 100 km. Migrating and nonmigrating tides have been detected on Earth and Mars, and migrating tides have been observed on Venus (Migliorini et al., 2012; Pechmann and Ingersoll, 1984; Peralta et al., 2012; Schofield and Taylor, 1983). In the case of Venus, which rotates every 243 Earth days, the thermal tides in the middle atmosphere reflect atmospheric rotation, clearly not the rotation of the solid planet. The atmosphere near the cloud tops at ~ 65–70 km altitude rotates at ~ 110 m s^{-1} past the subsolar point, establishing waves that migrate with the Sun but move opposite to the direction of the mean flow (Gierasch et al., 1997).

Tides are important in atmospheres. On Mars, feedback between tidal surface winds and lifting of dust high in the atmosphere may contribute to the generation of planet encircling dust storms (Leovy et al., 1973), while breaking of tides may be important for mixing atmospheric constituents. On Venus, tides may be implicated in superrotation, which we discuss next.

10.13.5.8   Superrotation

Superrotation is where the equatorial zonal wind speed is persistently greater than the speed of the underlying rotating planet, which applies to Venus (Belton et al., 1991; Peralta et al., 2007), Titan (Bird et al., 2005; Kostiuk et al., 2006), Jupiter (Ingersoll et al., 2004), and Saturn (Del Genio et al., 2009). The angular momentum of a planet's surface is maximal

at the equator, and so, the superrotation cannot be maintained by some simple transport of angular momentum (Hide, 1969, 1970), as, for example, occurs from equator to high latitudes in Hadley cells. Also, since viscosity should tend to dissipate high equatorial winds, superrotation is puzzling.

Generally, it has been proposed that equatorial superrotation might be maintained by eddies with the kind of 'upgradient' transport discussed in Section 10.13.5.4 (e.g., Gierasch, 1975) (although gravitational torque acting on the atmosphere is an alternative idea (Gold and Soter, 1971; Schubert, 1983)). Eddies could carry prograde momentum systematically toward the jet region, either by motions in the vertical plane with upward and zonal velocities correlated below the maximum wind level and downward and zonal velocities correlated above the maximum or by motions in the horizontal plane with equatorward and prograde winds correlated (Schneider and Liu, 2009). If the former case applies, buoyancy waves may be implicated; in the latter case, Rossby waves. Either way, generation of wave activity by some process near the equatorial wind maximum would be required.

Attempts to model superrotation on Venus have been made with varying degrees of success, and models that work have generally assumed background superrotation below the cloud base (e.g., Del Genio and Zhou, 1996; Hollingsworth et al.,

2007; Lebonnois et al., 2010; Yamamoto and Takahashi, 2009). The waves near the superrotating level on Venus may be atmospheric tides (Newman and Leovy, 1992). It is unlikely to be a coincidence that the peak winds occur near a maximum in the vertical profile of solar heating maximum (Figure 17) (Gierasch et al., 1997; Leovy, 1987; Pechmann and Ingersoll, 1984; Schofield and Taylor, 1983). However, the underlying physics of equatorial superrotation remains an area of research (Mitchell and Vallis, 2010).

10.13.6 Outstanding Questions

Although the Space Age has greatly improved our knowledge of the atmospheres of the solar system, including the Earth, a long list of unsolved problems remains. Planetary atmospheres as a whole are very undersampled, with no in situ measurements at all for Saturn, Uranus, and Neptune, a possibly unrepresentative descent profile from Jupiter, poor knowledge of the atmosphere of Venus below the clouds, and barely any measurements of winds in all extraterrestrial atmospheres. Even on Earth, matters of basic enquiry remain. These include, for example, how the Hadley circulation interacts with eddies (Levine and Schneider, 2011), how stratospheric circulation and
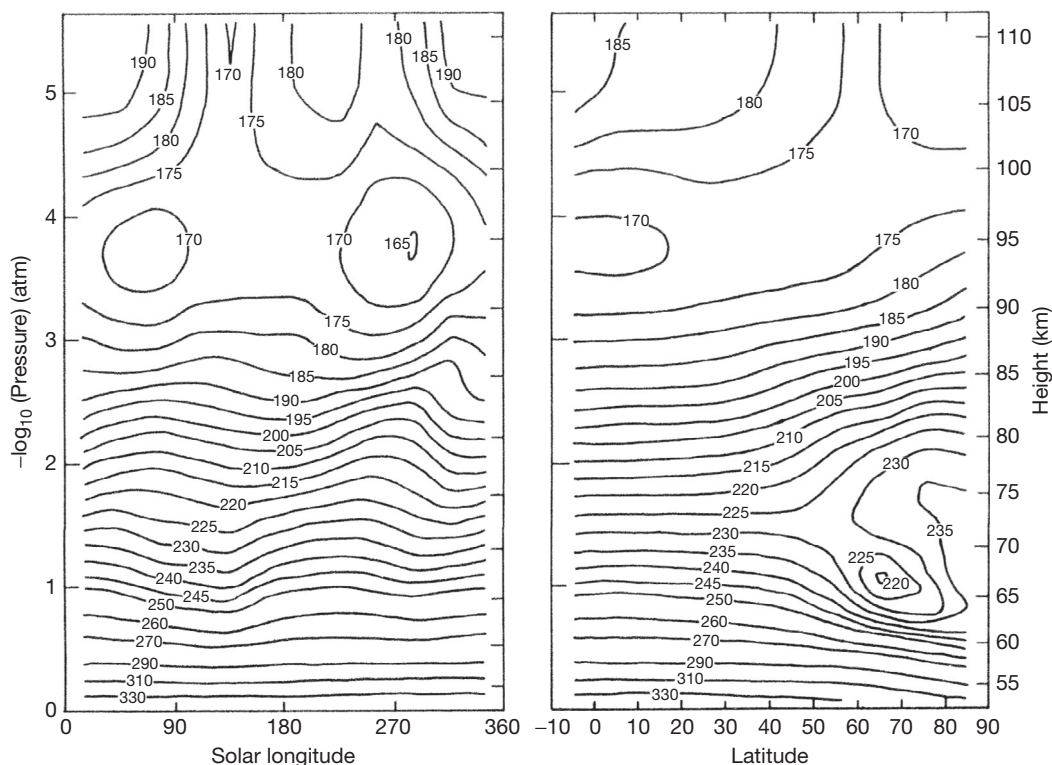

Figure 17 Cross sections of temperature (K) in the atmosphere of Venus above 55 km altitude (Schofield and Taylor, 1983). On the left, the temperature field is averaged between 0 and 30°N and shown in Sun-following coordinates where zero longitude is noon and 180° is the antisolar point. There is a minimum temperature of 170 K at 95 km altitude, above which the equator-to-pole temperature gradient is reversed. On the right, temperatures are shown as a zonal mean cross section. From above the cloud tops (70 km) to 95 km, a semidiurnal variation is revealed by waves in the temperature contours with a phase that moves in an eastward direction at higher altitude (left). The phase in the solar longitude plot on the left suggests a Sun-following eastward-propagating oscillation forced at lower altitudes. Gierasch PJ, Goody RM, Young RE, et al. (1997) The general circulation of the Venus atmosphere: An assessment. In: Bougher SW, Hunten DM, and Phillips RJ (eds.) *Venus II*, pp. 459–500. Tucson, AZ: University of Arizona Press.

chemistry affects the troposphere (Thompson et al., 2011), and the response of cloud formation (Boucher et al., 2013) and the stability of ice sheets to climate forcing (McNeall et al., 2011).

After the Earth, Mars has the most observed atmosphere. On Mars, global dust storms occur in some Martian years and not others (Martin and Zurek, 1993). But we do not know why. What are the mechanisms for storm initiation, growth, and decay and how are these storms connected to circulation features such as tides and planetary waves? Also, the role of clouds and surface exchange in the water cycle on Mars and its interaction with the dust cycle remains to be elucidated.

On Venus, winds and temperature fields in the lower atmosphere are essential for understanding the circulation and yet are poorly measured or understood. Clouds play such an important role for Venus' climate that further elucidation of their size distribution, shapes, and composition and the distribution of minor sulfur and chlorine species would also help define chemistry, climate, and dynamics. Also, many reactions relevant to chemistry on Venus that involve elemental sulfur lack laboratory data.

We do not have a fundamental understanding of the differences between the giant-planet atmospheric circulations. There are two main puzzles. The first is the different jet structures on Uranus and Neptune compared with those on Jupiter and Saturn. The latter have several jets in each hemisphere (Jupiter has 5–6 eastward jets and Saturn has 4), whereas the ice giants have only one jet (Figure 14). Whereas the equatorial jets are retrograde on the ice giants, they are prograde on the gas giants. Also, the fastest jets are on Neptune, and although Uranus is tipped on its side, its meridional profile of zonal winds is much like Neptune's and vaguely like the Earth's. Clearly, incident sunlight plays less of an overall role than rotation, while obliquity seems strangely unimportant for the jet structure. The second main puzzle is equatorial superrotation on Jupiter and Saturn. The superrotation is so strong on these gas giants that it is probably very deep. Vertical wind shear is required for the buoyancy wave mechanism that may be important for Venus yet appears lacking based on Galileo probe results (Section 10.13.5.8). So unlike on Venus, there is no clear mechanism for generating sufficiently strong buoyancy wave momentum fluxes. The horizontal shear zones associated with superrotation on Jupiter and Saturn are much wider than the scales of eddies that might transport momentum horizontally to drive superrotation. What drives superrotation on Saturn and Jupiter? And why is it absent on Uranus and Neptune, which have strong equatorial easterlies?

Finally, this chapter omitted atmospheric evolution for reasons of space. But it is clear from the history of the research literature in planetary science that initial assumptions of Earth-like conditions on the other rocky bodies, Venus and Mars, proved to be drastically erroneous. The reasons are related to great differences in how these bodies evolved, which is another story (Catling and Kasting, in press).

Acknowledgments

References

Abe Y (2011) Protoatmospheres and surface environment of protoplanets. *Earth, Moon, and Planets* 108: 9–14.

Andrews DG (2010) *An Introduction to Atmospheric Physics*, 2nd edn. New York: Cambridge University Press.

Appleby JF (1986) Radiative convective equilibrium models of Uranus and Neptune. *Icarus* 65: 383–405.

Appleby JF and Hogan JS (1984) Radiative-convective equilibrium models of Jupiter and Saturn. *Icarus* 59: 336–366.

Armstrong BH (1968) Theory of the diffusivity factor for atmospheric radiation. *Journal of Quantitative Spectroscopy and Radiative Transfer* 8: 1577–1599.

Atkins PW and De Paula J (2010) *Physical Chemistry*, 9th edn. New York: W.H. Freeman.

Atkinson DH, Ingersoll AP, and Seiff A (1997) Deep winds on Jupiter as measured by the Galileo probe. *Nature* 388: 649–650.

Atreya SK, Lorenz RD, and Waite JH (2009) Volatile origin and cycles: Nitrogen and methane. In: Brown RH, Lebreton J-P, and Waite JH (eds.) *Titan from Cassini-Huygens*, pp. 77–99. New York: Springer.

Atreya SK, Mahaffy PR, Niemann HB, Wong MH, and Owen TC (2003) Composition and origin of the atmosphere of Jupiter – An update, and implications for the extrasolar giant planets. *Planetary and Space Science* 51: 105–112.

Baker NL and Leovy CB (1987) Zonal winds near Venus cloud top level: A model study of the interaction between the zonal mean circulation and the semidiurnal tide. *Icarus* 69: 202–220.

Banfield D, Conrath BJ, Gierasch PJ, Wilson RJ, and Smith MD (2004) Traveling waves in the Martian atmosphere from MGS TES Nadir data. *Icarus* 170: 365–403.

Belton MJS, Gierasch PJ, Smith MD, et al. (1991) Images from Galileo of the Venus cloud deck. *Science* 253: 1531–1536.

Bent HA (1965) *The Second Law: An Introduction to Classical and Statistical Thermodynamics*. New York: Oxford University Press.

Berner RA (2004) *The Phanerozoic Carbon Cycle*. New York: Oxford University Press.

Bird MK, Allison M, Asmar SW, et al. (2005) The vertical profile of winds on Titan. *Nature* 438: 800–802.

Boucher O, Randall D, Artaxo P, et al. (2013) Clouds and aerosols. In: Stocker TF, Qin D, Plattner G-K, Tignor M, Allen SK, Boschung J, Nauels A, Xia Y, Bex V, and Midgley PM (eds.) *Climate Change 2013: The Physical Science Basis*, pp. 571–657. New York: Cambridge University Press.

Brewer AW (1949) Evidence for a world circulation provided by the measurements of helium and water vapour distribution in the stratosphere. *Quarterly Journal of the Royal Meteorological Society* 75: 351–363.

Brown GN and Ziegler WT (1979) Vapor pressure and heats of sublimation of liquids and solids of interest in cryogenics below 1-atm pressure. In: Timmerhaus K and Snyder HA (eds.) *Advances in Cryogenic Engineering*, pp. 662–670. New York: Plenum Press.

Buick R (2007) The earliest records of life on Earth. In: Sullivan WT and Baross J (eds.) *Planets and Life: The Emerging Science of Astrobiology*, pp. 237–264. Cambridge: Cambridge University Press.

Bullock MA and Grinspoon DH (2001) The recent evolution of climate on Venus. *Icarus* 150: 19–37.

Busse FH (1976) Simple model of convection in Jovian atmosphere. *Icarus* 29: 255–260.

Busse FH (1983) A model of mean zonal flows in the major planets. *Geophysical and Astrophysical Fluid Dynamics* 23: 153–174.

Carlson RW (1999) A tenuous carbon dioxide atmosphere on Jupiter's moon Callisto. *Science* 283: 820–821.

Catling DC (2014) The great oxidation event transition. In: Holland HD and Turekian KK (eds.) *Treatise on Geochemistry*, pp. 177–195. New York: Elsevier.

Catling DC, Claire MW, Zahnle KJ, et al. (2010) Atmospheric origins of perchlorate on Mars and in the Atacama. *Journal of Geophysical Research* 115: E00E11.

Catling DC and Kasting JF (in press) *Atmospheric Evolution on Inhabited and Lifeless Worlds*. New York: Cambridge University Press.

Catling DC and Zahnle KL (2009) The planetary air leak. *Scientific American* 300: 36–43.

Chamberlain JW and Hunten DM (1987) *Theory of Planetary Atmospheres*. Orlando, FL: Academic Press.

Chambers JE (2014) Planet formation. In: Holland HD and Turekian KK (eds.) *Treatise on Geochemistry*, pp. 55–72. New York: Elsevier.

Chapman GA, Cookson AM, and Preminger DG (2012) Comparison of TSI from SORCE TIM with SFO ground-based photometry. *Solar Physics* 276: 35–41.

Chapman S and Lindzen RS (1970) *Atmospheric Tides: Thermal and Gravitational*. New York, NY: Gordon and Breach.

Cho JYK and Polvani LM (1996) The morphogenesis of bands and zonal winds in the atmospheres on the giant outer planets. *Science* 273: 335–337.

Colburn D, Pollack J, and Haberle R (1989) Diurnal variations in optical depth at Mars. *Icarus* 79: 159–189.

Collins M and James IN (1995) Regular baroclinic transient waves in a simplified global circulation model of the martian atmosphere. *Journal of Geophysical Research* 100: 14421–14432.

Cook KH (2004) Hadley circulation dynamics. In: Diaz HF and Bradley RS (eds.) *The Hadley Circulation: Past, Present and Future*, pp. 61–83. Dordrecht: Kluwer.

Courtin R, Mckay CP, and Pollack J (1992) The greenhouse effect within the Solar System. *Recherche* 23: 542–549.

Crisp D (1986) Radiative forcing of the Venus mesosphere. I – Solar fluxes and heating rates. *Icarus* 67: 484–514.

Crisp D (1989) Radiative forcing of the Venus mesosphere. II – Thermal fluxes, cooling rates, and radiative equilibrium temperatures. *Icarus* 77: 391–413.

Crisp D and Titov D (1997) The thermal balance of the Venus atmosphere. In: Bougher SW, Hunten DM, and Phillips RJ (eds.) *Venus II*, pp. 353–384. Tucson, AZ: University of Arizona Press.

Crutzen PJ (1976) Possible importance of CSO for sulfate layer of stratosphere. *Geophysical Research Letters* 3: 73–76.

Crutzen PJ (1979) Role of NO and NO_2 in the chemistry of the troposphere and stratosphere. *Annual Review of Earth and Planetary Sciences* 7: 443–472.

Curtis AR and Goody RM (1956) Thermal radiation in the upper atmosphere. *Proceedings of the Royal Society of London A* 236: 193–206.

Del Genio AD, Achterberg RK, Baines KH, et al. (2009) Saturn atmospheric structure and dynamics. In: Dougherty M, Esposito L, and Krimigis S (eds.) *Saturn from Cassini-Huygens*, pp. 113–160. New York: Springer.

Del Genio AD and Suozzo RJ (1987) A comparative study of rapidly and slowly rotating dynamic regimes in a terrestrial general circulation model. *Journal of Atmospheric Sciences* 44: 973–986.

Del Genio AD and Zhou W (1996) Simulations of superrotation on slowly rotating planets: Sensitivity to rotation and initial condition. *Icarus* 120: 332–343.

Dima IM and Wallace JM (2003) On the seasonality of the Hadley cell. *Journal of the Atmospheric Sciences* 60: 1522–1527.

Dobson GMB (1956) Origin and distribution of the polyatomic molecules in the atmosphere. *Proceedings of the Royal Society of London A* 236: 187–193.

Fegley B (2014) Venus. In: Holland HD and Turekian KK (eds.) *Treatise on Geochemistry*, pp. 127–148. New York: Elsevier.

Forbes JM (2002) Wave coupling in terrestrial planetary atmospheres. In: Mendillo M, Nagy AF, and Waite JH (eds.) *Atmospheres in the Solar System: Comparative Aeronomy*, pp. 171–190. Washington, D.C.: American Geophysical Union.

Gierasch PJ (1975) Meridional circulation and maintenance of Venus atmospheric rotation. *Journal of the Atmospheric Sciences* 32: 1038–1044.

Gierasch PJ, Goody RM, Young RE, et al. (1997) The general circulation of the Venus atmosphere: An assessment. In: Bougher SW, Hunten DM, and Phillips RJ (eds.) *Venus II*, pp. 459–500. Tucson, AZ: University of Arizona Press.

Gold T and Soter S (1971) Atmospheric tides and 4-day circulation on Venus. *Icarus* 14: 16–20.

Goldblatt C, Robinson TD, Zahnle KJ, and Crisp D (2013) Low simulated radiation limit for runaway greenhouse climates. *Nature Geoscience* 6: 661–667.

Goody RM and Yung YL (1989) *Atmospheric Radiation: Theoretical Basis*, 2nd edn. New York: Oxford University Press.

Greeley R, Bender KC, Saunders RS, Schubert G, and Weitz C (1997) Aeolian processes and features on Venus. In: Bougher SW, Hunten DM, and Phillips RJ (eds.) *Venus II*, pp. 547–589. Tucson, AZ: University of Arizona Press.

Griffith CA and Zahnle K (1995) Influx of cometary volatiles to planetary Moons: The atmospheres of 1000 possible Titans. *Journal of Geophysical Research* 100: 16907–16922.

Guillot T (1995) Condensation of methane, ammonia, and water and the inhibition of convection in giant planets. *Science* 269: 1697–1699.

Haberle RM, McKay CP, Gwynne OE, et al. (1993a) Atmospheric effects on the utility of solar power on Mars. In: Lewis J and Matthews MS (eds.) *Resources of Near-Earth Space*, pp. 845–885. Tucson, AZ: University of Arizona Press.

Haberle RM, Pollack JB, Barnes JR, et al. (1993b) Mars atmospheric dynamics as simulated by the NASA Ames General Circulation Model. 1. The zonal-mean circulation. *Journal of Geophysical Research* 98: 3093–3123.

Hadley G (1735) Concerning the cause of the general trade-winds. *Philosophical Transactions of the Royal Society of London* 39: 58–62.

Hall DT, Feldman PD, McGrath MA, and Strobel DF (1998) The far-ultraviolet oxygen airglow of Europa and Ganymede. *Astrophysical Journal* 499: 475–481.

Han TT, Ping JS, and Zhang SJ (2011) Global features and trends of the tropopause derived from GPS/CHAMP RO data. *Science China – Physics Mechanics & Astronomy* 54: 365–374.

Hanel RA, Conrath BJ, Herath LW, Kunde VG, and Pirraglia JA (1981) Albedo, internal heat, and energy balance of Jupiter: Preliminary results of the Voyager infrared investigation. *Journal of Geophysical Research* 86: 8705–8712.

Hanel RA, Conrath BJ, Kunde VG, et al. (1972) The Nimbus 4 infrared spectroscopy. Experiment, I: Calibrated thermal emission spectra. *Journal of Geophysical Research* 77: 2629–2641.

Hansen CJ, Shemansky DE, Esposito LW, et al. (2011) The composition and structure of the Enceladus plume. *Geophysical Research Letters* 38.

Hartmann DL, Klein Tank AMG, Rusticucci M, et al. (2013) Observations: Atmosphere and surface. In: Stocker TF, Qin D, Plattner G-K, Tignor M, Allen SK, Boschung J, Nauels A, Xia Y, Bex V, and Midgley PM (eds.) *Climate Change 2013: The Physical Science Basis*, pp. 159–254. New York: Cambridge University Press.

Held IM (1975) Momentum transport by quasi-geostrophic eddies. *Journal of the Atmospheric Sciences* 32: 1494–1497.

Held IM (2000) General circulation of the atmosphere. In: Thiffeault J-L (ed.) *2000 Program in Geophysical Fluid Dynamics*, pp. 1–54. Woods Hole, MA: Woods Hole Oceanographic Institution (http://www.whoi.edu/page.do?pid=13076).

Held IM and Hou AY (1980) Non-linear axially-symmetric circulations in a nearly inviscid atmosphere. *Journal of the Atmospheric Sciences* 37: 515–533.

Heng K, Hayek W, Pont F, and Sing DK (2012) On the effects of clouds and hazes in the atmospheres of hot Jupiters: Semi-analytical temperature-pressure profiles. *Monthly Notices of the Royal Astronomical Society* 420: 20–36.

Hide R (1969) Dynamics of atmospheres of major planets with an appendix on viscous boundary layer at rigid bounding surface of an electrically-conducting rotating fluid in presence of a magnetic field. *Journal of the Atmospheric Sciences* 26: 841–853.

Hide R (1970) Equatorial jets in planetary atmospheres. *Nature* 225: 254–255.

Hide R and Mason PJ (1975) Sloping convection in a rotating fluid. *Advances in Physics* 24: 47–100.

Hinson DP, Wang HQ, and Smith MD (2012) A multi-year survey of dynamics near the surface in the northern hemisphere of Mars: Short-period baroclinic waves and dust storms. *Icarus* 219: 307–320.

Hoinka KP (1998) Statistics of the global tropopause pressure. *Monthly Weather Review* 126: 3303–3325.

Hollingsworth JL and Barnes JR (1996) Forced stationary planetary waves in Mars's winter atmosphere. *Journal of the Atmospheric Sciences* 53: 428–448.

Hollingsworth JL, Young RE, Schubert G, Covey C, and Grossman AS (2007) A simple-physics global circulation model for Venus: Sensitivity assessments of atmospheric superrotation. *Geophysical Research Letters* 34.

Holton JR (2004) *An Introduction to Dynamic Meteorology, International geophysics series*, 4th edn. New York: Elsevier Academic Press.

Houben H (2013) Thermophysical fluid dynamics: The key to the structures of fluid objects. *AGU Fall Meeting Conference, San Francisco December 9–13 2013*, abstract #P21C-1743.

Houghton JT (2002) *The Physics of Atmospheres*, 3rd edn. New York: Cambridge University Press.

Hu RY, Seager S, and Bains W (2012) Photochemistry in terrestrial exoplanet atmospheres. I. Photochemistry model and benchmark cases. *Astrophysical Journal* 761.

Hu RY, Seager S, and Bains W (2013) Photochemistry in terrestrial exoplanet atmospheres. II. H_2S and SO_2 photochemistry in anoxic atmospheres. *Astrophysical Journal* 769.

Huang HP and Robinson WA (1998) Two-dimensional turbulence and persistent zonal jets in a global barotropic model. *Journal of the Atmospheric Sciences* 55: 611–632.

Hunten DM (1973) The escape of light gases from planetary atmospheres. *Journal of the Atmospheric Sciences* 30: 1481–1494.

Ingersoll AP (1969) The runaway greenhouse: A history of water on Venus. *Journal of the Atmospheric Sciences* 26: 1191–1198.

Ingersoll AP (1990) Atmospheric dynamics of the outer planets. *Science* 248: 308–315.

Ingersoll AP (2013) *Planetary Climates, Princeton Primers in Climate*. Princeton, NJ: Princeton University Press.

Ingersoll AP, Dowling TE, Gierasch PJ, et al. (2004) Dynamics of Jupiter's atmosphere. In: Bagenal F, Dowling TE, and McKinnon WB (eds.) *Jupiter: The Planet, Satellites, and Magnetosphere*. New York: Cambridge University Press.

Irwin P (2009) *Giant Planets of our Solar System: Atmospheres, Composition, and Structure*, 2nd edn. Chichester, UK: Springer.

Jaumann R, Kirk RL, Lorenz RD, et al. (2009) Geology and surface processes on Titan. In: Brown RH, Lebreton J-P, and Waite JH (eds.) *Titan from Cassini-Huygens*, pp. 75–140. New York: Springer.

Johnson RE, Burger MH, Cassidy TA, Leblanc F, Marconi M, and Smyth WH (2009) Composition and detection of Europa's sputter-induced atmosphere. In: Pappalardo RT, McKinnon WB, and Khurana K (eds.) *Europa*, pp. 507–527. Tucson, AZ: University of Arizona Press.

Johnson RE, Volkov AN, and Erwin JT (2013) Molecular-kinetic simulations of escape from the ex-planet and exoplanets: Criterion for transonic flow. *Astrophysical Journal Letters* 768.

Joshi MM, Lewis SR, Read PL, and Catling DC (1994) Western boundary currents in the atmosphere of Mars. *Nature* 367: 548–551.

Joshi MM, Lewis SR, Read PL, and Catling DC (1995) Western boundary currents in the Martian atmosphere: Numerical simulations and observational evidence. *Journal of Geophysical Research* 100: 5485–5500.

Kahn RA, Martin TZ, and Zurek RW (1992) The martian dust cycle. In: Kieffer HH, Jakosky BM, Snyder CW, and Matthews MS (eds.) *Mars*, pp. 1017–1053. Tucson, AZ: University of Arizona Press.

Karl TR and Trenberth KE (2003) Modern global climate change. *Science* 302: 1719–1723.

Kasting JF (1988) Runaway and moist greenhouse atmospheres and the evolution of Earth and Venus. *Icarus* 74: 472–494.

Kasting JF (1991) CO_2 condensation and the climate of early Mars. *Icarus* 94: 1–13.

Kasting JF and Ackerman TP (1986) Climatic consequences of very high CO_2 levels in the earth's early atmosphere. *Science* 234: 1383–1385.

Kirschke S, Bousquet P, Ciais P, et al. (2013) Three decades of global methane sources and sinks. *Nature Geoscience* 6: 813–823.

Kliore AJ, Anabtawi A, Herrera RG, et al. (2002) Ionosphere of Callisto from Galileo radio occultation observations. *Journal of Geophysical Research* 107.

Kopp G and Lean JL (2011) A new, lower value of total solar irradiance: Evidence and climate significance. *Geophysical Research Letters* 38.

Kostiuk T, Livengood TA, Sonnabend G, et al. (2006) Stratospheric global winds on Titan at the time of Huygens descent. *Journal of Geophysical Research* 111: E07S03.

Krasnopolsky VA (2010) The photochemical model of Titan's atmosphere and ionosphere: A version without hydrodynamic escape. *Planetary and Space Science* 58: 1507–1515.

Krasnopolsky VA (2011) Atmospheric chemistry on Venus, Earth, and Mars: Main features and comparison. *Planetary and Space Science* 59: 952–964.

Krasnopolsky VA and Feldman PD (2001) Detection of molecular hydrogen in the atmosphere of Mars. *Science* 294: 1914–1917.

Krasnopolsky VA and Lefevre F (2013) Chemistry of the atmospheres of Mars, Venus, and Titan. In: Mackwell SJ, Simon-Miller AA, Harder JW, and Bullock MA (eds.) *Comparative Climatology of Terrestrial Planets*, pp. 231–275. Tucson, AZ: University of Arizona Press.

Krasnopolsky VA and Pollack JB (1994) H_2O-H_2SO_4 system in Venus' clouds and OCS, CO, and H_2SO_4 profiles in Venus' troposphere. *Icarus* 109: 58–78.

Lacis AA, Hansen JE, Russell GL, Oinas V, and Jonas J (2013) The role of long-lived greenhouse gases as principal LW control knob that governs the global surface temperature for past and future climate change. *Tellus Series B-Chemical and Physical Meteorology* 65: 19734. http://dx.doi.org/10.3402/tellusb.v65i0.19734.

Lacis AA, Schmidt GA, Rind D, and Ruedy RA (2010) Atmospheric CO_2: Principal control knob governing Earth's temperature. *Science* 330: 356–359.

Lammer H (2013) *Origin and Evolution of Planetary Atmospheres: Implications for Habitability*. New York: Springer.

Lammer H, Kasting JF, Chassefiere E, Johnson RE, Kulikov YN, and Tian F (2008) Atmospheric escape and evolution of terrestrial planets and satellites. *Space Science Reviews* 139: 399–436.

Lavvas PP, Coustenis A, and Vardavas IM (2008a) Coupling photochemistry with haze formation in Titan's atmosphere, part I: Model description. *Planetary and Space Science* 56: 27–66.

Lavvas PP, Coustenis A, and Vardavas IM (2008b) Coupling photochemistry with haze formation in Titan's atmosphere, Part II: Results and validation with Cassini/Huygens data. *Planetary and Space Science* 56: 67–99.

Lebonnois S, Hourdin F, Eymet V, Crespin A, Fournier R, and Forget F (2010) Superrotation of Venus' atmosphere analyzed with a full general circulation model. *Journal of Geophysical Research* 115.

Lee S and Kim HK (2003) The dynamical relationship between subtropical and eddy-driven jets. *Journal of the Atmospheric Sciences* 60: 1490–1503.

Lefevre F and Forget F (2009) Observed variations of methane on Mars unexplained by known atmospheric chemistry and physics. *Nature* 460: 720–723.

Leighton RB and Murray BC (1966) Behaviour of carbon dioxide and other volatiles on Mars. *Science* 153: 136–144.

Lellouch E, de Bergh C, Sicardy B, Kaufl HU, and Smette A (2011) The tenuous atmospheres of Pluto and Triton explored by CRIRES on the VLT. *ESO Messenger* 145: 20–23.

Lellouch E, Paubert G, Moses JI, Schneider NM, and Strobel DF (2003) Volcanically emitted sodium chloride as a source for Io's neutral clouds and plasma torus. *Nature* 421: 45–47.

Leovy CB (1987) Zonal winds near Venus cloud top level: An analytic model of the equatorial wind speed. *Icarus* 69: 193–201.

Leovy CB, Zurek RW, and Pollack JB (1973) Mechanisms for Mars dust storms. *Journal of the Atmospheric Sciences* 30: 749–762.

Levine XJ and Schneider T (2011) Response of the Hadley circulation to climate change in an aquaplanet GCM coupled to a simple representation of ocean heat transport. *Journal of the Atmospheric Sciences* 67: 769–783.

Levy H (1971) Normal atmosphere – Large radical and formaldehyde concentrations predicted. *Science* 173: 141–143.

Lian Y and Showman AP (2010) Generation of equatorial jets by large-scale latent heating on the giant planets. *Icarus* 207: 373–393.

Liang MC, Lane BF, Pappalardo RT, Allen M, and Yung YL (2005) Atmosphere of Callisto. *Journal of Geophysical Research – Planets* 110.

Lindemann TA and Dobson GMB (1923) A theory of meteors, and the density and temperature of the outer atmosphere to which it leads. *Proceedings of the Royal Society of London A* 102: 411–437.

Lindzen RS (1971) Atmospheric tides. In: Reid WH (ed.) *Mathematical Problems in the Geophysical Sciences, No. 2: Inverse Problems, Dynamo Theory and Tides*, pp. 293–362. Providence, RI: American Mathematical Society.

Lindzen RS and Hou AY (1988) Hadley circulations for zonally averaged heating centred off the equator. *Journal of the Atmospheric Sciences* 45: 2416–2447.

Liou K-N (2002) *An Introduction to Atmospheric Radiation*, 2nd edn. Amsterdam, London: Academic Press.

Lodders K (2010) Atmospheric chemistry of the gas giant planets. *Geochemical News* 142: 1–11.

Lodders K and Fegley B (1998) *The Planetary Scientist's Companion*. New York: Oxford University Press.

López-Puertas M and Taylor FW (2001) *Non-LTE Radiative Transfer in the Atmosphere*. London: World Scientific.

Lorius C, Jouzel J, Raynaud D, Hansen J, and Letreut H (1990) The ice-core record: Climate sensitivity and future greenhouse warming. *Nature* 347: 139–145.

Lyons TW, Reinhard CT, and Planavsky NJ (2014) The rise of oxygen in Earth's early ocean and atmosphere. *Nature* 506: 307–315.

Magalhaes JA, Seiff A, and Young RE (2002) The stratification of Jupiter's troposphere at the Galileo probe entry site. *Icarus* 158: 410–433.

Mahaffy PR, Webster CR, Atreya SK, et al. (2013) Abundance and isotopic composition of gases in the martian atmosphere from the Curiosity rover. *Science* 341: 263–266.

Mak M (2011) *Atmospheric Dynamics*. Cambridge, NY: Cambridge University Press.

Manabe S and Strickler RF (1964) Thermal equilibrium of the atmosphere with a convective adjustment. *Journal of the Atmospheric Sciences* 21: 361–385.

Manabe S and Wetherald RT (1967) Thermal equilibrium of the atmosphere with a given distribution of relative humidity. *Journal of the Atmospheric Sciences* 24: 241–259.

Marinova MM, McKay CP, and Hashimoto H (2005) Radiative-convective model of warming Mars with artificial greenhouse gases. *Journal of Geophysical Research* 110.

Martin LJ and Zurek RW (1993) An analysis of the history of dust activity on Mars. *Journal of Geophysical Research* 98: 3221–3246.

Martyn DF and Pulley OO (1936) The temperature and constituents of the upper atmosphere. *Proceedings of the Royal Society of London A* 154: 455–486.

McElroy MB and Donahue TM (1972) Stability of the Martian atmosphere. *Science* 177: 986–988.

McGouldrick K, Toon OB, and Grinspoon DH (2011) Sulfuric acid aerosols in the atmospheres of the terrestrial planets. *Planetary and Space Science* 59: 934–941.

McKay CP, Lorenz RD, and Lunine JI (1999) Analytic solutions for the antigreenhouse effect: Titan and the early Earth. *Icarus* 137: 56–61.

McKay CP, Pollack JB, and Courtin R (1989) The thermal structure of Titan's atmosphere. *Icarus* 80: 23–53.

McKay CP, Pollack JB, and Courtin R (1991) The greenhouse and antigreenhouse effects on Titan. *Science* 253: 1118–1121.

McNeall D, Halloran PR, Good P, and Betts RA (2011) Analyzing abrupt and nonlinear climate changes and their impacts. *WIREs Climate Change* 2: 663–686.

Meadows VS and Crisp D (1996) Ground-based near-infrared observations of the Venus nightside: The thermal structure and water abundance near the surface. *Journal of Geophysical Research* 100: 4595–4622.

Melosh HJ and Vickery AM (1989) Impact erosion of the primordial atmosphere of Mars. *Nature* 338: 487–489.

Menou K, Cho JYK, Seager S, and Hansen BMS (2003) "Weather" variability of close-in extrasolar giant planets. *Astrophysical Journal* 587: L113–L116.

Menou K and Rauscher E (2009) Atmospheric circulation of hot Jupiters: A shallow three-dimensional model. *Astrophysical Journal* 700: 887–897.

Michalski G, Bohlke JK, and Thiemens M (2004) Long term atmospheric deposition as the source of nitrate and other salts in the Atacama Desert, Chile: New evidence from mass-independent oxygen isotopic compositions. *Geochimica et Cosmochimica Acta* 68: 4023–4038.

Migliorini A, Grassi D, Montabone L, Lebonnois S, Drossart P, and Piccioni G (2012) Investigation of air temperature on the nightside of Venus derived from VIRTIS-H on board Venus-Express. *Icarus* 217: 640–647.

Mitchell JL and Vallis GK (2010) The transition to superrotation in terrestrial atmospheres. *Journal of Geophysical Research* 115.

Montmessin F, Bertaux JL, Lefevre F, et al. (2011) A layer of ozone detected in the nightside upper atmosphere of Venus. *Icarus* 216: 82–85.

Moroz VI, Ekonomov AP, Moshkin BE, et al. (1985) Solar and thermal radiation in the Venus atmosphere. *Advances in Space Research* 5: 197–232.

Moses JI, Fouchet T, Yelle RV, et al. (2004) The stratosphere of Jupiter. In: Bagenal F, Dowling TE, and McKinnon WB (eds.) *Jupiter: The Planet, Satellites, and Magnetosphere*. New York: Cambridge University Press.

Moses JI, Visscher C, Fortney JJ, et al. (2011) Disequilibrium carbon, oxygen, and nitrogen chemistry in the atmospheres of HD 189733b and HD 209458b. *Astrophysical Journal* 737.

Moskalenko NI, Ilin YA, Parzhin CN, and Rodionov LV (1979) Pressure-induced infrared radiation absorption in atmospheres. *Bulletin of the Academy of Sciences of the USSR, Atmospheric and Oceanic Physics* 15: 632–637.

Nappo CJ (2002) *An Introduction to Atmospheric Gravity Waves*. London: Academic Press.

Navarra A and Boccaletti G (2002) Numerical general circulation experiments of sensitivity to Earth rotation rate. *Climate Dynamics* 19: 467–483.

Newman M and Leovy C (1992) Maintenance of strong rotational winds in Venus middle atmosphere by thermal tides. *Science* 257: 647–650.

Niemann HB, Atreya SK, Demick JE, et al. (2010) Composition of Titan's lower atmosphere and simple surface volatiles as measured by the Cassini–Huygens probe gas chromatograph mass spectrometer experiment. *Journal of Geophysical Research* 115.

Nutzman P, Charbonneau D, Winn JN, et al. (2009) A precise estimate of the radius of the exoplanet Hd 149026b from Spitzer photometry. *Astrophysical Journal* 692: 229–235.

Ortiz JL, Orton GS, Friedson AJ, Stewart ST, Fisher BM, and Spencer JR (1998) Evolution and persistence of 5-μm hot spots at the Galileo probe entry latitude. *Journal of Geophysical Research* 103: 23051–23069.

Parkinson TD and Hunten DM (1972) Spectroscopy and aeronomy of O_2 on Mars. *Journal of the Atmospheric Sciences* 29: 1380–1390.

Pavlov AA, Kasting JF, and Brown LL (2001) UV-shielding of NH_3 and O_2 by organic hazes in the Archean atmosphere. *Journal of Geophysical Research* 106: 23267–23287.

Pearl JC, Conrath BJ, Hanel RA, Pirraglia JA, and Coustenis A (1990) The albedo, effective temperature, and energy balance of Uranus, as determined from Voyager IRIS data. *Icarus* 84: 12–28.

Pechmann JB and Ingersoll AP (1984) Thermal tides in the atmosphere of Venus: Comparison of model results with observations. *Journal of the Atmospheric Sciences* 41: 3290–3313.

Peralta J, Hueso R, and Sanchez-Lavega A (2007) A reanalysis of Venus winds at two cloud levels from Galileo SSI images. *Icarus* 190: 469–477.

Peralta J, Luz D, Berry DL, et al. (2012) Solar migrating atmospheric tides in the winds of the polar region of Venus. *Icarus* 220: 958–970.

Petty GW (2006) *A First Course in Atmospheric Radiation*, 2nd edn. Madison, WI: Sundog Publishing.

Pierrehumbert RT (2010) *Principles of Planetary Climate*. Cambridge: Cambridge University Press.

Pollack JB (1991) Kuiper prize lecture: Present and past climates of the terrestrial planets. *Icarus* 91: 173–198.

Pollack JB, Colburn DS, Fraser M, Kahn R, Carlston CE, and Pidek D (1979) Properties and effects of dust particles suspended in the Martian atmosphere. *Journal of Geophysical Research* 84: 2929–2945.

Pollack JB, Toon OB, Ackerman TP, Mckay CP, and Turco RP (1983) Environmental effects of an impact-generated dust cloud: Implications for the cretaceous-tertiary extinctions. *Science* 219: 287–289.

Porco CC, Helfenstein P, Thomas PC, et al. (2006) Cassini observes the active South Pole of Enceladus. *Science* 311: 1393–1401.

Prinn RG (2014) Ozone, hydroxyl radical, and oxidative capacity. In: Holland HD and Turekian KK (eds.) *Treatise on Geochemistry*. New York: Elsevier.

Ramanathan V and Carmichael G (2008) Global and regional climate changes due to black carbon. *Nature Geoscience* 1: 221–227.

Ramanathan V and Inamdar A (2006) The radiative forcing due to clouds and water vapor. In: Kiehl JT and Ramanathan V (eds.) *Frontiers of Climate Modeling*, pp. 119–151. New York: Cambridge University Press.

Ramirez RM, Kopparapu R, Zugger ME, Robinson TD, Freedman R, and Kasting JF (2014) Warming early Mars with CO_2 and H_2. *Nature Geoscience* 7: 59–63.

Read PL and Lewis SR (2003) *The Martian Climate Revisited: Atmosphere and Environment of a Desert Planet*. London: Praxis.

Rhines PB (1975) Waves and turbulence on a beta plane. *Journal of Fluid Mechanics* 69: 417–443.

Richardson MI and Wilson RJ (2002) A topographically forced asymmetry in the martian circulation and climate. *Nature* 416: 298–301.

Robinson TD and Catling DC (2012) An analytic radiative-convective model for planetary atmospheres. *Astrophysical Journal* 757: 104. http://dx.doi.org/10.1088/0004-637X/757/1/104.

Robinson TD and Catling DC (2014) Common 0.1 bar tropopause in thick atmospheres set by pressure-dependent infrared transparency. *Nature Geoscience* 7: 12–15.

Robock A (2000) Volcanic eruptions and climate. *Reviews of Geophysics* 38: 191–219.

Robock A, Oman L, and Stenchikov GL (2007) Nuclear winter revisited with a modern climate model and current nuclear arsenals: Still catastrophic consequences. *Journal of Geophysical Research* 112.

Rodgers CD and Walshaw CD (1966) Computation of infra-red cooling rate in planetary atmospheres. *Quarterly Journal of the Royal Meteorological Society* 92: 67–92.

Russell JM, Luo MZ, Cicerone RJ, and Deaver LE (1996) Satellite confirmation of the dominance of chlorofluorocarbons in the global stratospheric chlorine budget. *Nature* 379: 526–529.

Sagan C (1977) Reducing greenhouses and temperature history of Earth and Mars. *Nature* 269: 224–226.

Salby ML (2012) *Physics of the Atmosphere and Climate*, 2nd edn. New York: Cambridge University Press.

Salyk C, Ingersoll AP, Lorre J, Vasavada A, and Del Genio AD (2006) Interaction between eddies and mean flow in Jupiter's atmosphere: Analysis of Cassini imaging data. *Icarus* 185: 430–442.

Samuelson RE, Hanel RA, Kunde VG, and Maguire WC (1981) Mean molecular weight and hydrogen abundance of Titan's atmosphere. *Nature* 292: 688–693.

Sanchez-Lavega A (2010) *An Introduction to Planetary Atmospheres*. Boca Raton, FL: CRC Press/Taylor & Francis.

Sanchez-Lavega A, Perez-Hoyos S, and Hueso R (2004) Clouds in planetary atmospheres: A useful application of the Clausius–Clapeyron equation. *American Journal of Physics* 72: 767–774.

Satoh M (2004) *Atmospheric Circulation Dynamics and General Circulation Models*. Chichester, UK: Praxis Publishing, Springer-Praxis Books in Environmental Sciences.

Sausen R and Santer BD (2003) Use of changes in tropopause height to detect human influences on climate. *Meteorologische Zeitschrift* 12: 131–136.

Schmidt GA, Ruedy RA, Miller RL, and Lacis AA (2010) Attribution of the present-day total greenhouse effect. *Journal of Geophysical Research* 115: D20106. http://dx.doi.org/10.1029/2010JD014287.

Schmitt B, Deberghe C, Lellouch E, Maillard JP, Barbe A, and Doute S (1994) Identification of 3 absorption bands in the 2 micron spectrum of Io. *Icarus* 111: 79–105.

Schneider T (2006) The general circulation of the atmosphere. *Annual Review of Earth and Planetary Sciences* 34: 655–688.

Schneider T and Liu JJ (2009) Formation of jets and equatorial superrotation on Jupiter. *Journal of the Atmospheric Sciences* 66: 579–601.

Schneider T and Walker CC (2006) Self-organization of atmospheric macroturbulence into critical states of weak nonlinear Eddy–Eddy interactions. *Journal of the Atmospheric Sciences* 63: 1569–1586.

Schofield JT and Taylor FW (1983) Measurements of the mean, solar-fixed temperature and cloud structure of the middle atmosphere of Venus. *Quarterly Journal of the Royal Meteorological Society* 109: 57–80.

Schubert G (1983) General circulation and the dynamical state of the Venus circulation. In: Hunten DM, Colin L, Donahue TM, and Moroz VI (eds.) *Venus*, pp. 681–765. Tucson, AZ: University of Arizona Press.

Seager S (2010) *Exoplanet Atmospheres: Physical Processes*. Princeton, NJ: Princeton University Press.

Seager S and Deming D (2010) Exoplanet atmospheres. *Annual Review of Astronomy and Astrophysics* 48: 631–672.

Seager S, Dotson R, and Lunar and Planetary Institute (2010) *Exoplanets, The University of Arizona space science series*. Tucson, AZ: University of Arizona Press.

Seiff A, Kirk DB, Young RE, et al. (1980) Measurements of thermal structure and thermal contrasts in the atmosphere of Venus and related dynamical observations: Results from the four Pioneer Venus probes. *Journal of Geophysical Research* 85: 7903–7933.

Sekiya M, Hayashi C, and Nakazawa K (1981) Dissipation of the primordial terrestrial atmosphere due to irradiation of the solar far-UV during T-Tauri stage. *Progress in Theoretical Physics* 66: 1301–1316.

Sekiya M, Nakazawa K, and Hayashi C (1980) Dissipation of the primordial terrestrial atmosphere due to irradiation of the solar EUV. *Progress in Theoretical Physics* 64: 1968–1985.

Settle M (1979) Formation and deposition of volcanic sulfate aerosols on Mars. *Journal of Geophysical Research* 84: 8343–8354.

Shetty S and Marcus PS (2010) Changes in Jupiter's Great Red Spot (1979–2006) and Oval BA (2000–2006). *Icarus* 210: 182–201.

Shine KP, Barnett JJ, and Randel WJ (2008) Temperature trends derived from Stratospheric Sounding Unit Radiances: The effect of increasing CO_2 on the weighting function. *Geophysical Research Letters* 35.

Showman AP, Cho JYK, and Menou K (2010) Atmospheric circulation of extrasolar planets. In: Seager S (ed.) *Exoplanets*, pp. 471–516. Tucson, AZ: University of Arizona Press.

Showman AP, Wordsworth RD, Merlis TM, and Kaspi Y (2013) Atmospheric circulation of terrestrial exoplanets. In: Mackwell SJ, Simon-Miller AA, Harder JW, and Bullock MA (eds.) *Comparative Climatology of Terrestrial Planets*, pp. 277–326. Tucson, AZ: University of Arizona Press.

Smith ML, Claire MW, Catling DC, and Zahnle KJ (2014) The formation of sulfate, nitrate and perchlorate salts in the martian atmosphere. *Icarus* 231: 51–64.

Smith MD, Pearl JC, Conrath BJ, and Christensen PR (2001) Thermal Emission Spectrometer results: Mars atmospheric thermal structure and aerosol distribution. *Journal of Geophysical Research* 106: 23929–23945.

Smyth WH and Marconi ML (2006) Europa's atmosphere, gas tori, and magnetospheric implications. *Icarus* 181: 510–526.

Spencer JR, Jessup KL, McGrath MA, Ballester GE, and Yelle R (2000) Discovery of gaseous S_2 in Io's Pele plume. *Science* 288: 1208–1210.

Starr VP (1948) An essay on the general circulation of the Earth's atmosphere. *Journal of Meteorology* 5: 39–43.

Stephens GL and Tjemkes SA (1993) Water vapour and its role in the Earth's greenhouse. *Australian Journal of Physics* 46: 149–166.

Taylor JR (2005) *Classical Mechanics*. Sausalito, CA: University Science Books.

Taylor FW (2010) *Planetary Atmospheres*. Oxford, NY: Oxford University Press.

Tenishev V, Combi MR, Teolis BD, and Waite JH (2010) An approach to numerical simulation of the gas distribution in the atmosphere of Enceladus. *Journal of Geophysical Research* 115.

Teolis BD, Jones GH, Miles PF, et al. (2010) Cassini finds an oxygen-carbon dioxide atmosphere at Saturn's icy moon Rhea. *Science* 330: 1813–1815.

Thomas GE and Stamnes K (1999) *Radiative Transfer in the Atmosphere and Ocean*. Cambridge, NY: Cambridge University Press, Cambridge Atmospheric and Space Science Series.

Thompson RORY (1971) Why there is an intense eastward current in the North Atlantic but not in the South Atlantic. *Journal of Physical Oceanography* 1: 235–237.

Thompson DWJ, Solomon S, Kushner PJ, England MH, Grise KM, and Karoly DJ (2011) Signatures of the Antarctic ozone hole in Southern Hemisphere surface climate change. *Nature Geoscience* 4: 741–749.

Tian F, Claire MW, Haqq-Misra JD, et al. (2010) Photochemical and climate consequences of sulfur outgassing on early Mars. *Earth and Planetary Science Letters* 295: 412–418.

Titov DV, Bullock MA, Crisp D, Renno NO, Taylor FW, and Zasova LV (2007) Radiation in the atmosphere of Venus. In: Esposito LW, Stofan ER, and Cravens TE (eds.) *Exploring Venus as a Terrestrial Planet*, pp. 121–138. Washington, D.C.: AGU.

Tokano T (2009) The dynamics of Titan's troposphere. *Philosophical Transactions of the Royal Society* A367: 633–648.

Tokano T (2010) Relevance of fast westerlies at equinox for the eastward elongation of Titan's dunes. *Aeolian Research* 2: 113–127.

Tokar RL, Johnson RE, Thomsen MF, et al. (2012) Detection of exospheric O_2^+ at Saturn's moon Dione. *Geophysical Research Letters* 39.

Tomasko MG and West RA (2009) Aerosols in Titan's atmosphere. In: Brown RH, Lebreton J-P, and Waite JH (eds.) *Titan from Cassini–Huygens*, pp. 297–322. New York: Springer.

Trafton LM (1966) Pressure-induced monochromatic translational absorption coefficients for homopolar and non-polar gases and gas mixtures with particular application to H_2. *Astrophysical Journal* 146, p. 558.

Trafton LM (1998) Planetary atmospheres: The role of collision-induced absorption. In: Vigasin AA and Slanina Z (eds.) *Molecular Complexes in Earth's Planetary, Cometary and Interstellar Atmospheres*, pp. 177–193. London: World Scientific.

Trafton LM, Hunten DM, Zahnle KJ, and McNutt RL (1997) Escape processes at Pluto and Charon. In: Stern SA and Tholen DJ (eds.) *Pluto and Charon*, pp. 475–522. Tucson, AZ: University of Arizona Press.

Trenberth KE, Fasullo JT, and Kiehl J (2009) Earth's global energy budget. *Bulletin of the American Meteorological Society* 90: 311–324.

Turco RP, Toon OB, Ackerman TP, Pollack JB, and Sagan C (1983) Nuclear winter: Global consequences of multiple nuclear explosions. *Science* 222: 1293–1300.

Vallis GK (2006) *Atmospheric and Oceanic Fluid Dynamics: Fundamentals and Large-scale circulation*. New York: Cambridge University Press.

Vardavas IM and Taylor FW (2007) *Radiation and Climate*. Oxford: Oxford University Press, International Series of Monographs on Physics.

Vasavada AR and Showman AP (2005) Jovian atmospheric dynamics: An update after Galileo and Cassini. *Reports on Progress in Physics* 68: 1935–1996.

Walker JCG (1977) *Evolution of the Atmosphere*. New York: Macmillan.

Walker JCG (1982) The earliest atmosphere of the Earth. *Precambrian Research* 17: 147–171.

Walker JCG (1986) Impact erosion of planetary atmospheres. *Icarus* 68: 87–98.

Walker JCG, Hays PB, and Kasting JF (1981) A negative feedback mechanism for the long-term stabilization of Earth's surface temperature. *Journal of Geophysical Research* 86: 9776–9782.

Wallace JM and Hobbs PV (2006) *Atmospheric Science: An Introductory Survey*, 2nd edn. Burlington, MA: Elsevier Academic Press, International geophysics series.

Watson AJ, Donahue TM, and Walker JCG (1981) The dynamics of a rapidly escaping atmosphere: applications to the evolution of Earth and Venus. *Icarus* 48: 150–166.

Weaver CP and Ramanathan V (1995) Deductions from a simple climate model: Factors governing surface temperature and atmospheric thermal structure. *Journal of Geophysical Research* 100: 11585–11591.

Webster CR, Mahaffy PR, Atreya SK, Flesch GJ, Farley KA, and Team MS (2013) Low upper limit to methane abundance on Mars. *Science* 342: 355–357.

West RA, Baines KH, Friedson AJ, Banfield D, Ragent B, and Taylor FW (2004) Jovian clouds and haze. In: Bagenal F, Dowling TE, and McKinnon WB (eds.) *Jupiter: The Planet, Satellites, and Magnetosphere*, pp. 79–104. New York: Cambridge University Press.

West RA, Baines KH, Karkoschka E, and Sanchez-Lavega A (2009) Clouds and aerosols in Saturn's atmosphere. In: Dougherty M, Esposito L, and Krimigis S (eds.) *Saturn from Cassini–Huygens*, pp. 161–180. New York: Springer.

West RA, Baines KH, and Pollack JB (1991) Clouds and aerosols in the Uranian atmosphere. In: Bergstralh JT, Miner ED, and Matthews MS (eds.) *Uranus*, pp. 296–324. Tucson, AZ: University of Arizona Press.

Williams GP (1978) Planetary circulations.1. Barotropic representation of Jovian and terrestrial turbulence. *Journal of the Atmospheric Sciences* 35: 1399–1426.

Wilson EH and Atreya SK (2004) Current state of modeling the photochemistry of Titan's mutually dependent atmosphere and ionosphere. *Journal of Geophysical Research* 109: E06002. http://dx.doi.org/10.1029/2003JE002181.

Wilson RJ, Banfield D, Conrath BJ, and Smith MD (2002) Traveling waves in the Northern Hemisphere of Mars. *Geophysical Research Letters* 29.

Wolf ET and Toon OB (2010) Fractal organic hazes provided an ultraviolet shield for early Earth. *Science* 328: 1266–1268.

Wordsworth R, Forget F, and Eymet V (2010) Infrared collision-induced and far-line absorption in dense CO_2 atmospheres. *Icarus* 210: 992–997.

Wordsworth R and Pierrehumbert R (2013) Hydrogen-nitrogen greenhouse warming in Earth's early atmosphere. *Science* 339: 64–67.

Yamamoto M and Takahashi M (2009) Dynamical effects of solar heating below the cloud layer in a Venus-like atmosphere. *Journal of Geophysical Research* 114.

Yang J, Gong P, Fu R, et al. (2013) The role of satellite remote sensing in climate change studies. *Nature Climate Change* 3: 875–883.

Yelle RV, Griffith CA, and Young LA (2001) Structure of the Jovian stratosphere at the Galileo probe entry site. *Icarus* 152: 331–346.

Yung YL, Allen M, and Pinto JP (1984) Photochemistry of the atmosphere of Titan: Comparison between model and observations. *The Astrophysical Journal, Supplement Series* 55: 465–506.

Yung YL and DeMore WB (1999) *Photochemistry of Planetary Atmospheres*. New York: Oxford University Press.

Zahnle K, Freedman RS, and Catling DC (2011) Is there methane on Mars? *Icarus* 212: 493–503.

Zahnle K, Haberle RM, Catling DC, and Kasting JF (2008) Photochemical instability of the ancient Martian atmosphere. *Journal of Geophysal Research* 113: E11004.

Zahnle KJ and Kasting JF (1986) Mass fractionation during transonic escape and implications for loss of water from Mars and Venus. *Icarus* 68: 462–480.

Zahnle K, Kasting JF, and Pollack JB (1990) Mass fractionation of noble gases in diffusion-limited hydrodynamic hydrogen escape. *Icarus* 84: 502–527.

Zahnle K, Pollack JB, Grinspoon D, and Dones L (1992) Impact-generated atmospheres over Titan, Ganymede, and Callisto. *Icarus* 95: 1–23.

Zalucha AM, Gulbis AAS, Zhu X, Strobel DF, and Elliot JL (2011) An analysis of Pluto occultation light curves using an atmospheric radiative-conductive model. *Icarus* 211: 804–818.

Zelinka MD and Hartmann DL (2011) The observed sensitivity of high clouds to mean surface temperature anomalies in the tropics. *Journal of Geophysical Research* 116.

Zerkle AL, Claire M, Domagal-Goldman SD, Farquhar J, and Poulton SW (2012) A bistable organic-rich atmosphere on the Neoarchaean Earth. *Nature Geoscience* 5: 359–363.

Zhang X, Nixon CA, Shia RL, et al. (2013) Radiative forcing of the stratosphere of Jupiter, Part I: Atmospheric cooling rates from Voyager to Cassini. *Planetary and Space Science* 88: 3–25.